DESIGN OF A VARIABLE DUMP LOAD SWITCHING CONTROL SYSTEM FOR PICO HYDROPOWER PLANTS

BY

SAÏEF KSATRYA ALIMOESTAR

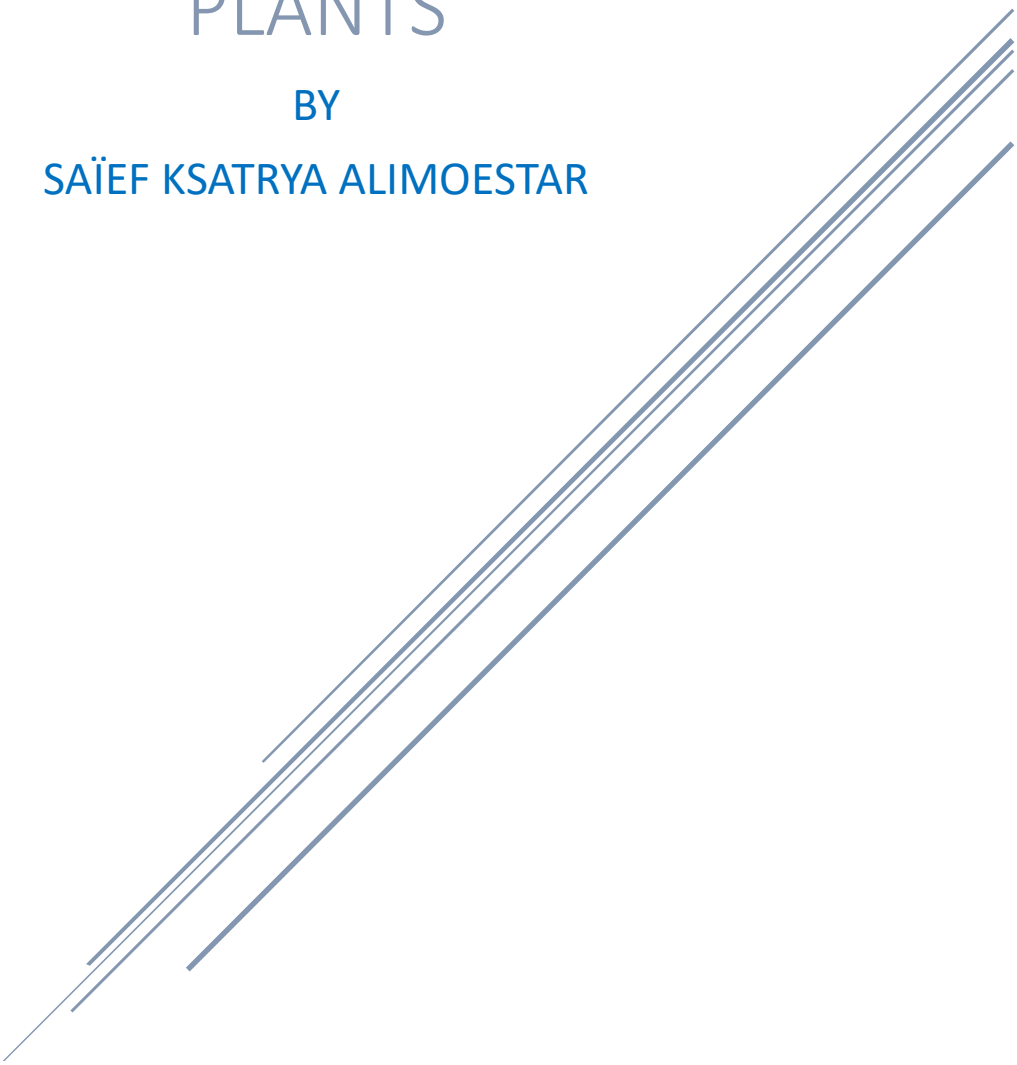

ANTON DE KOM
UNIVERSITEIT VAN SURINAME

Institute of Graduate Studies & Research (IGSR)
Renewable Energy Technologies

By

Saïef Ksatrya Alimoestar

In partial fulfillment of the requirements for the degree of

Master of Science

In

Renewable Energy Technology

At the Institute for Graduate Studies & Research,

Which will be defended publicly on 22 January 2020

Supervisor	: Dr. R. van Els	UNB
Thesis committee	: C. Ally MSc.	AdeKUS
	R. Mac Donald MSc.	AdeKUS
	Dr. Ir. R. Nannan	AdeKUS

Acknowledgements

To my parents (Rosita & August), my wife (Jessica), my son (Zahir), my grandmother (Leginah) and the rest of my family for their love and support.

To my supervisor Dr. Rudi van Els, who guided me in Brasilia for internship and during the thesis in Suriname. May you keep guiding students of Suriname to gain knowledge about hydropower.

To the Electrical Engineering department of the University of Suriname for the use of their laboratory and equipment.

To my roommate during the internship, Aboikoni Andy, for the great times in Brazil and the interior of Suriname and for his moral and academic support during thesis phase.

To my colleagues and friends at the energy laboratory: Dhanes Akash, Kasi Sandeshkoemar and Ramnaresh Wikash for their moral and academic support, and for the pleasant working environment they have created.

Summary

Suriname is part of the Amazon rainforest and has a lot of hydropower potential that can be used to implement Pico- and Micro hydropower unit to generate electricity 24 hours a day for the dispersed communities that live in the interior along the rivers. One example of this way of decentralized rural electrification was the Micro hydropower plant of Puketi. In 2017 the Gran Holo micro-hydropower plant construction phase was completed, but due to some technical issues related to its dump load control system this plant is not yet operational. One of the main technical challenges of these Pico- and Micro hydropower plants is to optimize the electricity generation with simple, yet robust and easy to use control system, as these systems will be used in remote locals with limited access to technical support. That is why the focus of this research is to design a control system for these hydropower systems to keep the frequency and voltage at the load terminals within respectively a -5% to +10% and ± 10%. The control system was designed for a Pico Indalma Turbine and therefore a simulation of the turbine generator and control system was implemented in Matlab. Besides this, an experimental setup was built with the proposed controller and a variable frequency drive, induction motor and generator emulating the turbine and generators characteristics. This research also contributes to the use of a VFD in combination with a motor to replicate the Indalma turbine behavior within a certain speed range. The dump load control system has been built using an Arduino microcontroller, 8 relays and for the dump loads incandescent lightbulbs were used. From the theoretical (simulations) results it is noticeable that voltage at the generator terminals fluctuates between 124.5 V and 127V, which is within the ±10% margin. The theoretical (simulations) results also show that the frequency fluctuation is around 1.5 Hz (58 and 59.5 Hz). The experimental results show a voltage fluctuation between 115 V and 102 V, whereby its average value is around 108 V. If this is taken as the base line than the voltage range should be between 118 V (+10%) and 97 V (-10%). The frequency at the generator terminals fluctuates between 46.7 and 55.0 Hz, with an average of 51.5 Hz. From the theoretical results it's clear that the designed control system is accurate enough, since the voltage at generator terminals is within the 10% margin and the frequency is within the -5% to +10% margin. The experimental results also indicates that the voltage fluctuation is within the 10% margin. The dump load control system worked as expected and this principle could be used for an up scaled system with some modifications, whereby the Gran Holo hydropower plant is one of the possibilities.

List of symbols & abbreviations

Symbol	Description	Unit
A	Area	m^2
D	Pipe diameter	m
F	Frequency	Hz
I	Current	A
M	mass	kg
P	Pressure	N/m^2
P	Power	W
$\dot{Q}$	Flow	m^3/s
T	Time	s
U	Voltage	V
V	Volume	l , dm^3
V	Velocity	m/s
L	distance	m

Abbreviations	
AdeKUS	Anton de Kom University of Suriname
DEV	Bureau of Electricity Service
DSM	Demand Side Management
EBS	Energie Bedrijven Suriname
EPAR	Energy Supply Paramaribo
IEEE	Institute of Electrical and Electronics Engineers
IPP	Independent Power Producers
MOSFET	Metal Oxide Semiconductor Field Effect Transistor
MWC	Meters Water Column
PMSG	Permanent Magnet Synchronous Generator
PPA	Power Purchase Agreements
PSK	Phase Shift Keying
RET	Renewable Energy Technology
TTL	Transistor-Transistor Logic
UARTs	Universally Asynchronous Receiver/Transmitter

USB	Universal Serial Bus
VFD	Variable Frequency Drive
VSD	Variable Speed Drive

Table of Contents

List of figures

List of tables

1 Introduction

Suriname is part of the Amazon rainforest, just as neighboring Guyana, French Guyana and the northern part of Brazil and has a population of 542.000 inhabitants. The country is divided in 10 districts, where Paramaribo is the capital city. The largest district is Sipaliwini, which occupies 79.90% of the country and 7% of the total population lives in this district widespread. This area is also called the interior or hinterland of Suriname [1]. In order to bring development to this part of the country, a crucial step is to provide the villages in the interior with constant energy supply (electricity). Electricity has become one of the most important needs for mankind's development and it plays a significant role in the improvement of the socio-economic conditions [2][3]. Some of these villages in the hinterland are located nearby sites with Micro- and Pico-hydropower potentials, which can be used to generate electricity and these hydropower plants could be a relative cheap and a clean alternative for power generation[4].

In Suriname 37% (189 MW) of the total energy generation (506.9MW) is generated using hydropower at the Suralco hydropower plant at Brokopondo. This plant has a generating capacity of 189MW. This plant is operational since 1965, which makes it one of the oldest large hydropower plants that is still operational in the Amazon region. The water reservoir has an area of 1560 km^2. Currently there are 3 Kaplan turbines and 3 fixed blade turbines installed. During normal operation 4 out of the 6 turbines are working. This is done to keep 2 turbines as back-ups in case there is an issue with one of the 4 turbines in operation [5].

Suriname has an estimated hydro potential of 2,419 MW. From this potential only ±190 MW has been explored until now, which includes Afobaka 189MW, Gran Holo 135 kW and Puketi 40 kW. Table 1.1 presents Micro hydropower potential sites in Suriname examined since 1981.

Table 1.1: Micro hydropower potential sites

	Naipal 2003 [6]			Naipal 2012 [7]			Internship rapport 2019 [8]			King 1981 [9]		
location	flow(m^3/s)	head(m)	power(kW)	flow(m^3/s)	head(m)	power(kW)	flow(m^3/s)	head(m)	power(kW)	flow(m^3/s)	head(m)	power(kW)
Puketi	-	-	-	-	-	-	-	-	-	-	-	40
Tapawatra	14.3	4.2	200	5	3.2	300	-	4	25	-	-	80 + 40
Gran Dan	17.7	6.0	530	-	-	-	-	-	-	-	-	-
Dangogo	4.9	1.2	25	-	-	-	-	-	-	-	-	-
Felulasi (Afobasu)	5.0	1.6	40	-	-	-	-	3 – 4	20-50	-	-	-
Felulasi (Mindrihati)	15.0	3.1	250	-	-	-	-	-	-	-	-	-
Gran-olo	-	-	-	5	3.5	650	-	-	-	-	-	-
Manbari	-	-	-	5	2.0	375	-	-	-	-	-	-
PG2	-	-	-	5	1.0	160	-	-	-	-	-	-
Tepu	-	-	-	-	-	100	-	-	-	-	-	-
Gran Dan	-	-	-	5	6.0	600	-	-	-	-	-	-
Afobasu Sula	-	-	-	5	1.6	120	-	-	-	-	-	-
Mindrihati sula	-	-	-	5	3.1	200	-	-	-	-	-	-
Aprisina sula	-	-	-	5	0.8	300	-	-	-	-	-	-
Atjoni	-	-	-	-	-	200	-	-	-	-	-	-
Bushpapaja sula	-	-	-	-	-	100	-	-	-	-	-	-
Karina Ituru	-	-	-	3	2.2	100	-	-	-	-	-	-

From 1981 to 1988 Suriname had a Pico hydropower plant at Puketi. This micro hydropower plant supplied the villages Puketi and Futupasi of electricity, which was generated with a 40KW Ossberger Crossflow SH52A/G (model type Michell-Banki) turbine [10].Villages like Puketi and Futupasi are an example of villages that used to be supplied by the micro hydropower plant at Puketi, which worked for almost seven years. Its control system was mechanically controlled and was based on the flow control principle. Thus, controlling the flow of water to the turbine [11].

From October 2005 to February 2017 construction of the Gran Holo micro hydropower plant took place, which is located in the Tapanahony River [11][12][13]. After construction the commissioning phase started, during which the hydropower plant did not function as expected. The EBS, who acted as a consultant during the commissioning, stated in their reported problems with operation of the control system [14]. The control system of this micro-hydropower plant is based on dump loads which are controlled using relays. These relays are in turn activated by a PLC

unit, which is supposed to keep the voltage at the generator terminals within a specified margin [15].

The function of a control system for a hydropower plant is to keep the frequency and voltage within a specified margin. The consequences for a poor control system can lead to voltage and frequency rise or fall. Which in turn can damage or destroy the electrical equipment connected to this hydropower plant [16][17]. Note that control systems for Pico- and Micro hydropower plant are designed for the specific installation, there is no universal controller for every Pico- and Micro hydropower plant [18].

To understand the working principle of a hydropower plant controller, good knowledge of such systems are needed. And in Suriname there are few people with such knowledge, which may be of the reasons why the Gran Holo hydropower plant is not yet operational. Since the main issue with this plant is its control system, this thesis focuses on building a simplified control system that can replace the current control system of Gran Holo micro-hydropower plant. That being said the control system will be based on the shunt load governor principle to build an electronic dump load controller. This controller must keep the voltage at the generator terminals within a ±10% margin of 127V by dumping the excess energy in the dump loads. This prevents the rise in voltage and frequency when energy demand is lower than production. Since the EBS uses the NEN1010 standard, which states a ± 10% voltage margin for electricity supply to the local households, this will be the reference point for this research [19].

1.1 `Objective

1.1.1 General objective

Design, model, simulate and built a dump load control system for micro hydropower systems, which controls dump loads to keep the voltage at the generator terminals within a 10% margin. Moreover, given the context of operation, additional important points are low cost, robust, easy to install and low maintenance.

1.1.2 Specific objective

1. Design the control system, which will keep the frequency and voltage at the load terminals within respectively a -5% to +10% and ± 10% margin;

2. Simulate a control system for micro hydropower systems, using a simplified model for the 6” Indalma hydraulic turbine;

3. Design the dump load control system as similar as possible to the control system of Gran Holo hydropower plant.

1.2 Methodology

To achieve the above proposed objectives the following steps were undertaken:

- Literature study on hydropower, Indalma hydraulic turbine and the control of hydraulic turbines;

- Implementing a research test setup;

- The modeling and simulation of the control system;

- Design and execution of the control system.

This thesis rapport is divided into six (6) chapters, which have sections and subsections. The content of each chapter is discussed below:

- The second chapter is a review of the literature regarding: hydropower and the types of hydropower plants, the Indalma hydraulic turbine and the control of this turbine.

- The third chapter presents the research test setup, which was used for experiments regarding the dump load controller.

- The fourth chapter presents the control hardware and software. This chapter also gives a detailed overview how this control hardware was built.

- The fifth chapter discusses the modeling and simulations of the dump load control system. Furthermore, the parameters on which the system is depended on, is described and simulation models are presented.

- Chapter six presents the results and analysis.

- Finally, the last chapter concludes the thesis by presenting the conclusions, and provides suggestions for future work.

2 Literature review

This chapter provides the basic understanding of hydropower and hydraulic turbines. The classifications for five specific hydraulic turbine types are also discussed. It also presents the relevant hydraulic turbines and their characteristics, which have been used in Suriname. Furthermore, this chapter discusses three different ways to control hydraulic turbines.

2.1 Hydropower

Hydropower is a form of renewable energy based on the natural cycle of water, which has been around since the 19th century. Thus, making hydropower the most mature and reliable renewable energy resource. The only large-scale and cost-efficient energy storage technology available today is hydropower, if the environmental aspect is left out of the equation. Even though other energy storage technologies have promising futures, hydropower is still the only technology which has proven to be economically beneficial for large-scale storage [20]. In 2015 hydropower was the most used renewable energy source globally. Electricity generated by hydropower plants supplied 71% of all renewable electricity. At the end of 2015, hydropower plants were supplying 6.79% of the world's energy demand, which accounted for 1209 GW [21]. In 2018 the world average cost for electricity produced by hydropower was USD 0.047/ kWh, which was the cheapest method of all [22]. The hydropower sector alone gave employment to 2.05 million people worldwide [23].

Hydropower plants can be classified in six categories, namely according to capacity, head, purpose, facility types, hydrological relation and transmission system. This is illustrated in Figure 2.1. When classified according to power range or the capacity the focus is placed on the electric energy that the hydropower plant can produce.

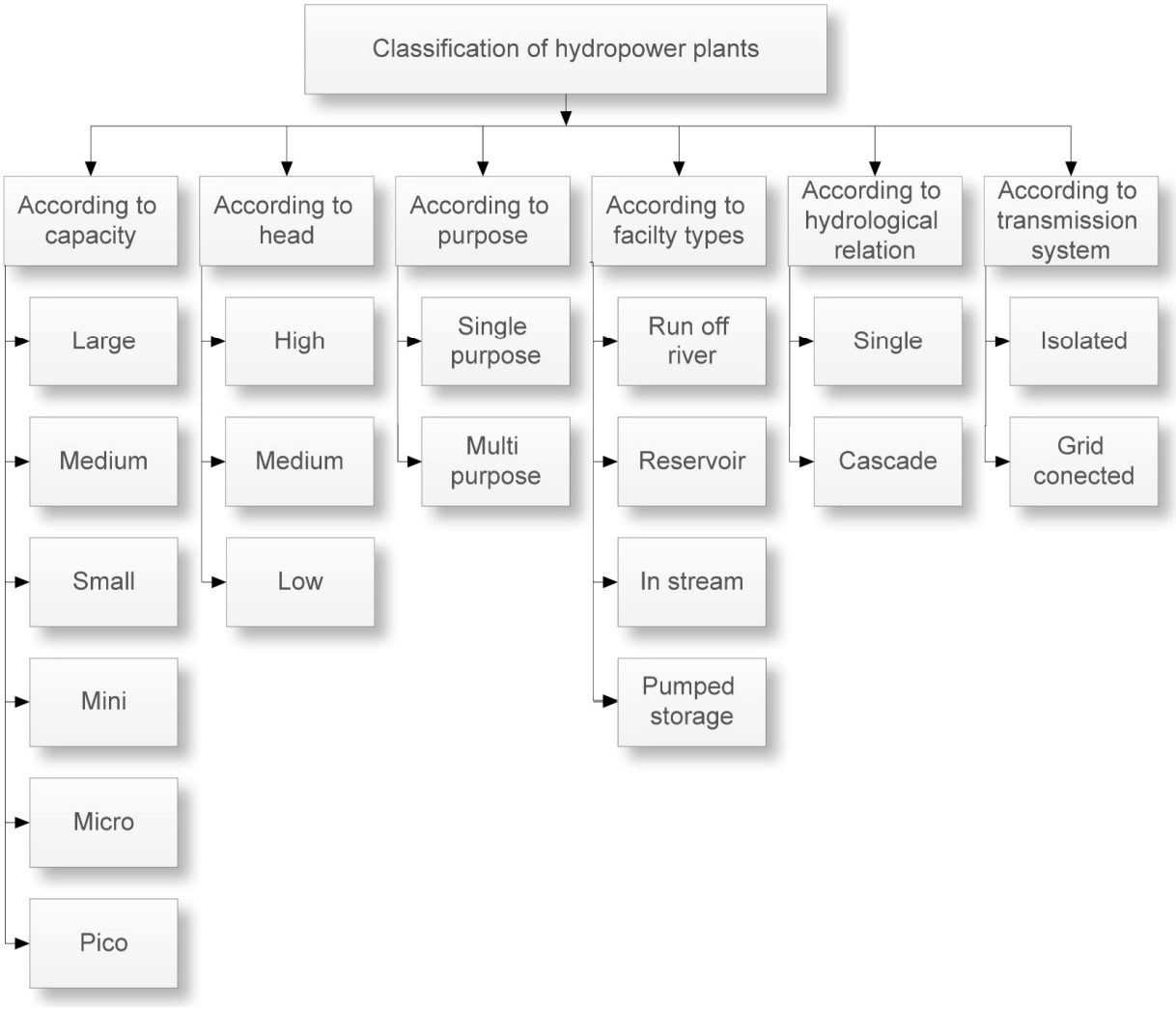

Figure 2.1: Hydropower plant classification [24]

This study will focus on hydropower in the ranges of Pico, Micro and mini. Table 2.1 presents the classification of the hydropower plants according to their power capacity.

Table 2.1: Classification according to power capacity

Size	Power capacity (kW)	Techniques
Pico	1-10	Mostly run off the river
Micro	10-100	Mostly run off the river
Mini	100-1000	Mostly run off the river and small dams

In South America the majority of the countries make use of hydropower to generate electricity [25]. In the amazon region there are a lot of villages nearby rapids and rivers. For these villages Micro- and Pico- hydropower plants are an option for rural electrification [26]. The Acaizal and Cachoeira do Aruá Micro-hydropower systems are two examples of rural electrification using hydropower [8].

The village Acaizal in Santarém in the district Para of Brazil, has two 10" Indalma turbines working in parallel to drive an 80 kW generator. This hydropower system has been working without any control system whatsoever for more than 13 years. The hydropower system is owned by the village and is under supervision of cooperation of the village [8].

Cachoeira do Aruá is a village situated in Santarém in the district Para of Brazil, where electricity was generated using hydropower since 2003. In 2017 the hydropower installation has been upgraded from a single 50 kW Indalma turbine to two 70 kW Indalma turbines working in parallel without a control system. This system has a penstock diameter of one meter and a head of 6 meters over a length of 200 meters. The present Indalma turbines have a 25 inch water inlet. The Micro hydropower plant is being supervised by a trained villager [8].

The typical components in a Micro- and Pico hydropower plant are the intake weir, the channel, the penstock and the powerhouse with turbine and generator. Figure 2.2 illustrates the typical layout for a Micro- and Pico hydropower plant. Micro- and Pico hydropower plants often

don’t require sophisticated dams or water reservoirs, such systems are also called “run off the river” systems. Part of the water stream of the river is diverted to the turbine through a pen-stock, which was also the case at the hydropower plants of Acaizal and Cachoeira do Aruá [8][27]. The turbine converts the potential- and kinetic energy of the water stream into mechanical energy, which is again converted to electrical energy by the generator. The conversion from hydraulic power to electrical power is illustrated in Figure 2.3. As the demand of energy is not constant throughout the day, the generation has to be controlled in order to maintain a stable voltage and frequency. Conventionally, the frequency is controlled by mechanical governors, however these governors are expensive, complex and slow in response [20][28].

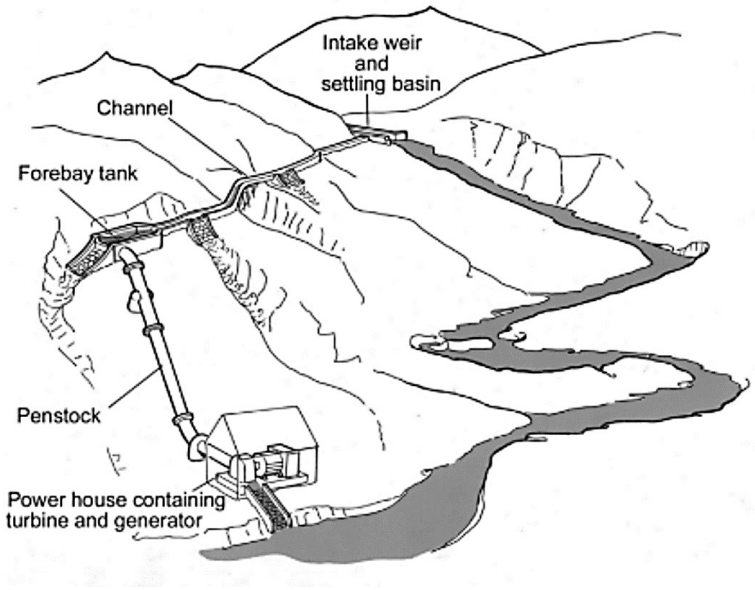

Figure 2.2: Typical Micro- and Pico hydropower plant layout [27]

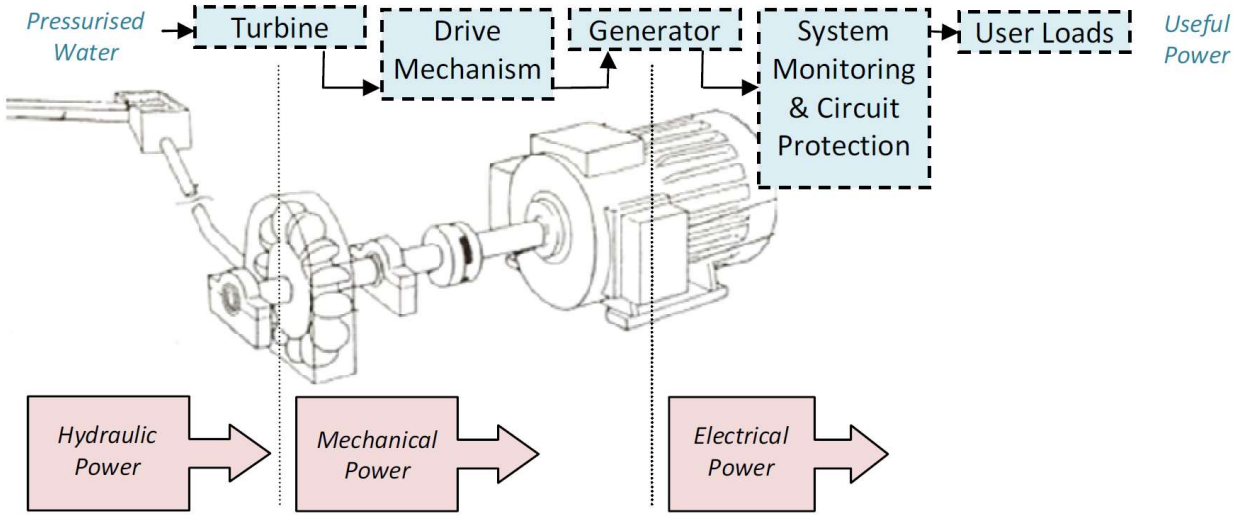

Figure 2.3: Conversion hydraulic power [16]

2.2 Hydraulic turbines installed in Suriname

As mentioned in the above section the hydraulic turbines are a crucial part of a Micro – or Pico hydropower plant. The hydraulic turbine is responsible for the conversion of the hydraulic energy of the water to mechanical energy. The working principle of a hydraulic turbine is water flows in through the water inlet, which comes in contact with the turbine blades and brings them in motion. Since the turbine blades are fixed on the rotor shaft, the shaft starts to rotate. There are different types of hydraulic turbines, for various applications. The relevant hydraulic turbines, which are installed in Suriname are presented in Table 2.2. This table also shows the location, installed capacity and the operational period of these turbines.

Table 2.2: Hydraulic turbines in Suriname

Hydraulic turbine type	**Location/project**	**Installed Capacity (kW)**	**Operational period**
Cross-flow	Puketi micro hydropower plant	40	1981 – 1988
S-type	Gran Holo mini hydropower plant	300	Not yet operational
Indalma	AdeKUS Pico hydropower experimental setup	5	2014 – present (only in operation during experiments)

Hydraulic turbines are classified based on the mechanism by which water interacts with the turbine propeller. These turbines can be classified in different ways, namely on the basis of (1) energy transfer, (2) the geometry of the flow path, and the (3) specific speed. Hydro turbines that are classified based on energy transfer are dived in two general classes, either (a) impulse or (b) reaction turbines [29].

1) (a) When friction and gravity effects are neglected in impulse turbines, the fluid pressure and the relative velocity do not change as the fluid passes over the blades. Impulse turbines do not run full of fluid and do not need a draft tube, i.e., the outlet tube, which is submerged in water. The impulse turbines are working with high head and low flow. Both the pressure and the relative velocity change over the rotor as they flow through a reaction turbine. The Pelton turbine is an example of an impulse turbine.

   (b) Reaction turbines run fully filled with the working fluid and therefore need a draft tube, which is fully submerged in water (thus these turbines should always be filled with water). Furthermore, reaction turbines are low head and high flow rate turbines. Kaplan -, Francis- and the Indalma turbine are examples of reaction turbines.

2) Hydraulic turbines that are classified based geometry of the flow path can be divided in three categories: (a) radial flow turbines, (b) axial flow turbines and (c) mixed flow turbines.

   a) In radial flow turbines the fluid flows in a plane that is partially or fully perpendicular to the axis of rotation.

b) Axial flow turbines: hereby the fluid flows partially or fully parallel to the axis of rotation.

c) Mixed flow turbines: in these turbines the fluid flows in a radial and axial direction.

These turbines encompass a variety of designs between the extremes of fully radial and fully axial flow machines.

3) Hydraulic turbines that are classified based on specific speed are divided in three main categories: (a) Pelton-, (b) Francis- or the (c) Kaplan turbines. The specific speed of each turbine is usually given by the manufacturer. But if the specific speed is unknown, this could be acquired experimentally.

Table 2.3: Head classification for hydro turbines

Classification	Head (m)	Typical turbine type
High head	>100	**Pelton, Francis, etc.**
Medium	30-100	**Francis, Kaplan, etc.**
Low head	2-30	**Crossflow, Indalma**

Before placing a hydraulic turbine model in a specific location it's always necessary to know the hydropower potential. If there is a very low potential this is economically not feasible to place a hydropower system at such a location, unless there is no other form of electricity generation possible. The hydropower potential of a river or waterfall can be calculated theoretically using equation 1, where the power (P) is proportional to the head (H), flow rate (Q) and gravity (g) [27]. Note that this is a theoretical value, in practice less power is obtained.

$$P(w) = Q(\frac{m}{s}) \times H(m) \times g(m^3 \cdot kg^{-1} \cdot s^{-2}) \quad [1]$$

2.3 Hydraulic turbine characteristics

When hydraulic turbine characteristics are considered one of the most important factor is the specific speed (Ωs), which is mostly given by the turbine manufacturer. This is an expression which relates the inlet head (H), the volumetric flow rate (Q), and the rotational speed (Ω) as written in Equation 2. This equation is primarily used to select the most suitable rotating flow machine for a given set of conditions, which could be: Pelton turbine, Francis turbine or Kaplan turbine [29].

$$\Omega_s = \frac{\Omega \dot{Q}^{\frac{1}{2}}}{(gH)^{\frac{3}{4}}} \qquad \frac{\left[\frac{\text{rad}}{\text{s}}\right]\left[\frac{\text{m}^3}{\text{s}}\right]}{\left[\frac{\text{m}}{\text{s}^2}\right][\text{m}]} \qquad [2]$$

From the specific speed gained from Equation 2 a turbine can be chosen according to Figure 2.4, which shows the specific speed range for various turbines. But if for a certain location the water flow and the head is known than Figure 2.5 is used to determine which turbine is suited for such a location.

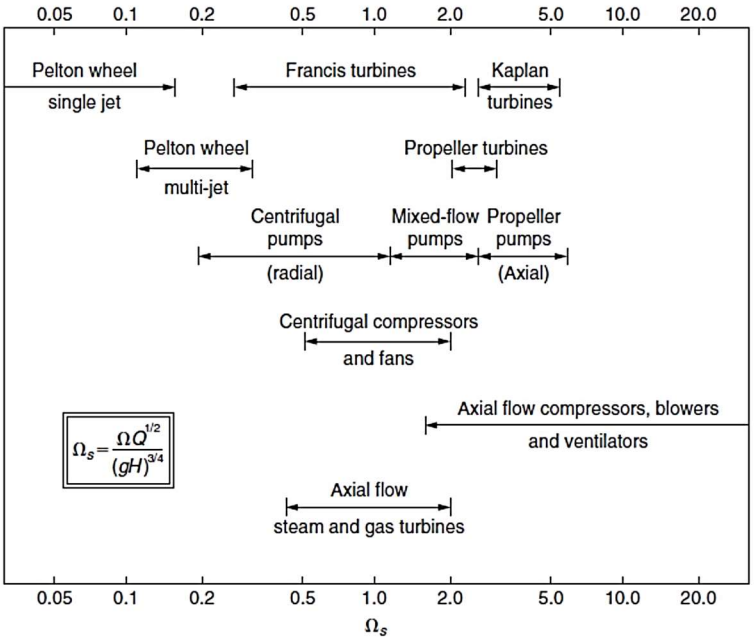

Figure 2.4: Specific speed range for various turbines [30]

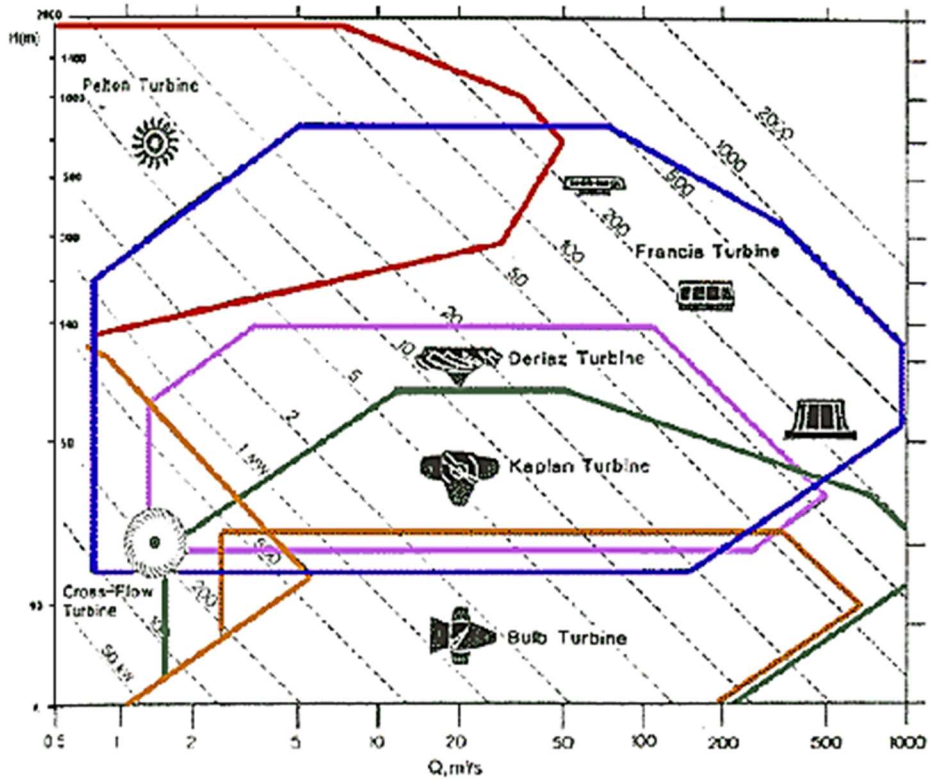

Figure 2.5: Head vs flow for typical turbines [30]

2.3.1 Ossberger (Cross-flow)

The Ossberger cross-flow turbine is named after the German Fritz Ossberger, who was granted the patent for his turbine in 1933. The name cross-flow turbine comes from its unique design whereby water flows through or across the rotor. Figure 2.6 illustrates an Ossberger cross-flow turbine, with a vertical water flow. According to the flow the cross-flow turbine can be categorized in vertical flow and horizontal flow turbines. The unique structure of a cross-flow turbine, makes it excellent for smaller hydroelectric sites with low head and high flow with power outputs between 5-100 kW. Water flows from the inlet through the runner and it crosses the channels confined by each blade couple twice. After transferring the potential energy of the water, to mechanical energy of the runner, the water leaves the turbine through another channel. Additional efficiency is released by going through the runner twice. The advantage the cross-flow turbine has over other hydraulic turbines is that it helps to clean the runner form clog, sand, leaves, twigs, etc. Cleaning of the runner prevents losses and efficiency drop. From Figure 2.8 it is clear that the cross-flow turbine has the highest efficiency when it's used under its nominal flow rate, compared to other hydraulic turbines [31]. This type of cross-flow turbine was first used in Suriname in the 1980 at the Puketi hydropower plant.

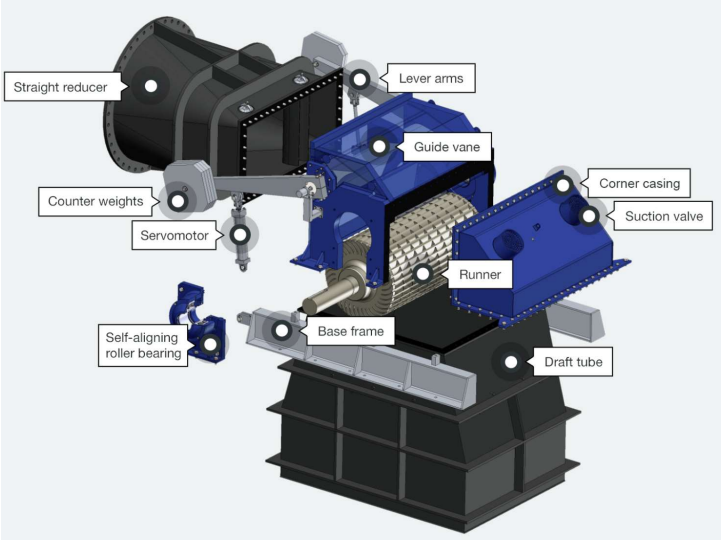

Figure 2.6: Ossberger cross-flow turbine [32]

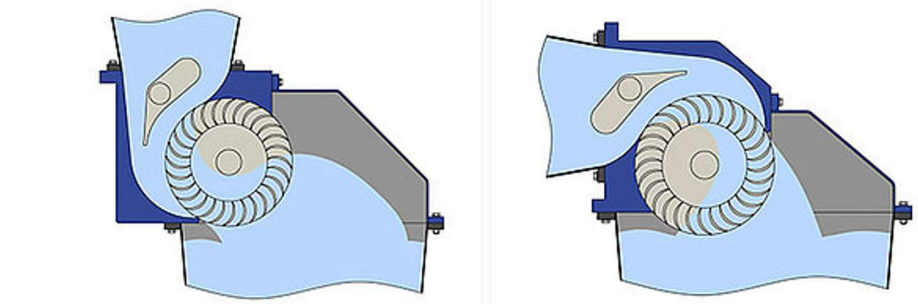

A B

Figure 2.7: Cross-flow turbine with (A) vertical flow (B) horizontal flow [32]

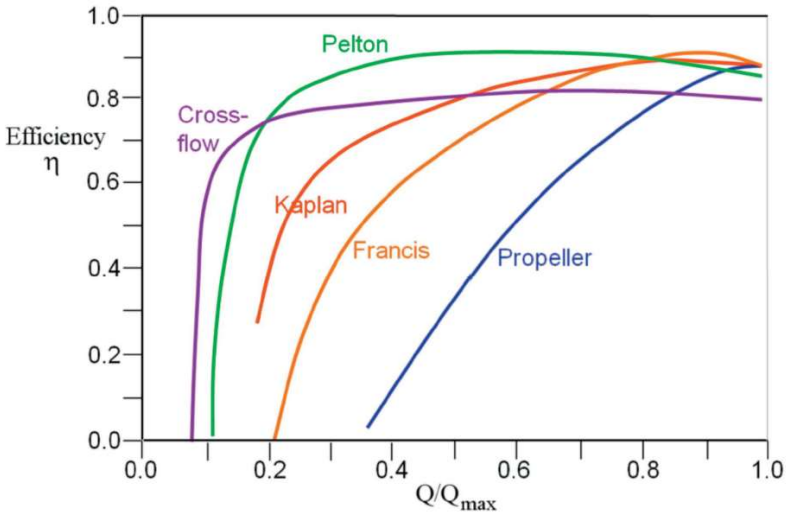

Figure 2.8: Efficiency vs discharge for various hydraulic turbines [31]

2.3.2 S-type turbine

The S-type turbine are mostly used for "run off the river" systems with relatively low head, where a small dam is required to anchor the powerhouse and raise the water level at the location. The turbine itself could be a fixed blade model or an adjustable blade model, such as the S-type Kaplan turbine. This is S-type Kaplan turbine is first used in Suriname at Gran Holo micro hydropower plant. This type of turbine is a special variation of the traditional Kaplan turbine, whereby the generator is outside of the water channel (see Figure 2.9). This variation has three main advantages, which are:

1. Makes it easier to reach generator for maintenance;

2. Since the generator is outside of the water channel, the system is more robust.

3. The total pressure is utilized, which consists of the suction and discharge pressure.

The main disadvantage of the S-type turbine, compared to run of the river type turbines are the higher installation costs, which comes from civil works for the required small dam and the tail (water output channel) that has to be submerged in water [7][17].

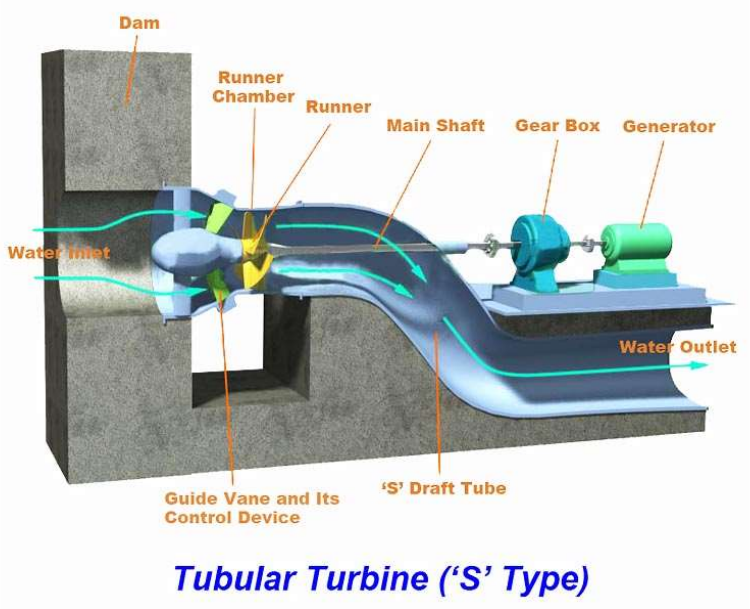

Figure 2.9: Kaplan S-type turbine [33]

2.3.3 Indalma hydraulic turbine

The Indalma hydraulic turbine was invented, patented and developed by Indalma Company located in Santarém, Pará – Brazil. This turbine was developed by studying the Francis turbine and its main goal was to be used in remote areas in the Amazon region. Therefore, the turbine does not have a rotor with movable blades or even a distributor with guided blades. It has no moving parts to regulate the water inlet, which makes it more robust and cheaper. Adjusting its speed and power through water in flow is only possible by a manual drive for opening the water inlet butterfly valve [34][35].

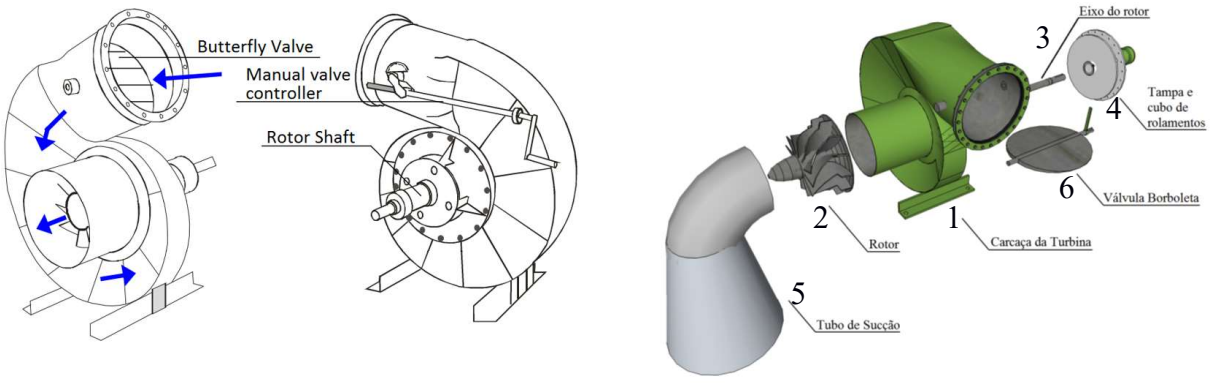

Figure 2.10: Indalma turbine main components[34][35]

The main components of the Indalma turbine (see Figure 2.10) are:

1. The turbine casing, sometimes called a snail – where the flow of water flows and is forced to go to the center;

2. The turbine rotor – the flow of water rotates the rotor, thus potential and kinetic energy of the water flow is converted to mechanical energy;

3. The rotor shaft – responsible for transmitting the mechanical power generated by the flow to the electric generation system;

4. The housing cover and the bearing hub – are responsible for mechanism, both the fixed part (housing) and the moving part (shaft). For such, seals and seals are used. This component also serves as the basis for bearings that support the rotor shaft.

5. Draft tube – this is the part of the turbine where water flows out of the turbine and downstream of the river.

6. Butterfly valve and its lever for manual operation – it is verified that the Butterfly valve mechanism is very simple and has no sophistication, or even an additional function that assists in the implementation of a control system.

2.4 Control of hydraulic turbines

The Pico- and Micro hydropower plants installed in the Amazon region usually are not installed with a control system. The flow to the turbine is manually adjusted according to the season. For example, in Santarem the village of Cachoeira do Aruá has a 25” Indalma turbine, which in the dry season the manual valve that controls the flow to the turbine is fully open and in the rainy season this valve is adjusted according to the flow. Even though the flow is almost constant the load of the household varies, due to on/off switching of electrical devices or home applications. Since the flow is constant, this load increase will result in voltage and frequency decrease. If the load decreases, this will result in voltage and frequency increase. So, to make such a system work without control system means the villagers need to be aware of their current situation and need to know the basics of the whole system. In the case of the village Cachoeira do Aruá, the villagers know that at dawn the street lights and those of the houses turn on, so to balance

out the supply and demand, they pull the plug of their freezers and fridges. Such Pico- and Micro hydropower plants without control systems have certain advantages, such as; the system is cheaper and more robust. The disadvantages are flow must be manually controlled at season change, inefficient and discomforting for users.

To control hydraulic turbines used in Pico- and Micro hydropower systems there are three (3) possible methods. The first method is to design the system in such a way that operation of the turbine is at the back side of the power curve. The second method is control of the power output of the turbine by controlling the water inlet valve of the turbine. The third method is to run the turbine at fixed operation point (fixed power output) and dissipate the surplus energy in dump load or load ballast [17]. These methods are discussed in the following subsections.

2.4.1 Operation at the back side of the power curve

Normally the operating point of a turbine is at the top off the curve shown in Figure 2.11. So, if there is no controller then at decreasing load the turbine speed will increase accordingly until its runaway speed. And if the load increases above the peak power then the frequency and speed will decrease. Therefore, operation will be at the left side of the curve also known as the instable area. In order to use the turbine without flow or power controller, the turbine has to be operated at the back side of the power curve. This method is based on shifting the operation point of the turbine to an operation point 75% of the runaway speed, thus to the backside of the curve (see Figure 2.11). By doing so the system has a speed variation of max. 33% in both directions, thus more flexibility for the entire system. Note that this method does not use an external controller [17][29].

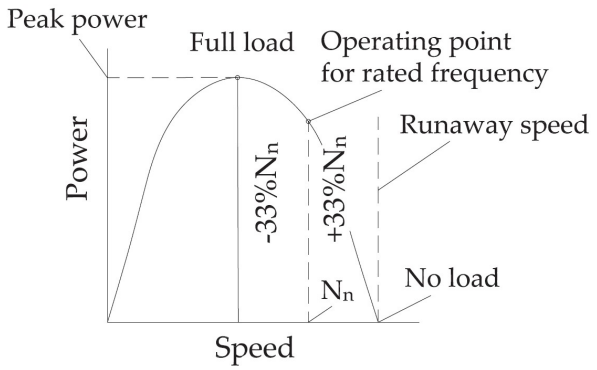

Figure 2.11: The operation point for the operation at the back side principle[17]

Previous experimental study at UNB GAMA-Brasilia with this principle on the 4" Indalma turbine indicated that the turbine has a self-regulating capacity in terms of frequency of 15% and in terms of power of 30%. This means that the turbine can handle a 15% fluctuation in frequency and a 30% fluctuation in power. In shaft power output the self-regulating capacity was between -23.4% and + 4.8%. Therefore between these intervals the turbine operates in stable conditions (see Figure 2.12) [29]. Note the overall curve can be neglected between these intervals. In de above described stable condition (interval between de redlines of Figure 2.12) the relation between power and speed is linear.

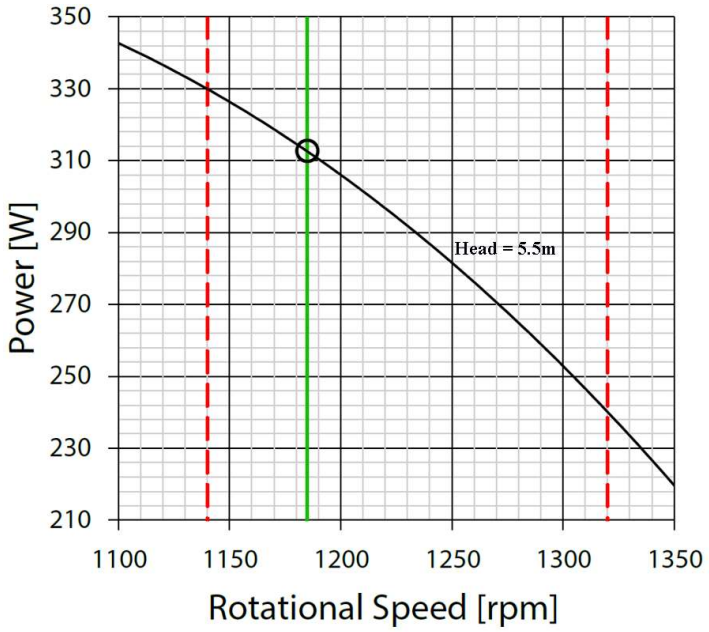

Figure 2.12: Indalma operation point and regulating ranges (H=5.5m) [29]

2.4.2 Flow control

The main controller of the hydraulic turbine is the governor, which varies the water flow through the turbine to control its speed or power output. Generator speed and system frequency may be adjusted by the governor. Governing system as per IEEE standard 75 (includes the following: (a) Speed sensing elements, (b) Governor control actuators, (c) Hydraulic pressure supply system and (d) Turbine control servomotors, which are normally supplied as part of the turbine. Figure 2.13 illustrates a typical block diagram of the Governor system.

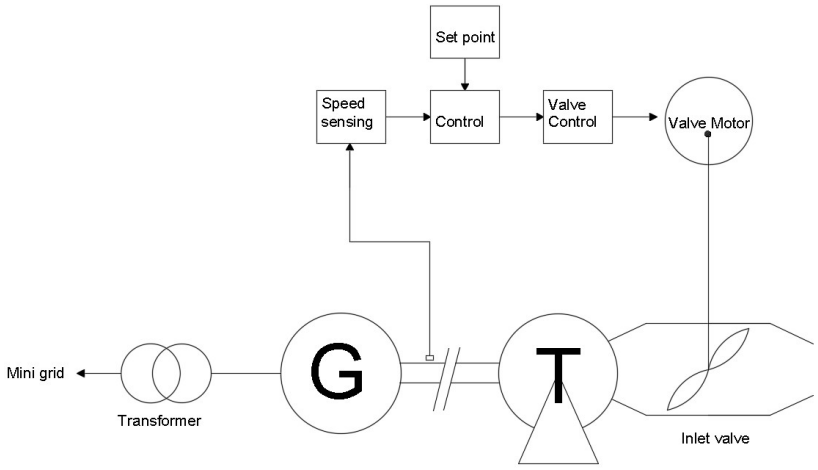

Figure 2.13: Typical block diagram of the Governor system

Governor control systems for hydro turbines are basically a feedback control, which senses the speed and power of the generator or the water level of the fore bay of the hydroelectric installation, etc. and in accordance with the deviation of the actual set point from the reference point, it takes actions by operating the discharge/load controlling devices. The control section may be mechanical, analog electronic or digital electronic. The actuator is a component of the control system that acts upon an environment and responds by converting the energy into mechanical motion. This can either be opening or closing the water inlet to the turbine. However, for Micro and smaller hydropower plants the flow control method is not a suitable option due to the high capital cost. The reason for the high capital cost is due to the extra infrastructure needed for the valve that will control the flow to the turbine and the control system which should be robust.

2.4.3 Load control

An alternative to the above mentioned methods is the load or shunt load governor (SLG). For Pico- and Micro hydro systems this load control method can save about 40% on capital cost as it requires no extra electromechanical components to control the inlet valve [36]. With the SLG based system the input to turbine is kept constant, which means that energy production also remains constant. To balance out the production and demand, an additional dump load is connected at generator terminal. In most cases a resistor bank is used as a dump load, which is controlled by an analog, electronic or microprocessor based electronic circuit. This circuit switches the dump

loads according to the grid load in such a manner that the total load on generator terminal (dump load plus grid load) remains constant. When designed correctly the generator will operate at its optimal operation point, thus keeping the speed (frequency) variation within the specified limits. Since there is no extra stress on the generator and turbine this system is robust and needs almost no maintenance. Disadvantage of this control system is the waste of the extra (surplus) energy, which is dissipated in the dump loads and therefore this control system is only recommended for Micro and smaller hydropower plants [36]. Figure 2.14 illustrates the shunt load governor principle, which will be used in the design of the control system for the Pico/Micro hydropower plant.

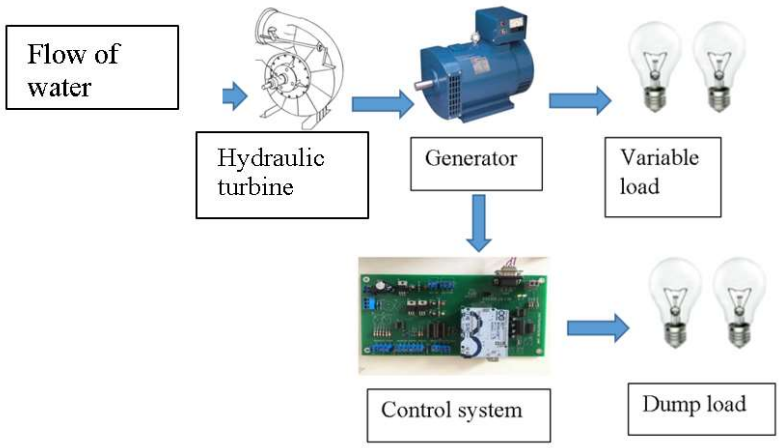

Figure 2.14: Shunt load governor principle [36]

In the next section an example of a load control system is presented

2.4.4 Gran Holo control system

The Gran Holo micro hydropower plant has a 150 kW Permanent Magnet Brushless Generator, which is directly connected through a shaft and gear box to the S-type hydro turbine. The Gran Holo micro hydropower plant is designed to operate at a hydraulic head (H) between 2-6 meters. The minimum flowrate is 15 m^3/s and its maximum is 50 m^3/s [37]. Figure 2.15 shows the Gran Holo hydropower plant during dry and rainy season, whereas Figure 2.16 gives a sketch of the power house of Gran Holo. Figure 2.17 shows the installed turbine, gearbox and generator. Note that here the same principle applies as discussed in Figure 2.9.

(a) (b)

Figure 2.15: Gran Holo hydropower plant in the dry season (a) and rainy season (b)

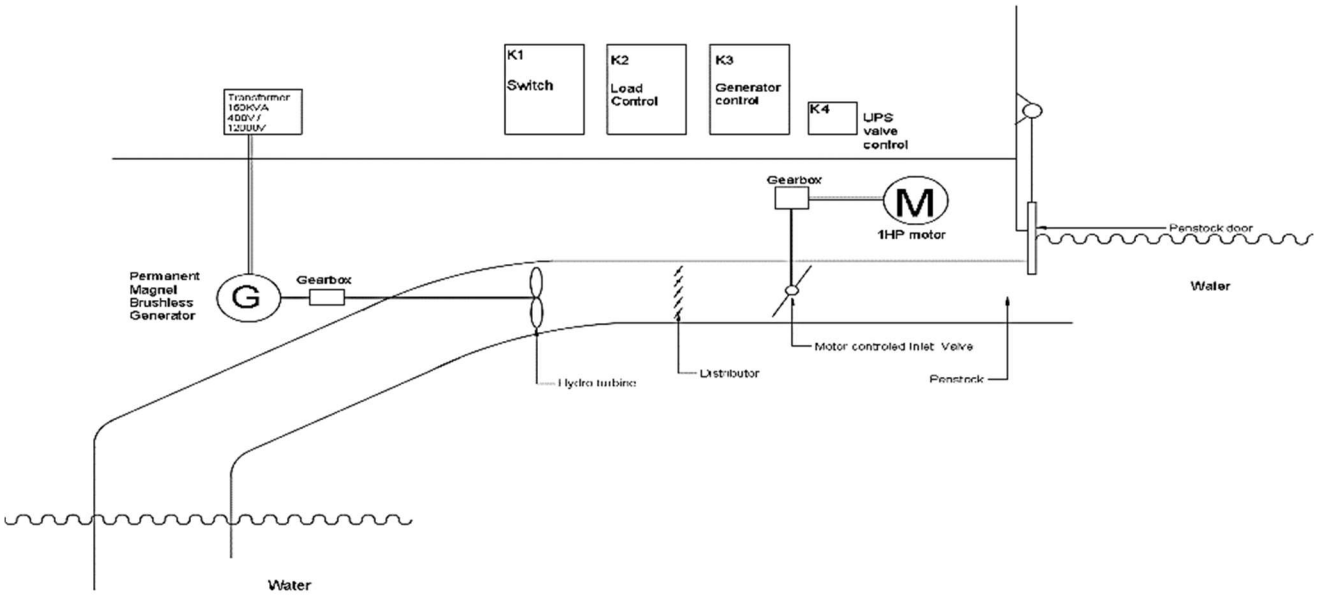

Figure 2.16: Gran Holo powerhouse sketch

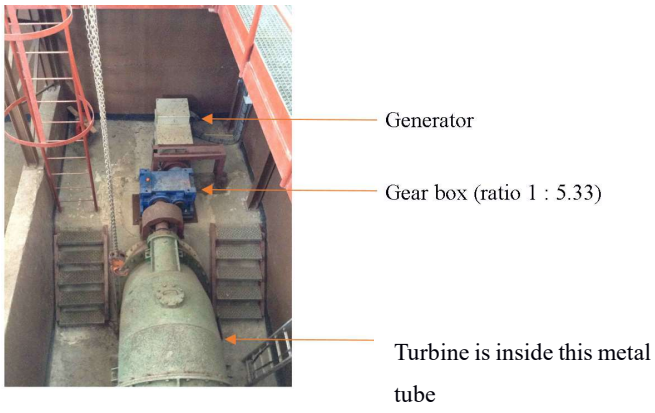

Figure 2.17: Gran Holo turbine, gear box and generator [15]

The control system of Gran Holo micro hydropower plant is based on a variable load dissipation (load controlled) to keep the load on the generator constant, regardless to the change in load on the transmission line[1]. The system principal is based on comparing the RPM of the turbine shaft, line voltage, current and frequency at the generator side, with the reference values for each of these parameters. If there is a positive difference the control system connects more resistive dump loads to the grid and if there is a negative difference the control system connects less resistive dump loads to the grid. Thus the generator generates at maximum power and the control system controls the power flow to the dump load and transmission line. Figure 2.18 gives an overview of the Gran Holo hydropower system [15].

[1] These findings or done based on reports off studies done by the EBS and R. van Els [14][15].

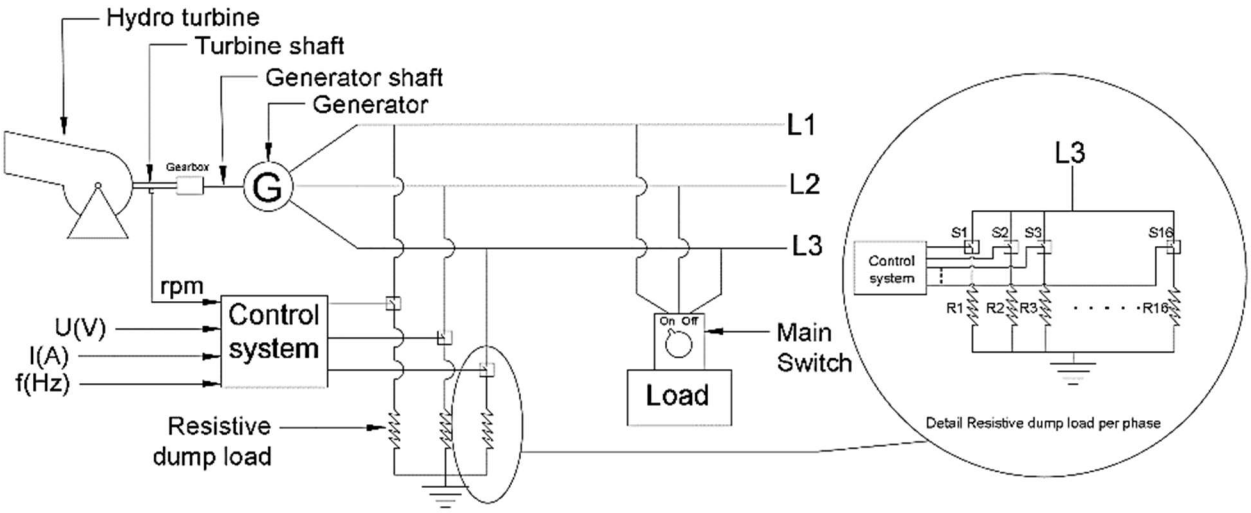

Figure 2.18: Gran Holo hydropower system

The brain of the control system is a PLC (Programmable Logic Controller). This PLC receives input data from the switch unit, load controller and valve controller. Besides receiving data it also controls the switch unit, load controller and valve controller. The function of the switch unit is to turn the power supply to the villages on or off. The load controller, controls the amount of resistive dump loads which are connected to the generator, to dissipate the surplus energy. The amount of resistive dump loads is switched "on" or "off" with relays.

This control system is constructed using 5 load ballast banks (dump loads). If assumed that they are connected on the 400V grid of the generator then the dump loads could dissipate a maximum of 110 kW. These dump loads are controlled by the PLC, which is located in the generator control unit. This PLC controls 41 switching circuits (using relays) through 2 opto-isolator boards that most probably connect the individual dump load circuits to the generator control unit [15].

2.5 Dump load controller

For dump load controllers there have been some research done already. Some of them are also made for micro hydropower. This section will shine some light on two different dump load control models designed for micro hydropower plants.

In India 2015 three Electrical engineers designed an electronic based dump load controller for grid isolated asynchronous generator. The dump load controller was designed using a rectifier in combination with an IGBT as chopper switch, a capacitor and a DC dump load resistance. This controller operates on voltage and frequency changes, whereby these changes control the firing angle to the IGBT. Thus, controlling the amount of energy that is consumed in the dump load. Figure 2.19 presents this designed dump load controller [38].

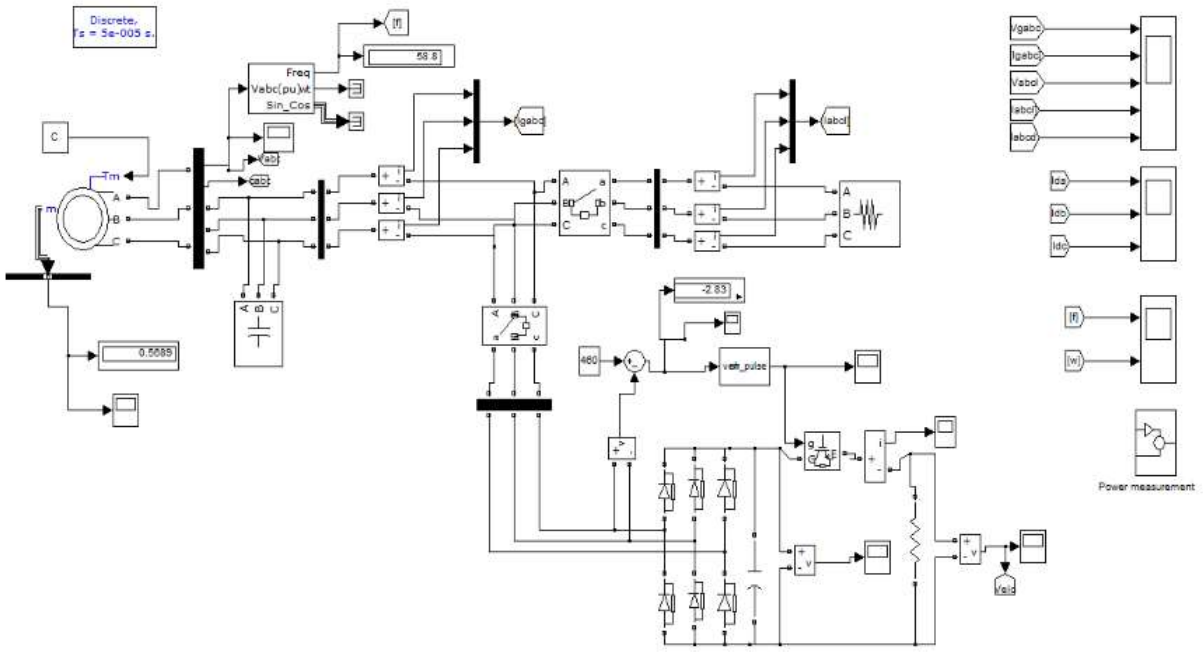

Figure 2.19: Simulink model of electronic based dump load controller

In Nepal 2016, Gyawali N designed an electronic load controller (ELC) for a micro hydropower plant. This ELC scheme consist of an Active Power Filter (APF) and DC chopper, which gives the ELC the ability to overcome issues from the effects of reactive power, harmonic current and unbalanced current in load. Gyawali claims that "The ELC model incorporates an IGBT based VSC with three-phase four-wire topology . It operates on current controlled mode with center-tapped neutral wire to provide the path for the neutral current. Besides, the ELC also includes a DC chopper to deviate controlled current through the dump load connected at the DC bus." Figure 2.20 presents the ELC model of Gyawali N [39].

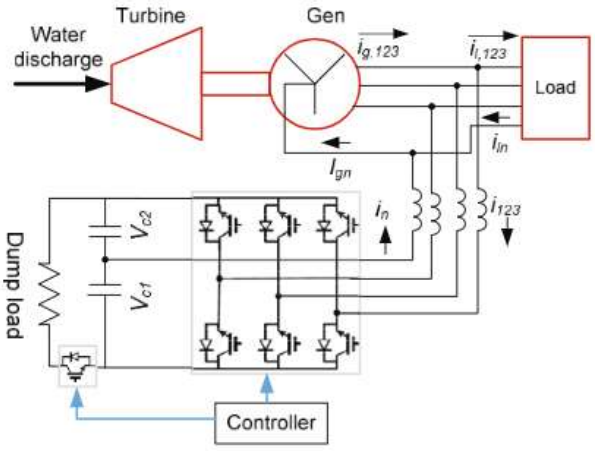

Figure 2.20: Electronic load controller model

2.6 Demand side management

Demand side management (DSM) is an approach to balance out the production and the demand of energy. Previous studies have shown how effective this method is for peak shaving, also known as load shedding [40] [41]. In general DSM is done to lower the peak load by switching off certain loads in a smart grid. Examples of the loads that could be switched off using DSM in a smart grid are swimming pool pumps, washing machines, charging of electrical vehicles, etc. [42] DSM have a 10 times faster response time than generators, which is proven by researchers in Australia in 2008 [40]. DSM could be used in different ways [43]. In this study the DSM function can be seen in the dump load controller, whereby its function is to balance the dump load and actual load on the system.

3 Research test setup

This chapter presents the research test setup that was built in the energy laboratory of the AdeKUS to simulate the functioning of Indalma turbine in a specific operation point and its interaction with the proposed load controller. Since there is neither water circuit nor Indalma turbine in the energy laboratory, an experimental setup was designed to emulate the turbine characteristics with a Variable Frequency Driver (VFD) and electric induction motor controlled by a special external circuit board. This configuration was adapted from other researches with wind turbines where the behavior of these turbines was simulated with VFD and electric motors. [44][45][46]. In this method of simulating the turbine characteristic with the VFD and motor can be used for a wide speed range. The setup was adapted to simulate the operation of the Indalma turbine in a specific operation point through a lookup table implemented by the external circuit board coupled to the generator and the proposed load controller as show in Figure 3.1. How the characteristics of the turbine are simulated using VFD and motor is discussed later in the virtual Indalma sub section.

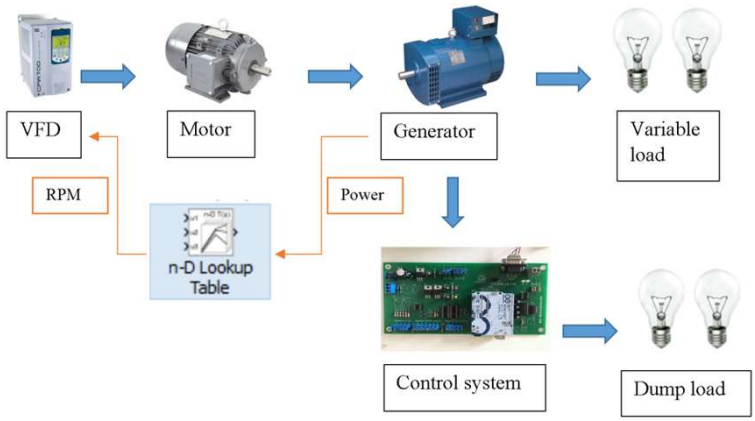

Figure 3.1: The research setup overview

This research test setup was built using the available VFD, motor and generator at that time presented in Table 3.1.

Table 3.1: Specification of the available VFD, motor and generator data

	VFD	Motor	Generator
Power	1.125 – 112.5 kW[2]	2.2 kW	5 kW
Voltage input	380 – 480 V	220 V	X
Voltage output	220 – 480 V	X	220 V
RPM	X	1700	1800
Frequency	Input frequency = 50 / 60 Hz Output frequency = 0 – 300 Hz	50 Hz	60 Hz

Note that the control system used in this research test setup is based on a combination of two (2) methods. The load control principle in combination with the operation on the back side of the curve principle. By doing so the control system will cost less due to less complexity of the controller and the Pico - or Micro hydropower system will be more robust. Its advantage above the operation on the back side of the curve principle would be that the operation point can be chosen closer to the peak power, thus generating more electrical energy at a more stable frequency.

3.1 Indalma turbine characteristics

There are measurements of two Indalma turbines done in previous studies. Figure 3.2 illustrates the RPM versus power curve of a 4" Indalma turbine at the hydropower laboratory of the University of Brasilia (UNB)[29]. Figure 3.3 shows the RPM versus power curve of the 6" Indalma turbine measured at the hydraulic laboratory at AdeKUS [47]. In the second figure the polynomial in red is the fitted curve through the measured points. From this fitted curve the

[2] Note that the VFD manual (WEG700) used HP as unit for power. For the conversion from HP to kW in this thesis the following is used: 1 HP = 750 W = 0.75 kW.

maximum mechanical power, measured using a Prony brake, is 1714 W at an RPM value of 624. The fitted curve equation is $y = -0.0044x^2 + 5.4923x$ and has an accuracy of 90.57 %. Comparing Figure 3.2 and Figure 3.3 it is noticeable that the forms of the fitted curves are identical. It's also noticeable that the measured points of the 4" turbine fit better to the curve, this is due to the more accurate measuring system used in UNB. Measurements were done using a digital acquisition system [29]. At AdeKUS measurements were done with analog instrumentation [47].

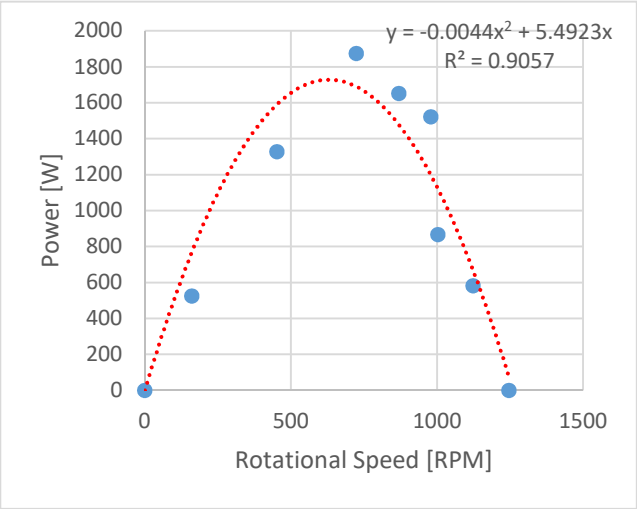

Figure 3.3: Power vs RPM curve of the 6" Indalma turbine [47]

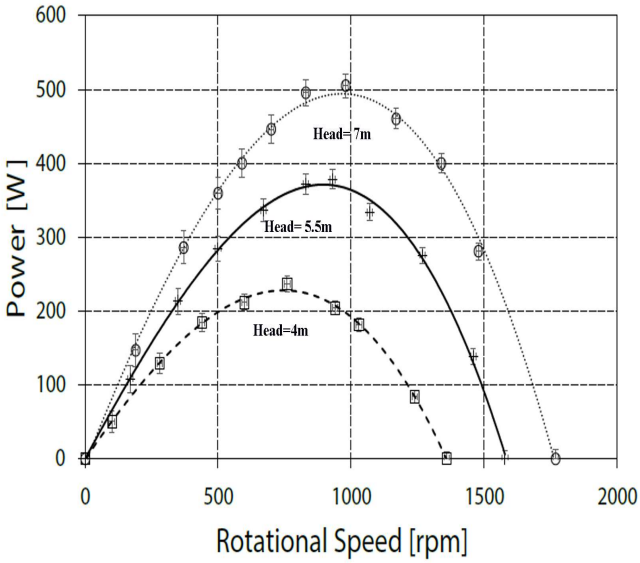

Figure 3.2: Power vs RPM curve of the 4" Indalma turbine [29]

Using one of the affinity laws (see Equation 3) the power versus RPM curve of the 6" turbine can be theoretically derived from the data of the 4"turbine [30]. Since the flow and rotational speed are assumed to be constant, Equation 3 can be simplified to equation 4 [48]. This theoretical power versus RPM curve is presented in Figure 3.4.

$$P = f_6[\frac{Q}{ND^3}] \quad [3]$$

Whereby P = power, f_6 = the function of the form attained by experiments, Q = flow, N = rotational speed and D = input diameter.

$$P_{6"} = P_{4"}[\frac{D_{6"}}{D_{4"}}]^3 \quad [4]$$

Whereby $P_{6"}$ and $P_{4"}$ = power of respectively 6" and 4" turbine. $D_{6"}$ and $D_{4"}$ = input diameter of respectively the 6" and 4" turbine.

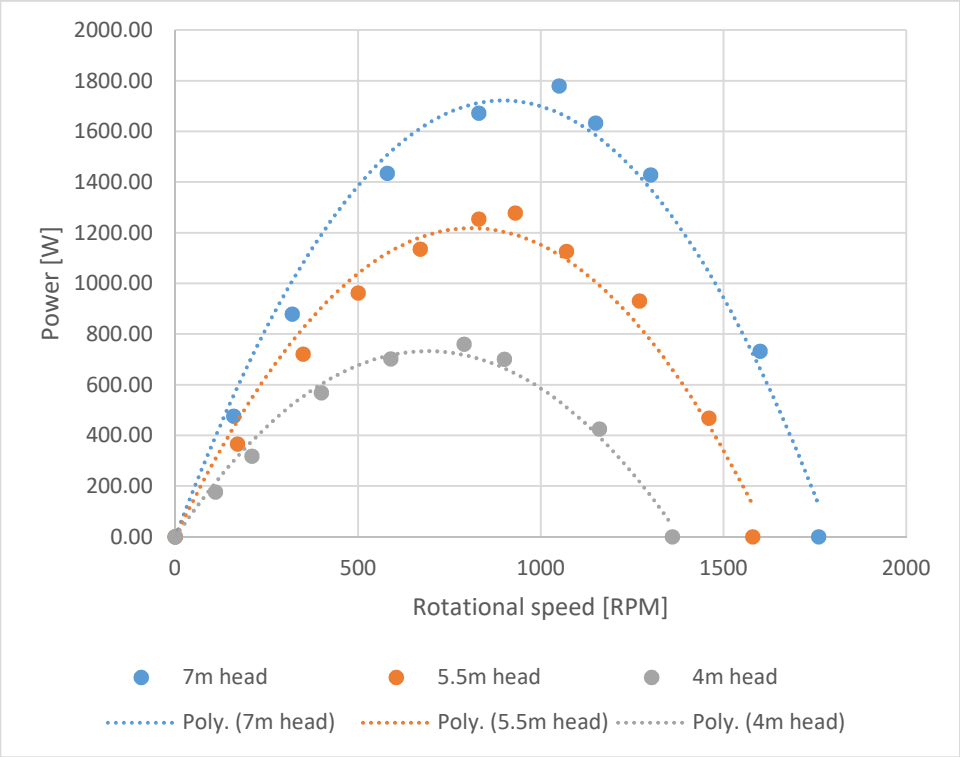

Figure 3.4: Theoretical power vs RPM curve of the 6" Indalma turbine

In Figure 3.5 the theoretical and measured data of the Indalma turbine are plotted. If the theoretical power vs RPM curve of the 6" Indalma turbine is compared to the measured power vs RPM curve, the following can be concluded:

1. The measured data reaches maximum power at a lower RPM;
2. The measured data works in a RPM range of 0 – 1246 and the highest power (1874 W) measured is at 723 RPM;
3. The measured data fits the theoretical curve of 7 m better than the two other theoretical curves;
4. The RPM measurements for the runaway speed from the experimental – and theoretical data differ more than 30% from each other. This difference could be related to the measuring systems used during the experiments (4" and 6" turbine).

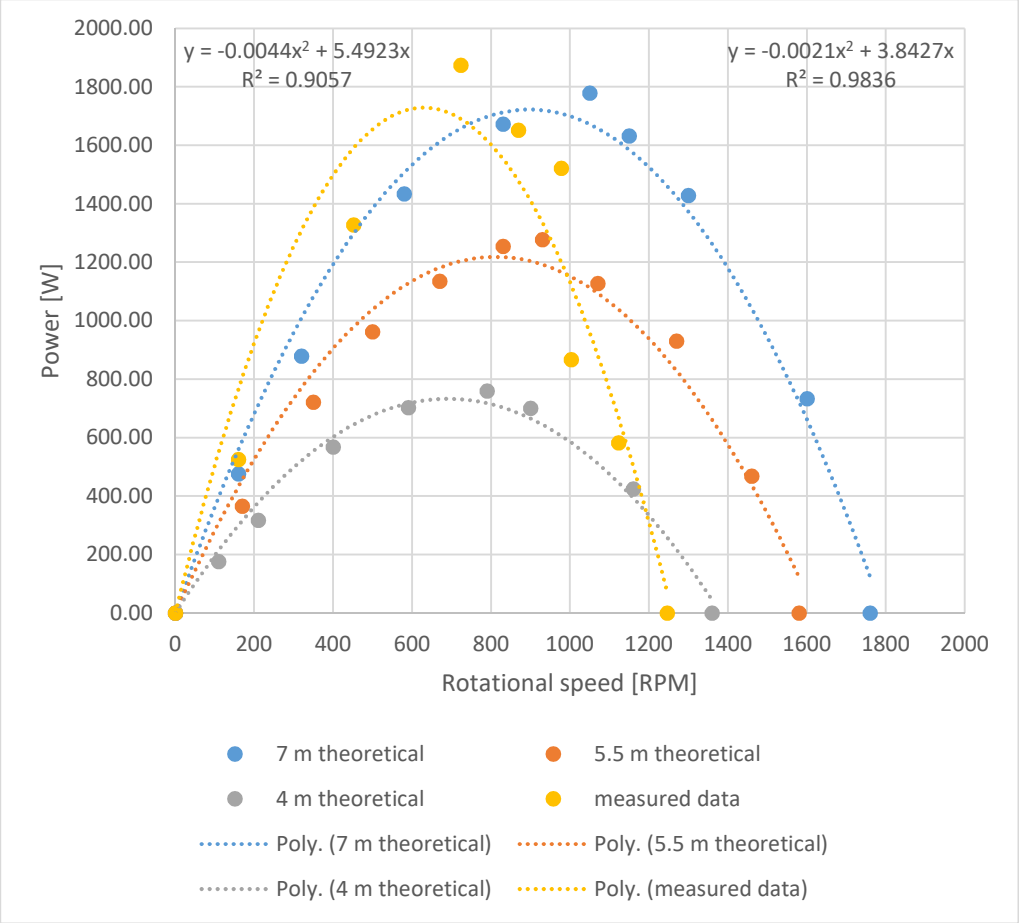

Figure 3.5: Different power vs RPM curves for the 6" Indalma turbine

3.2 Virtual 6" Indalma turbine

There is no 6" Indalma turbine in the research test setup, but since the characteristics are known this can be simulated using a VFD and motor. Several studies have proven this for more sofisticated applicatioins then the application used in this research [44][45][46]. A virtual 6" Indalma turbine can be implemented by using the Power-RPM curve and this was done by using an Arduino micrcontroller controlling the speed of the motor through the VFD. The arduino measures the RPM, current and voltage of the generator and sends an analog reference signal through its digital analog converter (PWM) output to the VFD as shown in Figure 3.6.

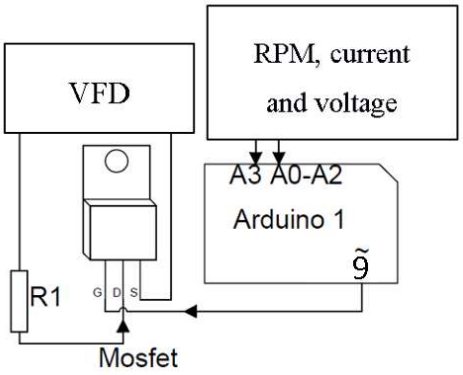

Figure 3.6: VFD speed control using Arduino

The analog reference signal is implemented with the Arduino PWM output (Pin 9) connected to the gate of a IRF630 MOSFET(see Figure 3.6). The drain of this MOSFET is connected to the 24 V DC supply of the VFD through a 10 kΩ resistor. The source of this MOSFET is connected to the analog reference input on the VFD (0 - 10 V). Note that signal passes through a low pass filter, which is built inside of the VFD to filter out higher harmonics. The analog reference input voltage range (0 - 10V) corresponds to a RPM range 0 – 100 % of the maximum RPM set point value (must be programmed into the VFD). The arduino calculates the power output of the generator using its measured current and voltage, and determines the speed of the turbine through the adjusted Power-RPM fucntion. As mentioned above in the sub section 2.4.1. The working area (interval for stable condition) can be considered a linear relation. This is used to implement the virtual Indalma principle.

The operational point (OP) of the 7m calculated data is at an RPM value of 1320 (as shown in Figure 3.7). The working area lies between the RPM values of 1254 and 1379 (area between orange lines of Figure 3.7), which corresponds to a frequency change of respectively – 5 % and + 10 %. This can easily be calculated since the change in RPM is proportional to the change in frequency. Between these intervals the power varies between 1305 and 1516 W.

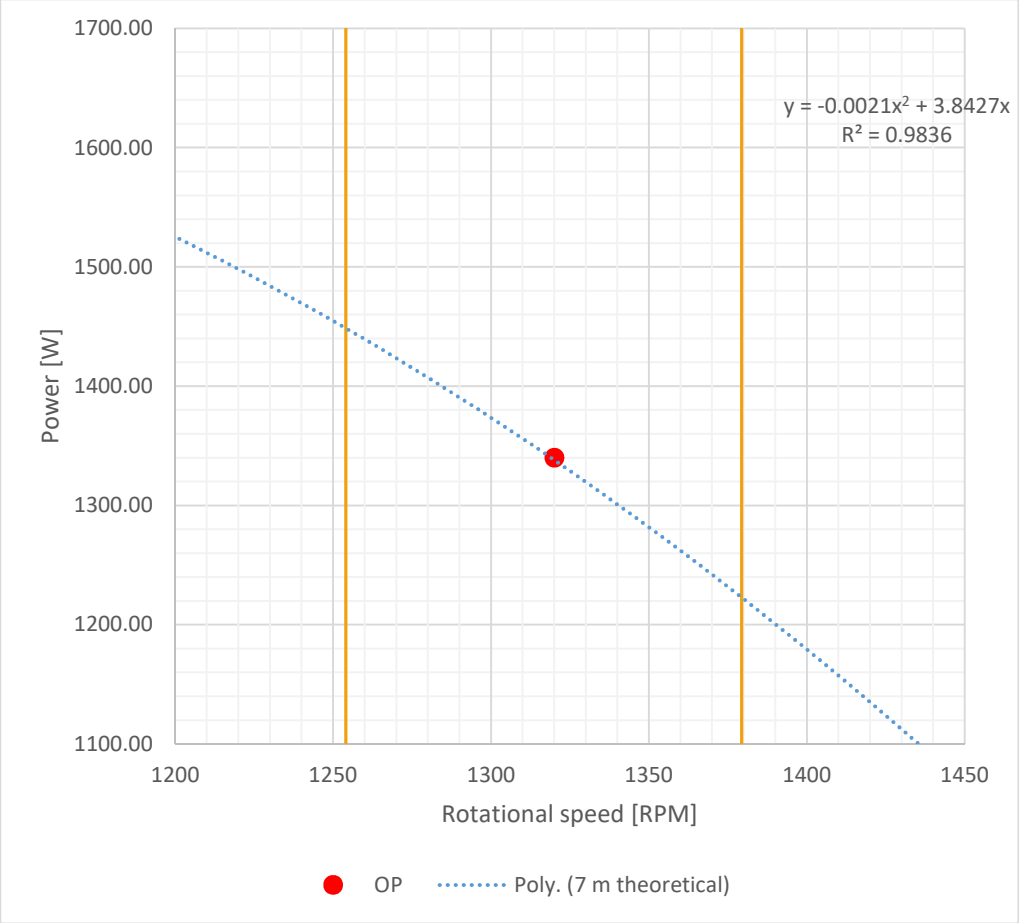

Figure 3.7: 7 m calculated data zoomed in at OP

To control the speed of the motor-generator set with a PWM signal, the curve for the PWM-RPM is needed to determine the RPM as a function of the PWM. Therefore measurements were done for different PWM values and the RPM was measured as shown in Figure 3.8. The PWM and RPM are related to each other as a lineair function (Equation 5 and 6).

$$PWM = -0.1412RPM + 246.77 \quad [5]$$

$$RPM = 7.0822PWM - 1747.66 \quad [6]$$

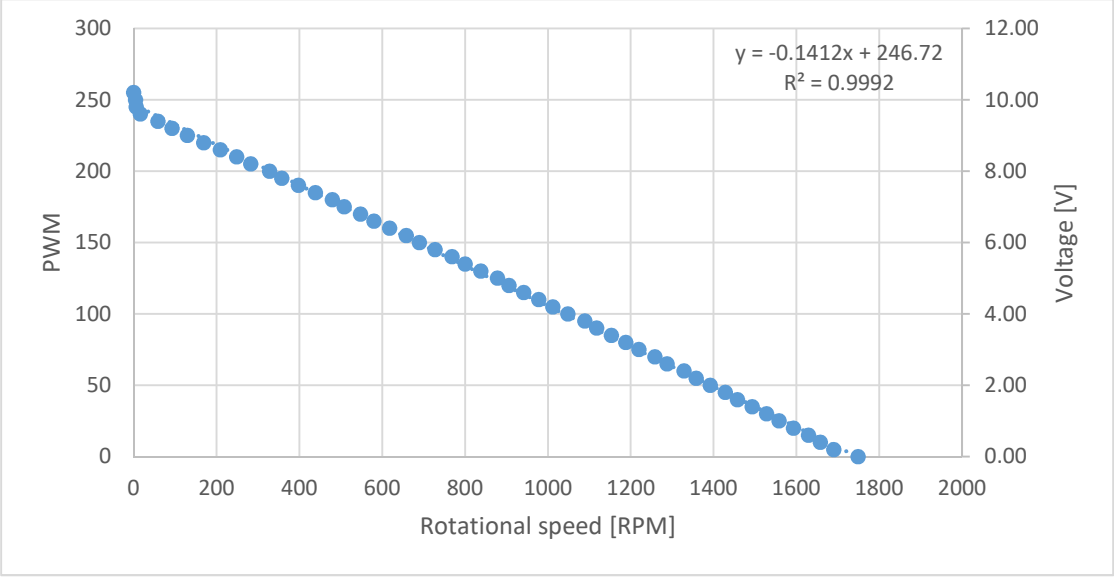

Figure 3.8: PWM-RPM curve

3.3 Dump load control method

In order to design the dump load control system, the motor-generator performance was measured under different loads. This was done by connecting the motor directly to the electric grid and placing different loads at the generator terminals. During the measurements at different loads the nominal speed (1800 RPM) of the generator could not be reached due to the fact that the motor was rated 1700 RPM. The loads were created using a combination of incandescent light bulbs of 15, 40, 60, 75 and 100W. The load varied from 0 – 1425 W, whereby the maximum voltage drop measured between line and neutral was 48.2 V and frequency drop was 11.86 Hz (20%). The results of these measurements are presented in Table 3.2, whereby the power (Power (W)) is calculated using voltage and current measured at the generator terminals and the total power (Load (W)) is the load connected on the generator.

Table 3.2: Generator performance under different loads

Generator measurement						load (light bulbs)				
U (V)	**I (A)**	**Power (W)**	**f(Hz)**	**RPM**	**Load (W)**	**15 W**	**40W**	**60W**	**75W**	**100W**
131.0	0.0	0.0	58.11	1743.3	0					0
130.3	0.1	13.0	58.09	1742.7	15	1				0
129.7	0.3	38.9	58.08	1742.4	40		1			0
129.3	0.4	51.7	58.09	1742.7	60			1		0
128.9	0.6	77.3	58.08	1742.4	75				1	0
128.2	0.8	102.6	58.07	1742.1	100					1

127.8	1.0	127.8	58.06	1741.8	115	1				1
127.4	1.1	140.1	58.05	1741.5	140		1			1
127.0	1.3	165.1	58.05	1741.5	160			1		1
126.8	1.4	177.5	58.05	1741.5	175				1	1
126.2	1.7	214.5	58.03	1740.9	200					2
126.0	1.9	239.4	58.04	1741.2	215	1				2
125.6	2.1	263.8	58.02	1740.6	240		1			2
125.3	2.2	275.7	58.01	1740.3	260			1		2
125.1	2.3	287.7	57.99	1739.7	275				1	2
125.1	2.3	287.7	57.99	1739.7	300					3
125.0	2.4	300.0	57.99	1739.7	315	1				3
124.6	2.6	324.0	57.99	1739.7	340		1			3
124.4	2.7	335.9	57.99	1739.7	360			1		3
124.2	2.9	360.2	57.97	1739.1	375				1	3
123.8	3.1	383.8	57.98	1739.4	400					4
123.7	3.3	408.2	57.97	1739.1	415	1				4
123.3	3.5	431.6	57.95	1738.5	440		1			4
123.1	3.6	443.2	57.94	1738.2	460			1		4
122.9	3.7	454.7	57.93	1737.9	475				1	4
123.1	3.9	480.1	57.93	1737.9	500					5
122.8	4.0	491.2	57.97	1739.1	515	1				5
122.6	4.1	502.7	57.95	1738.5	540		1			5
122.3	4.3	525.9	57.93	1737.9	560			1		5
122.1	4.4	537.2	57.92	1737.6	575				1	5
124.6	4.7	585.6	58	1740.0	600					6
123.8	4.8	594.2	58	1740.0	615	1				6
123.1	4.9	603.2	57.98	1739.4	640		1			6
121.1	5.0	605.5	57.89	1736.7	700					7
122.4	5.1	624.2	57.96	1738.8	660			1		6
122.1	5.3	647.1	57.94	1738.2	675				1	6
121.3	5.3	642.9	57.91	1737.3	715	1				7
120.7	5.5	663.9	57.87	1736.1	740		1			7
120.4	5.5	662.2	57.85	1735.5	775				1	7
120.1	5.7	684.6	57.86	1735.8	800					8
120.0	5.7	684.0	57.85	1735.5	815	1				8
120.5	5.8	698.9	57.86	1735.8	760			1		7
119.7	5.9	706.2	57.87	1736.1	840		1			8
119.4	6.0	716.4	57.84	1735.2	860			1		8
119.2	6.1	727.1	57.85	1735.5	875				1	8
118.7	6.4	759.7	57.8	1734.0	900					9
118.2	6.7	791.9	57.79	1733.7	940		1			9
118.1	6.9	814.9	57.82	1734.6	960			1		9
117.8	7.0	824.6	57.81	1734.3	975				1	9
117.3	7.4	868.0	57.76	1732.8	1000					10
112.3	7.9	887.17	55.87	1688	975	3	3	1	2	6

108.9	8.2	892.98	54.28	1649	1070	1	3	1	1	8
110.1	8.4	924.84	54.89	1658	1075	3	3	1	2	7
102	8.8	897.6	52.55	1592	1170	1	3	1	1	9
99.4	8.9	884.66	51.48	1556	1175	3	3	1	2	8
97.9	9	881.1	51.12	1552	1245	1	3	1	2	9
94.2	9.3	876.06	49.87	1510	1285	1	4	1	2	9
82.8	8.7	720.4	46.25	1505	1425	1	6	2	2	9

Figure 3.9 shows the measured frequency versus load (incandescent light bulbs, data from Table 3.2). One of the objectives is to keep the frequency within a -5% to +10% margin from the base line. If the base line is chosen to be 60 Hz, then the frequency should be between 57 and 66 Hz. This range is given in the same figure as the orange lines. Note that the current measured values for the motor-generator test setup never surpass 58.11 Hz, this is due to the undersized motor. From this figure it is clear that above a load of 975 W the frequency is not within the objective range.

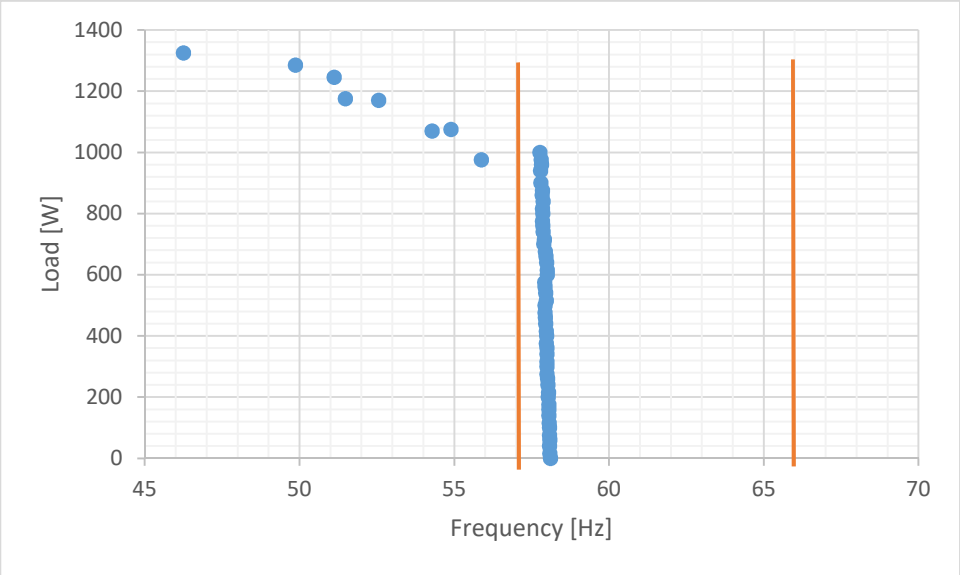

Figure 3.9: Frequency of the motor-generator setup at different loads

Figure 3.10 shows the measured voltage vs load (incandescent light bulbs, data from Table 3.2). Another objective of this research is to keep the voltage within a -10% to +10% margin from the base line. If the base line is chosen to be 127 V, then the voltage should be between 104.3 and 139.7 V. This range is given in the same figure as the orange lines. From the figure it is clear that above a load of 1170 W the voltage is not within the objective range.

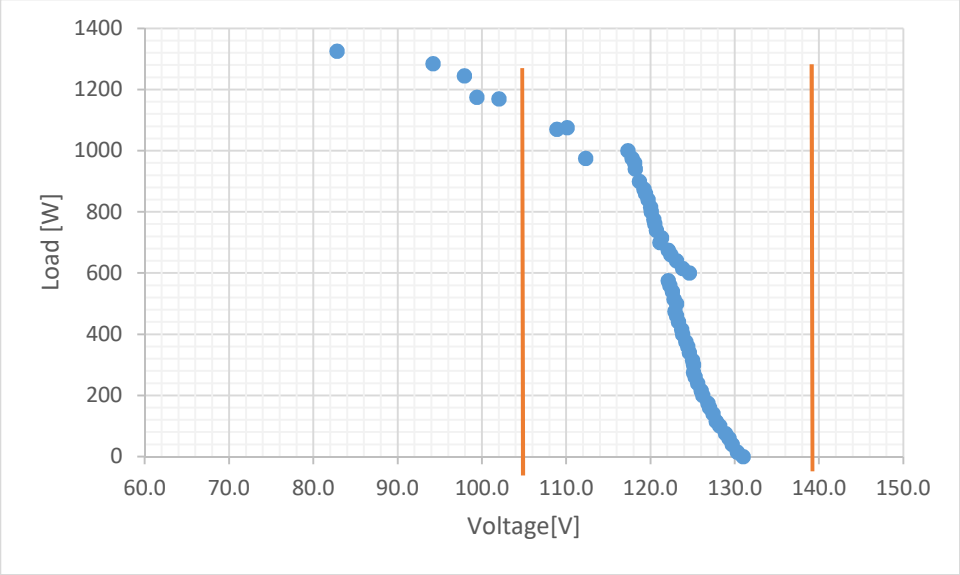

Figure 3.10: Voltage of the motor-generator setup at different loads

Thus, keeping in mind that the turbine characteristics should still be implemented it would be wise to choose a main load that is lower than 975 W. Therefore, the maximum main load is set to be 800 W. The variable dump load controller will be designed for a maximum of 800W as the maximum power it can handle. During experiments this value will never be exceeded.

To control the variable dump loads there are different kinds of techniques; PWM, PSK (Phase Shift Keying), relays, etc. This control system is based on relays, which is done to keep the control system as similar as possible to Gran Holo hydropower plant. A suitable AC dump load is the use of multiple incandescent light bulbs, with rating 127V 100W. This ensures a suitable dump load step range, which is increased or decreased by a step of 100W. The 100W step was chosen due to the limited relays (8 available relays).

The schematics of the designed and implemented dump load control system is illustrated in Figure 3.11. The main components used to design this control system are:

- Arduino Uno R3
- Current sensors (measures the RMS)
- Voltage sensor (measures the RMS)
- RPM sensor

- Incandescent light bulbs

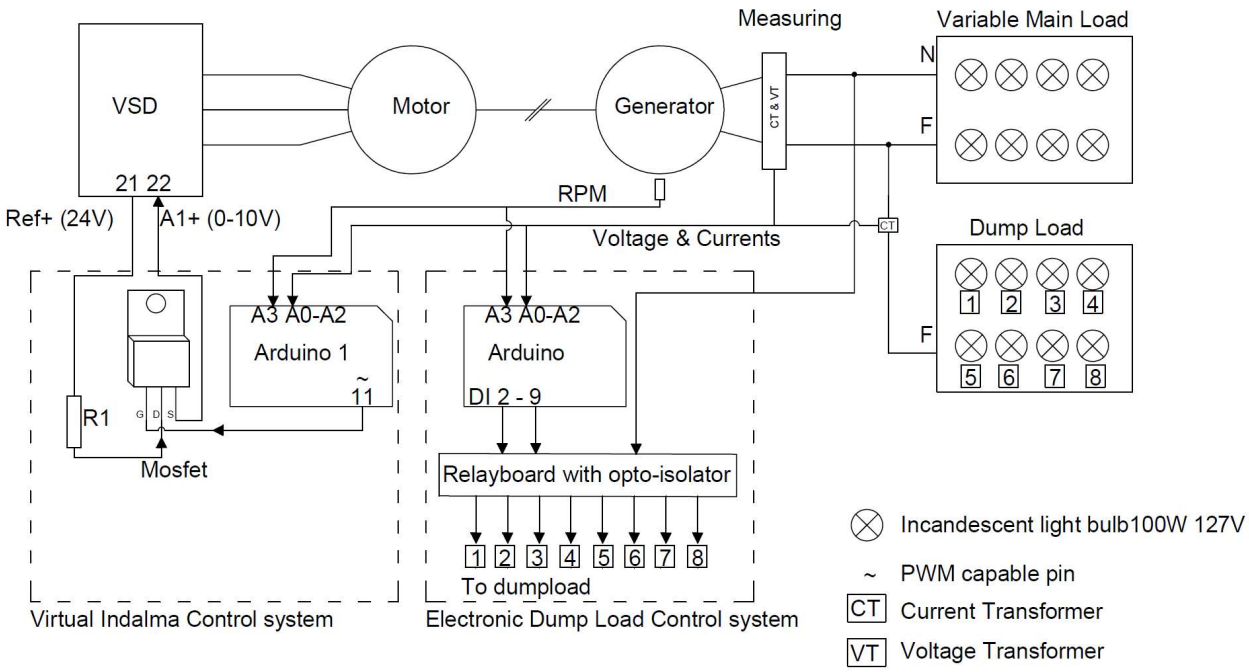

Figure 3.11: Schematic overview control system

Figure 3.12 illustrates the control system which was built during this research. In Figure 3.13 the control system proto type circuit board is shown. This circuit board is Arduino driven. The sensors provide data input for the Arduino, which in turn controls the dump load steps and VFD accordingly.

Figure 3.12: Dump load control system (from different angles)

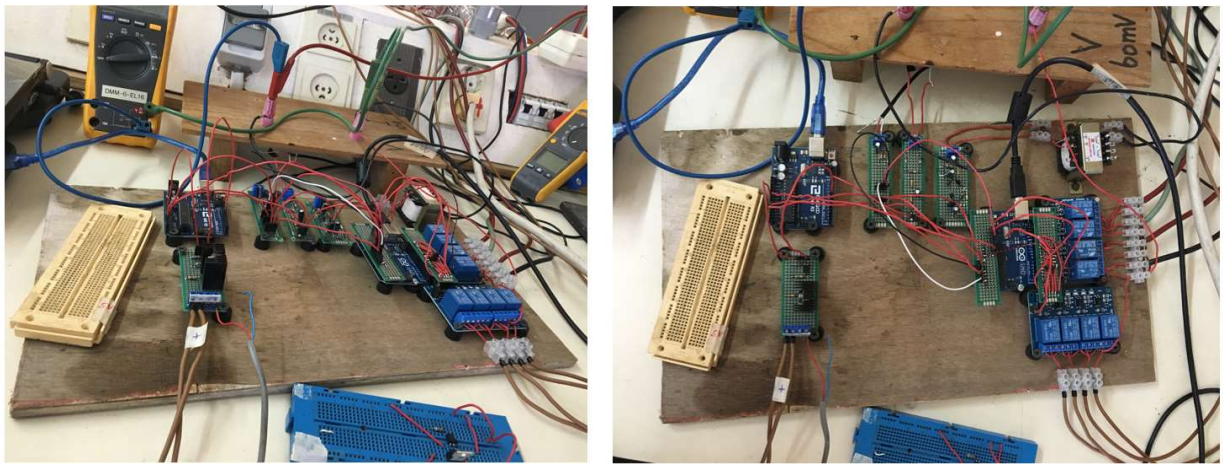

Figure 3.13: Dump load control proto type circuit board

4 Hardware and software implementation

This chapter presents the hardware and software implementation of the experimental setup. The control hardware is made using two Arduino Uno R3 microcontrollers. These microcontrollers are programmed using its own software, known as Arduino IDE. The version used is 1.8.5 and programming language is based on C++. Note that there are two hardware's made. The first is the dump load controller and the second is the virtual Indalma turbine. These hardware work independently, regardless of some of the inputs that they have in common.

Figure 4.1 illustrates an overview of this dump load control system. First the microcontroller reads the values of the RPM-, voltage- and current sensors. According to the programming code the Arduino then turns the dump load on or off, using switching modules.

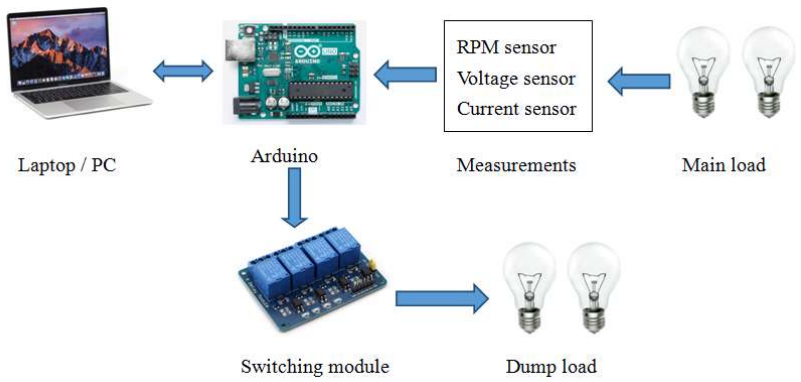

Figure 4.1: Dump load control system overview

Figure 4.2 illustrates an overview of the virtual Indalma turbine system. The microcontroller reads the values of the voltage- and current sensors. According to the programming code the Arduino then calculates the desired RPM value according to the RPM-power linear relation of **Error! Reference source not found.**.

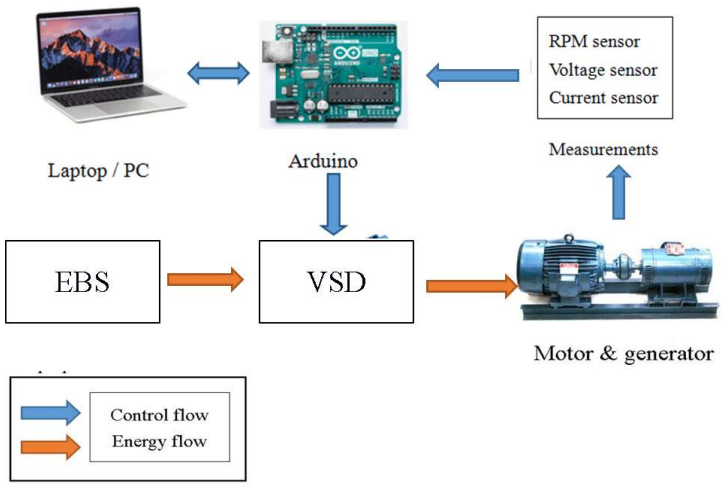

Figure 4.2: Virtual Indalma overview

4.1 Suitable dump load and dump load on/off switching

To build this control hardware there are two options to switch on the dump load, make use of power MOSFETS or use relays. Since the objectives is to keep the control system as similar as possible similar as Gran Holo hydropower plant relays will be used. The relay module, which is used has 4 channels and is Arduino compatible, as shown in Figure 4.3. The module is equipped with 4 high current relays (series number: SRD-05VDC-SL-C) rated: 250V AC 10A or 30V DC 10A [49].

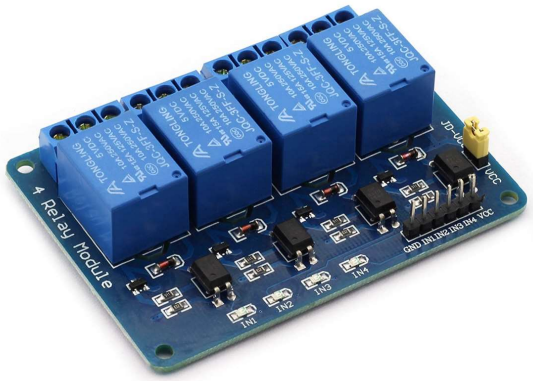

Figure 4.3: Arduino compatible relay module

4.2 RPM measurement

The RPM is measured using an inductive proximity sensor, which is programmed as an "on" or "off" switch. The sensor is installed in such a way that it detects the metal axis of the generator and when the key way passes through the sensor, the sensor becomes inactive, as shown in Figure 4.4. When this happens an interrupt function is triggered in the Arduino code. One full rotation of the axis gives two interrupts. By measuring the time between two interrupts, the RPM can be calculated using

$$RPM = \frac{1\,min}{\Delta t} \quad [7]$$

Since the time Δt in Equation 7 is measured in microseconds the 1 min is also transformed to microseconds. With the use of interrupt function in the Arduino code the time between "on" and "off" of the RPM sensor was used to determine the RPM. During the experiments the results for the RPM were flickering, probably noise or magnetic interference from the motor. To reduce this a debounce filter was used in combination with an average function, which takes 30 measurements and gives an average RPM value. This solved the issue at hand.

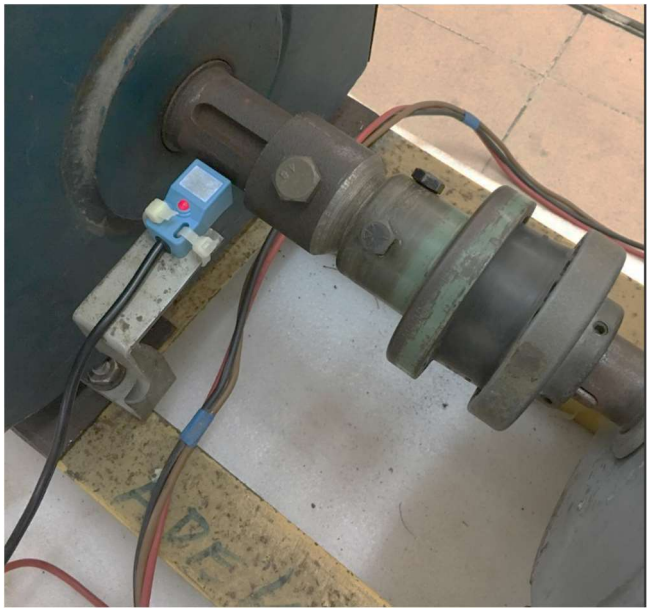

Figure 4.4: Inductive proximity sensor mounted on the Genset

4.3 Voltage measurement

The line-neutral voltage measurement system was designed to range 0 – 150V AC using a voltage divider to translate the measured voltage to a 0-5V DC signal, which is then processed by the Arduino (see Figure 4.7). The system was implemented with a transformer and a bridge rectifier. The voltage is measured at the generator terminals. During measurements the voltage between line-neutral had some noise in it. To reduce or filter this noise a bandpass filter was designed.

4.3.1 Bandpass Filter design

The bandpass filter is a combination of a high pass filter and a low pass filter, which only allows a frequency signal between certain ranges and cancels out all other outside this certain range. This bandpass filter was designed for a range of 57- 63Hz (60Hz ± 5%). The bandpass filter circuit has 2 capacitors and 2 resistors, C1 and R1 for the high pass filter and C2 and R2 for the low pass filter (Figure 4.5). To design this filter the available resistors and capacitors were used.

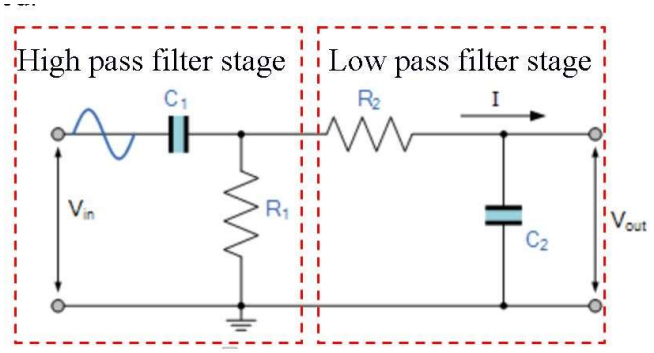

Figure 4.5: Bandpass filter circuit

4.3.1.1High pass filter stage

To design the high pass filter stage the lower cut off frequency (f_C) of 57 Hz was used. When using the available 10 µF capacitor, the resistor value R1 can be calculated from Equation 9 which was derived from Equation 8. This results in a high pass filter stage with a 300 Ω resistor

and 10 µF capacitor. The cut off frequency will then be 53.05 Hz, which was calculated using Equation 8.

$$f_C = f_L = \frac{1}{2\pi R_1 C_1} \quad [8]$$

$$R_1 = \frac{1}{2\pi f_L C_1} \quad [9]$$

4.3.1.2Low pass filter stage

To design the low pass filter stage the higher cut off frequency (f_C) of 63 Hz was used. When using the available 1 µF capacitor, the resistor value R1 can be calculated from Equation 9. The low pass filter stage was designed using a 300 Ω resistor in series with a 2.2 kΩ resistor and a 1 µF capacitor. The cut off frequency will then be 63.66 Hz, which was calculated using Equation 8. Thus this bandpass filter works between 53.05 - 63.66 Hz [50].

4.3.2 Measuring circuit

The voltage measuring circuit consists of the following components: resistors, capacitors, diodes and a 110/12 V transformer. Figure 4.6 shows the schematics to measure the voltage, whereby 1, 2 and 3 are respectively bandpass filter, rectifier and voltage divider with capacitors to smoothen the ripples. Every measuring circuit is build/soldered on a separate circuit board. This is done to minimize the effect of interference, which was a major issue in my initial circuit board when everything was soldered on a 16 cm x 10 cm circuit board. Figure 4.7 presents the hardware to measure the voltage.

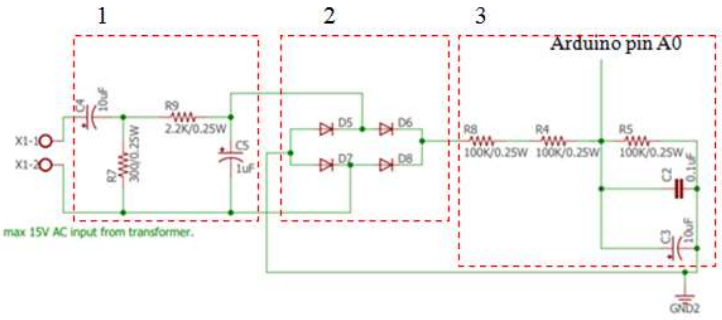

Figure 4.6: Voltage measuring circuit

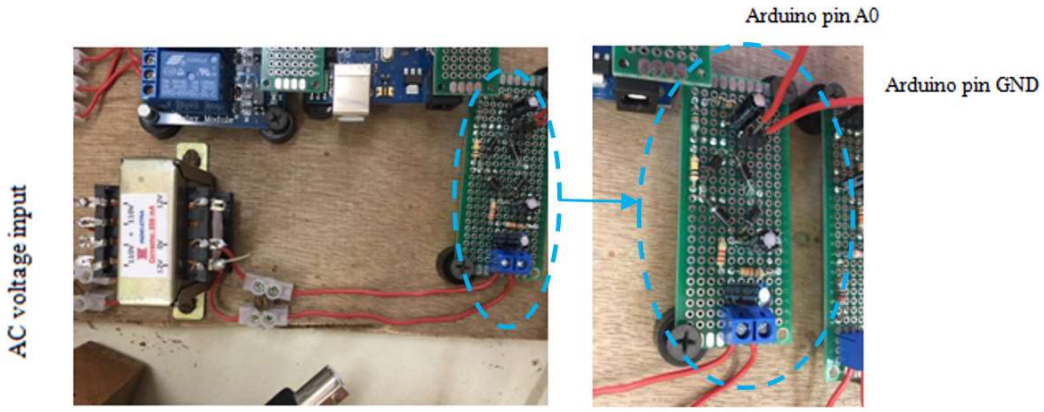

Figure 4.7: Voltage measuring hardware

4.4 Current measurement

The Arduino's analog input pins measures voltage between 0 and 5 V. Thus, the output of the current sensors needed to be translated to a voltage between 0 and 5 V. Current is measured at two different locations, at the load side and the dump load side. The two current sensors are of two different types. The main load current sensor is current based and the dump load current sensor is voltage based.

The main load current sensor can read currents up to 100A and give a current output between 0 and 50 mA according to the current being measured. To measure the current, the shunt method was used as the voltage across the shunt resistor has a linear relation to the current flowing through the shunt resistor. So, if the value of the shunt resistor is known and the voltage across that resistor is measured, then the current through the shunt resistor can be calculated using ohm's law (see equation 10). This calculation is done within the Arduino code. Figure 4.8 illustrates the circuit diagram, which was used to build the current measuring hardware. The measuring hardware is illustrated in Figure 4.10.

$$I = \frac{U}{R} \qquad [10]$$

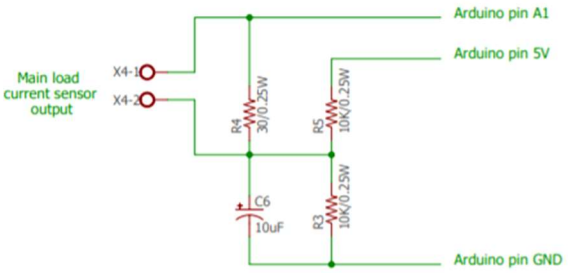

Figure 4.8: Main load current sensor circuit diagram

The dump load current sensor can read currents up to 30A and give a voltage output between 0 and 1 V according to the current being measured. Since the Arduino input can read voltages 0 – 5 V it was wise to expand the output voltage range of the sensor for more reliable readings. This is done as illustrated in Figure 4.9, while Figure 4.10 illustrates the circuit board implementation of the main- and dump load current sensor.

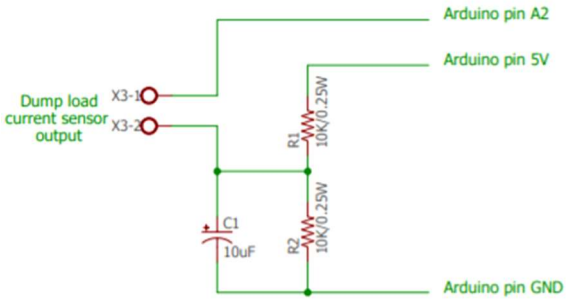

Figure 4.9: Dump load current sensor circuit diagram

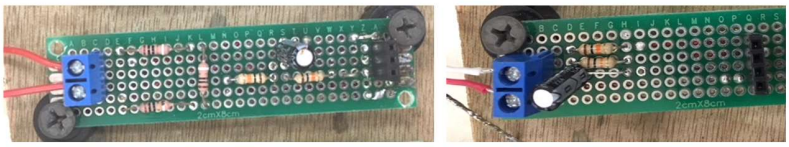

(a) *(b)*

Figure 4.10: Current measuring hardware of the main load (a) and the dump load (b)

4.5 Uncertainties

In this section the uncertainties for the current, voltage and power measurements are discussed. These measurements were performed with the Arduino, the float function being used

with one decimal accuracy for the voltage and current. The error for current equals 0.1 A and the error for voltage equals 0.1 V. Since power is dependent on current and voltage the error of the power measurements is calculated using Equation 11.

$$\frac{\Delta z}{z} = \sqrt{\left(\frac{\Delta x}{x}\right)^2 + \left(\frac{\Delta y}{y}\right)^2} \quad [11]$$

Whereby Z equals X multiplied by Y (Z = XY) or Z equals X divided by Y (Z=X/Y) [51][52][53]

The maximum voltage measured equals 131.0 V and the maximum current equals 9.3 A as shown in Table 3.2. When these values are used to calculate the power uncertainty this equals an uncertainty of 1.1 %.

The power uncertainty calculations:

$$Error \Rightarrow \frac{\Delta P}{P} = \sqrt{\left(\frac{\Delta U}{U}\right)^2 + \left(\frac{\Delta I}{I}\right)^2} = \sqrt{\left(\frac{0.1}{131.0}\right)^2 + \left(\frac{0.1}{9.3}\right)^2} \approx 0.011$$

$$Error\ in\ percentage\ (\%) \Rightarrow \frac{\Delta P}{P} \times 100\% = 1.1\%$$

4.6 Dump load controller and virtual Indalma turbine hardware

The hardware consists of two microcontrollers (Arduino's), switching modules, measuring sensors, dump load and main load (see Figure 4.11). The first Arduino implements the dump load system, which get input from the sensors and gives switching commands to the switching modules according to its programming. The practical choice for dump loads is the use of incandescent light bulbs of 100W. The energy that the dump load can handle must be equal to the maximum value of the main load. This ensures that the entire system does not collapse if there would be an issue with the transport net to the main load or the main load itself, but rather that the dump load will dissipate all the energy.

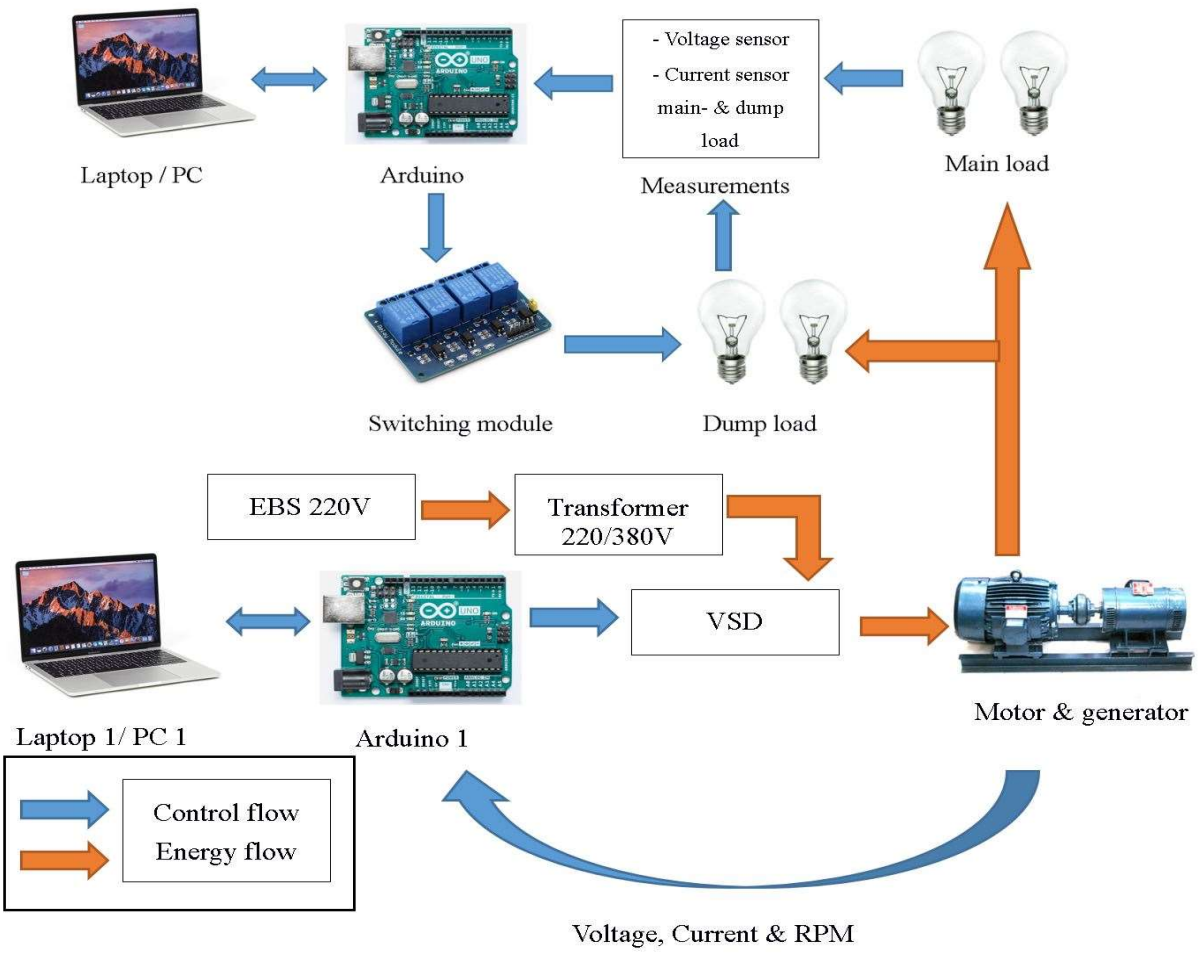

Figure 4.11: Control hardware diagram

The second Arduino is used to control the speed of the motor through an analog input of the VSD (see subsection virtual 6" Indalma). Figure 4.12 presents the implemented hardware of both dump load controller and virtual Indalma controller.

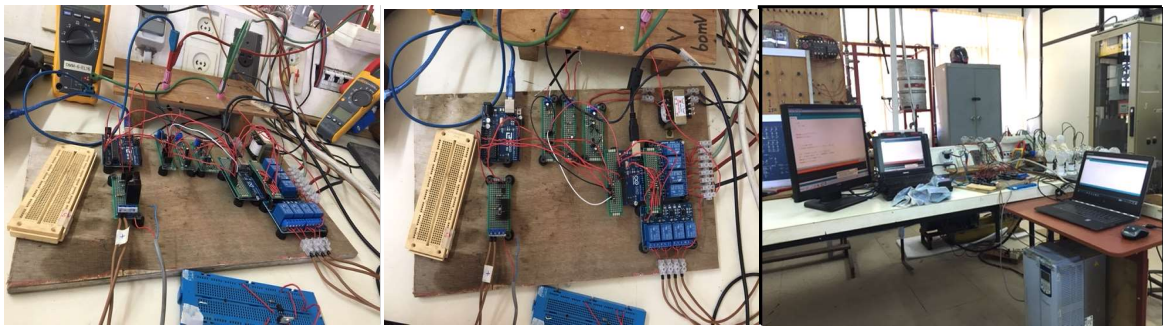

Figure 4.12: The control hardware

4.7 Implementation virtual Indalma

In Figure 4.13 the speed reference circuit that steers the VFD for the virtual Indalma turbine is presented. This circuit is controlled with the second Arduino through the optocoupler. The reason behind using an optocoupler is to create a physical separation between the Arduino circuit (5V) and the VSD input circuit (10V) to prevent damaging the Arduino due to overvoltage. The range of the analog input of the VSD is 0-10V that is translated for speed reference as 0-100% of the nominal speed. The VSD has its own 24V DC source terminals Ref+ and Ref-. The analog inputs are coded AI+ for positive side and AI – for the negative side as shown in Figure 4.14 [54]. Ref+, Ref-, AI+ and AI- from the speed reference circuit diagram are connected to the corresponding terminals of the VSD.

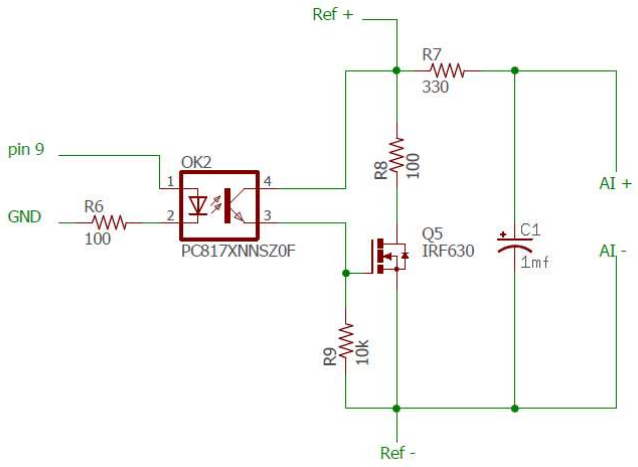

Figure 4.13: Speed reference circuit diagram

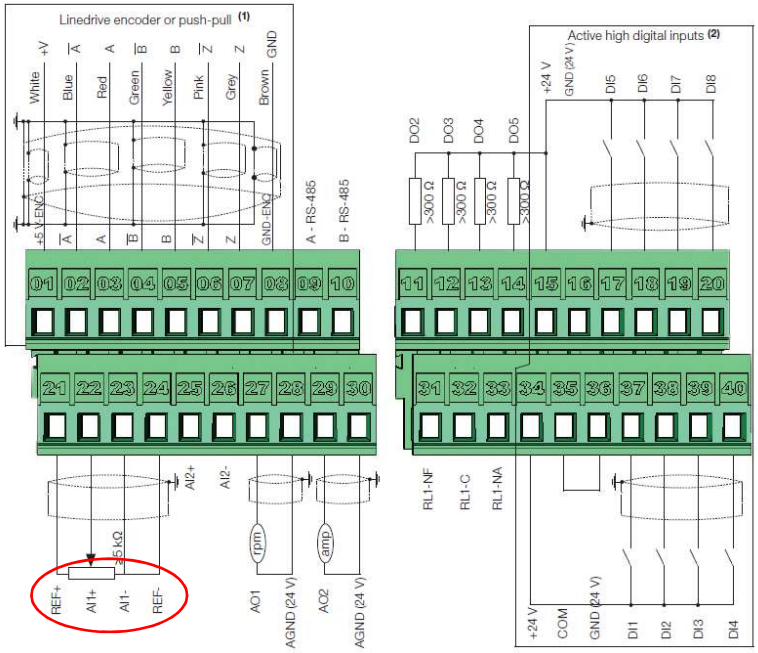

Figure 4.14: VSD Analog and digital in- and output connections [54]

4.8 Software

The software used to program the Arduino Uno R3 is Arduino IDE, version 1.8.5. The programming language is based on C++. Since there are two Arduino's in the setup (Figure 4.11), they are programmed separately. The first Arduino is used to control the relays. This Arduino gets inputs from the voltage sensor and both (load and dump load) current sensors.

The voltage sensor software code uses a while loop. This loop keeps repeating until the sample count equals the predefined number of samples, which was set to 10. In other words, the functions within this loop will repeat 10 times. The function within the while loop does the following: reads the analog sensor value (A0) and sums the total of 10 readings. If the 10 readings have been completed the while loop is broken and the program moves on. Then the average value of these readings is calculated and the sample count and sum is reset to zero (0), see Figure 4.15.

```
  // ------------------------------------------------------------VOLTAGE MEASURING
  // PIN A0
{ while (sample_count < NUM_SAMPLES) {   // take a number of analog samples and add them up
      value = analogRead(Vsensor);
      sum = sum + value;
      sample_count++;
    }

    voltage = ((float)sum / (float)NUM_SAMPLES * 5.00) / 1023.0;
    ACvoltage = float((voltage * 46.075) + 11.366);
    if (ACvoltage <= 60) {
      ACvoltage = 0.0;
    }

    sample_count = 0;
    sum = 0;
```

Figure 4.15: Arduino code for voltage measuring

The current sensors code also uses a while loop to calculate the average of 10 measurements, like the voltage measuring code. The advantage is that using this method gives a more accurate value for the measured signal. Figure 4.16 and Figure 4.17 shows the code for current measuring for the main – and dump load respectively.

```
    //-----------------------------------------------------------CURRENT MEASURING MAIN LOAD
    //PIN A1
  { while (Isample_count < NUM_SAMPLES) {    // take a number of analog samples and add them up
        double Irms = emon1.calcIrms(1480);  // Calculate Irms only
        Ical = float (Irms * 0.5891);
        Ivalue = float (Ical * 1);
        sumI = float (sumI + Ivalue);
        Isample_count++;
      }

      Iav = float((float)sumI / (float)NUM_SAMPLES );

      if (ACvoltage <= 30) {
        Iav = 0;
      }
      if (Iav <= 0.25) {
        Iav = 0;
      }
      Isample_count = 0;
      sumI = 0;
```

Figure 4.16: Arduino code for main load current measuring

```
128     //-------------------------------------------------------CURRENT MEASURING dumpload
129     //PIN A2
130   { while (Idsample_count < NUM_SAMPLES) { // take a number of analog samples and add them up
131         float Irms = emon2.calcIrms(1480); // Calculate Irms only
132         Idcurrent = float (Irms);
133         sumId = sumId + Idcurrent;
134         Idsample_count++;
135       }
136       IdCALcurrent = float(sumId / NUM_SAMPLES );
137       if (IdCALcurrent <= 0.15)
138       {
139         IdCALcurrent = 0;
140       }
141
142
143       Idsample_count = 0;
144       sumId = 0;
```

Figure 4.17: Arduino code for dump load current measuring

From the above inputs; voltage and currents, the power can be calculated by multiplying the voltage and the current. In Figure 4.18 the method of calculating the main load power (POWER), dump load power (POWERD), generator power supply (Pgen) and the equation for controlling the relays (POWERDL) are shown. Note that the power calculated is defined in terms of watt (W). From these calculations the relay modules are controlled. Since the dump load are incandescent lightbulbs and have a measured power consumption around 90 W each, then 8 lightbulbs, which are connected to two relay modules with each 4 channels, equals a total dump load of 720 W. The control of the dump load is therefore based on 8 step changes of each 90 W. The main load is a combination of lightbulbs with different power rating such as: 15, 40, 60, 75 and 100W. Different combinations can be acquired to achieve a variable main load from 0 – 800W. The download link to the script for this Arduino (control AC load 10) is presented in the Appendix C.

```
167     //-----------------------------------------------------------------POWER
168
169     POWER = (Iav * ACvoltage);
170     POWERD = (IdCALcurrent * ACvoltage);
171     Pgen = POWER + POWERD;
```

Figure 4.18: Arduino code for power calculations

The second Arduino, which is used to implement the 6” Indalma characteristics, is programmed independently from the first Arduino. It uses the RPM, voltage and currents sensors data and calculates the desired RPM and gives a PWM output signal. This signal is used to control the analog input voltage of the VFD thought a MOSET. The Arduino code for the voltage, current

and power calculations are similar to the above mentioned codes in the first Arduino. The PWM output signal code is given in Figure 4.19. The first step was to determine the RPM value of the turbine from the curve for a certain Power output of the generator. Once the corresponding RPM value is known, the PWM value is calculated. On the other hand, the measured RPM is used to compare with the RPM set point. The download link to the script for Arduino 1 (virtual Indalma) is presented in the Appendix C.

```
//-------------------------------------------------------------------VSD speed control
//rpm-power curve fitted equation: y = -0.0017x2 + 3.04155x (top punt (895,1360))
// -0.0017x2 + 3.0415x - y = 0
//a=-0.0017, b=3.0415, c=(-y), d = b*b-4*a*c
//y=power
{
  c = ( - POWER) * 10000;
  d = (b * b) - (4 * a * c);
  if (d < 0) {
    x = 0;
  }
  if (d == 0) {
    x = (-b / (2 * a));
  }
  if (d > 0) {
    x1 = (-b + sqrt(d)) / (2 * a);
    x2 = (-b - sqrt(d)) / (2 * a);
    if (x1 > x2) {
      x = x1;
    }
    else
      x = x2;
  }

  // x to pwm value
  // linear equation: y1 = -0.1412x+246.72

  yold = float(-(0.1412 * x) + 246.72) ;
  if (c > -10000) {
    yold = 0;
  }
  if (ynew != yold) {   // compare the new and old value
    yset = yold;
  }
else if ( yset < 0) {
    yset = 0;
  }
  else {
    yset = ynew;
  }
  yold = ynew;
  if (   yset <= 121.96 && yset >= 0) { //lower tan this top of the graph and u go to the left side of the parabola
    analogWrite(PWMpin, yset);
  }
  delay(5000);
}
```

Figure 4.19: Arduino 1 code for PWM output

Note that for the implementation of the virtual Indalma a second order function within a certain range was used instead of the lookup table. This was done because operation only takes place within the certain range (right side of the curve) and because implementing a look up table using Arduino gave some difficulties during the experiments.

5 Modeling and simulation of the control systems

This chapter presents the modeling of the control system using Matlab R2017b software. The focus of this research is the dump load controller. Therefore, simulations are focused on the dump load controller. Since the characteristics of the 6" Indalma turbine and the adjusted power-RPM curve are known, this is used as the mechanical input for the generator. The output of the generator is then used for the load and designed controller. Modeling started with the simplified model of the Pico hydropower setup. The second step was modeling of the dump load control system. Finally, simulations are discussed for two different situations.

5.1 Matlab model

The Matlab model consist of a permanent magnet synchronous generator and 4 subsystems namely speed control-, main load-, dump load- and the measurements subsystem. The speed of the rotor, voltage and current are measured of the generator. From the voltage and current, the power is calculated and fed to a look-up table which in turn is connected as a loop back to adjust the speed accordingly. This method is possible since there is data of the power curve of the 6" Indalma turbine. Figure 5.1 shows the Matlab model with which the simulations were done. In this model the VFD and the motor are neglected, whereby the mechanical input of the generator is directly connected to the speed controller. This is done because the focus point of this thesis is the dump load control system and not the hydropower plant itself. In other words, the focus area is after the generator.

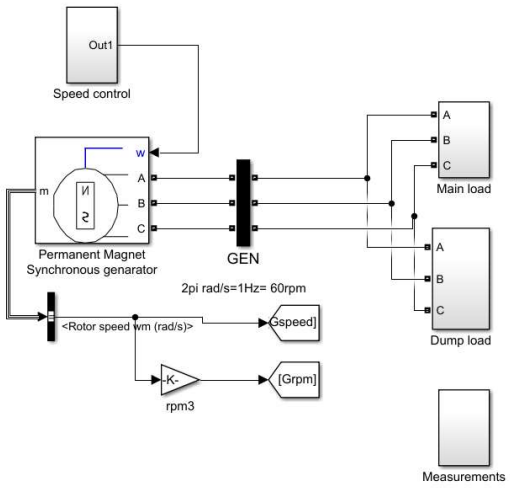

Figure 5.1: Simplified Matlab model of the laboratory setup

5.1.1 Permanent magnet synchronous generator

The permanent magnet synchronous generator (PMSG) block was used, because in the lab setup an actual permanent magnet synchronous generator is set up as generator. For modeling, the machine parameters that were used, were gained from the internal machine parameter computing function. Figure 5.2 shows the internal machine parameter computing function. From the specifications only the voltage constant have been changed to 220Vrms/1.8kRPM = 122.22 Vrms/kRPM. The default values are used for the rest of the parameters, since these were unknown. The parameter computing function calculated the block parameters, which is seen at the right side of Figure 5.2. Because Matlab is a well-known and worldwide used software by engineers to do simulations it is assumed that parameter computing function works correctly.

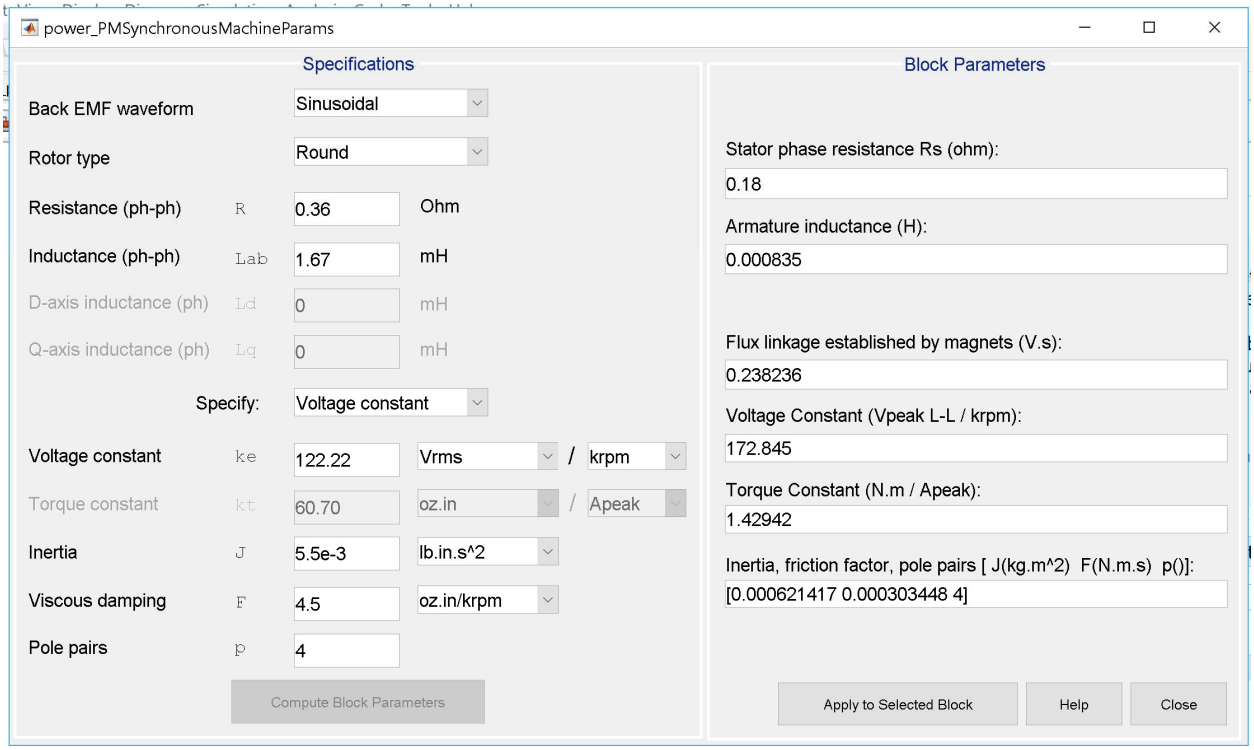

Figure 5.2: Internal machine parameter computing function

5.1.2 Electrical load

Each electrical load is connected to the generator terminals through a breaker. The function of this breaker is to simulate the switching of load in reality. Each dump load has a power capacity of 100W and the total load is 800W, which means the main load is also 800W since these two should be equal to each other. Figure 5.3 illustrates how the electrical load is modeled in Matlab.

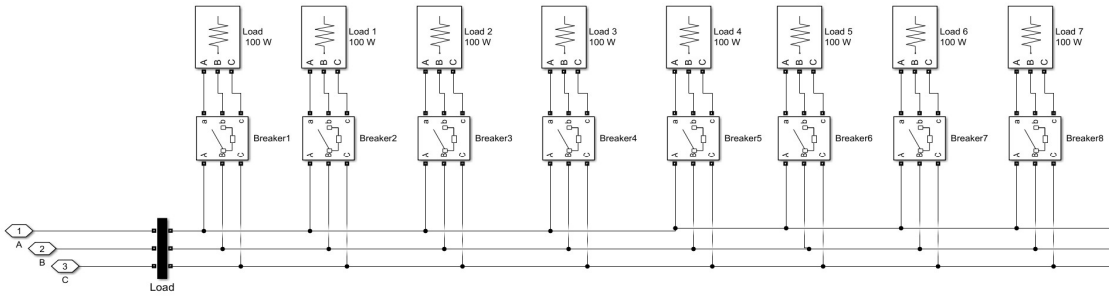

Figure 5.3: Electrical load

5.1.3 Speed controller

The speed controller is based on the RPM-power curve of the 6" Indalma turbine. This speed controller models the virtual Indalma discussed in chapter 3.2. In Figure 5.4 the model is illustrated. Note that there is a manual reference speed switch to switch between fixed RPM and turbine effect (virtual Indalma). The first option is to perform simulation with a fixed RPM and the second option is to perform simulations with the 6" Indalma turbine effect taken into consideration (7m theoretical data is used).

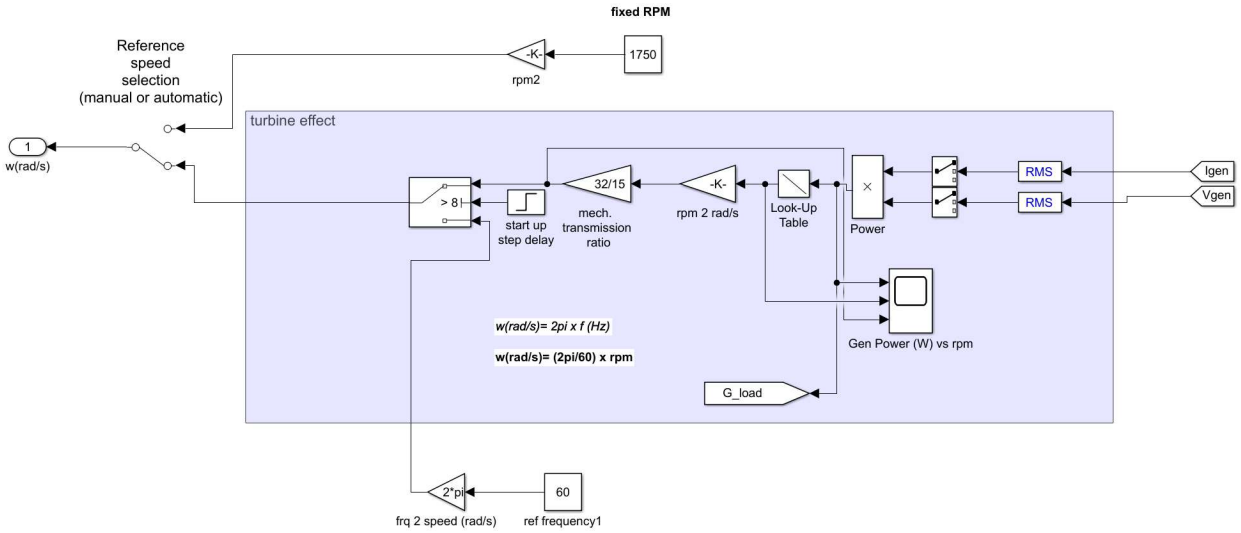

Figure 5.4: Speed controller model

5.2 Modeling of the simple dump load controller (proportional on/off controller with feedback)

The dump load controller is based on the flowchart in Figure 5.5, whereby the main purpose is to keep the voltage and at the generator terminals at a constant value. This can be achieved by keeping the power at the generator terminals almost constant. At all times equation 12 must be valid in order to obtain the above. If for some reason it's not valid the control system should switch a dump load on or off accordingly.

$$P_{gen} = P_L + P_{DL} \qquad [12]$$

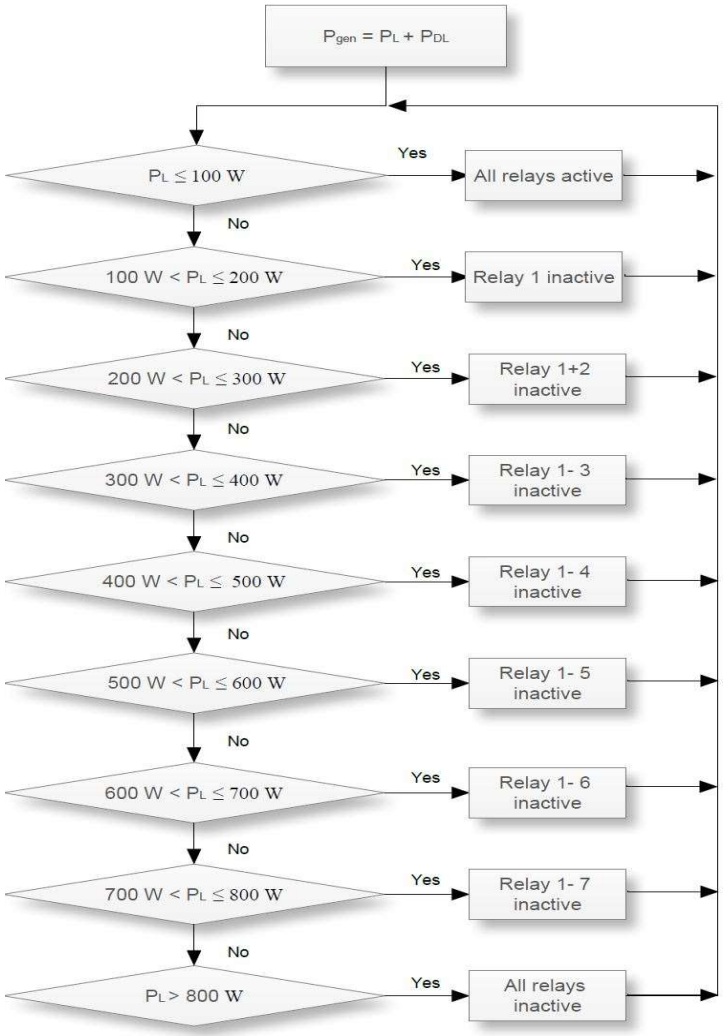

Figure 5.5: Flowchart control system

From the above flowchart it is clear that every step differs 100W from the last one. This is done on purpose since the eight dump loads (incandescent lamps) are each rated 100W. The model of the control system is presented in Figure 5.6. Between each dump load and generator terminals there is a breaker, which is controlled by a comparing function. This function compares the main load power to a certain threshold. If this is true than the breaker is switched on and the dump load is active.

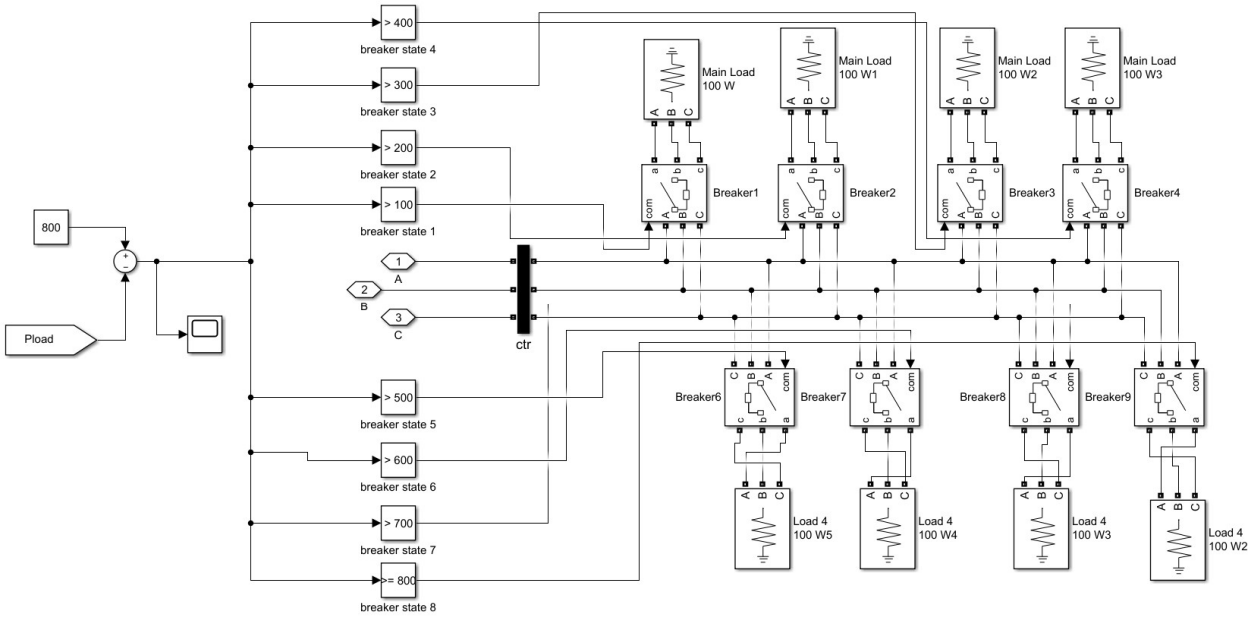

Figure 5.6: Dump load controller model

5.3 Simulation and validation

The simulations done in Matlab are presented in this section. Furthermore, the validation of these simulation results is also discussed as well as recommendations for future studies. The main focus is to simulate the designed micro hydropower controller, which will keep the voltage at the generator terminals almost constant. The simulations are divided in two parts. The first part focuses on the performance of the controller, whereby the turbine characteristics are neglected. And for the second part the turbine characteristics are considered.

For the first simulation the turbine characteristics are neglected, thus the rotational speed of the Indalma turbine (5kW) will be kept constant. The purpose is to simulate a case during a certain period when the flow is almost constant and therefore the generation of electrical power is also constant. The variable dump load switching control system will keep the frequency and voltage of the network at a desired level, although the main load can vary. The dump load switching is dependent on the load of the grid (main load), which will be varied during the simulation. The higher the grid load (main load), the less power the control system will dissipate in the dump load.

During the second simulation the turbine characteristics are considered. This means there will be a loop back from generator terminals to calculate the actual turbine speed at the load at that time. This value will then be fed to the PMSG.

The electrical load is set to switch on and off on fixed times, using a three-phase breaker with internal switching times. These switching times of the electrical load is illustrated in Table 5.1, this table also indicates that there are electrical loads of 100W, 200W and 300W. Since the dump load control system is designed for 800W max. The dump load equation equals:

$$P_{DL} = 800 - P_L \quad [13]$$

This means that if $P_L = 0$, then $P_{DL} = 800$. Thus, the controller will dissipate the full load of 800W. P_{DL} is linearly dependent on P_L and the Sum of both should always equal 800W.

Table 5.1: Electrical load switching time

Electrical load switched on (W)	Total electrical load (W)	On switching time (s)	Dump load (W)
100	100	5	700
100	200	10	600
200	400	15	400
200	600	20	200
100	700	25	100
100	800	30	0

In Figure 5.7 the results of the first simulation is presented using 6 graphs. From top left to bottom right these figures will be discussed. The first figure (top left / Vload) illustrates the voltage (phase to ground) at the main load terminals, which is produced by the PMSG at a constant speed of 377 rad/s (1800 RPM). Second graph on the left (Iload) illustrates the current drawn by the electrical load (main load). In the third graph on the left (P_Load) the power is illustrated which is drawn by the main load, since the three-phase breakers are switched on from 5 – 35 seconds the graph shows an increase in power. This step increase equals the load that is connected to each three-phase breaker. The first graph on the right (Vctr) presents the phase to ground dump load rail voltage. The second graph on the right (Ictr) presents the current drawn by the active dump loads. The last graph presents the power drawn by the active dump loads and this has the inverse form of the power drawn by the main load (third graph on the left).

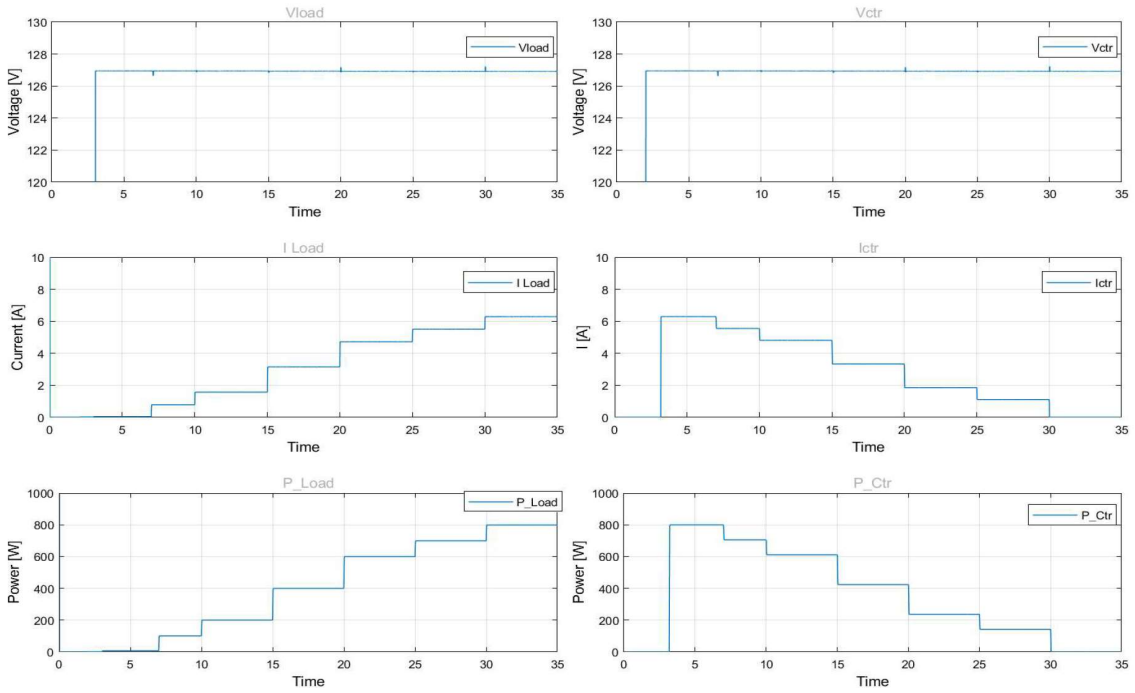

Figure 5.7: First simulation results

In Figure 5.8 the P_Load and P_CTR (dump load) are given in one graph. Notice that in this graph P_CTR decreases with the same value that P_Load increases. In the same graph P_Gen stands for P generator and there are spikes (illustrated with the black circles in Figure 5.8) in the graph, which are caused by the controller execution delay. This delay is constant throughout the simulation and equals 55 ms (55 milliseconds).

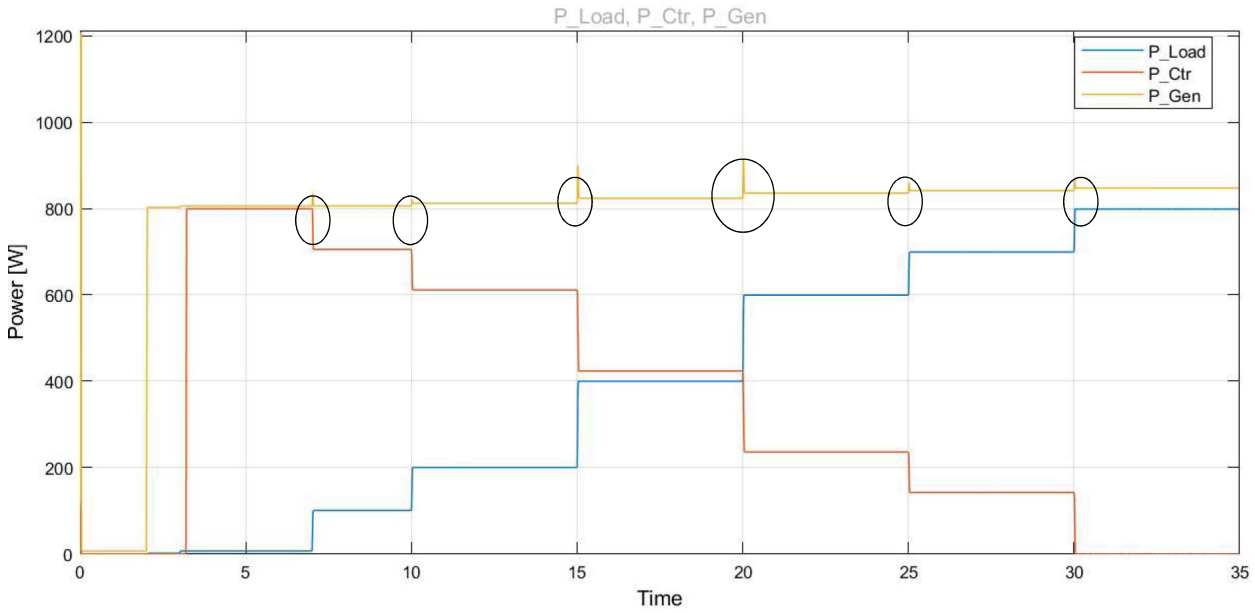

Figure 5.8: P load vs P control

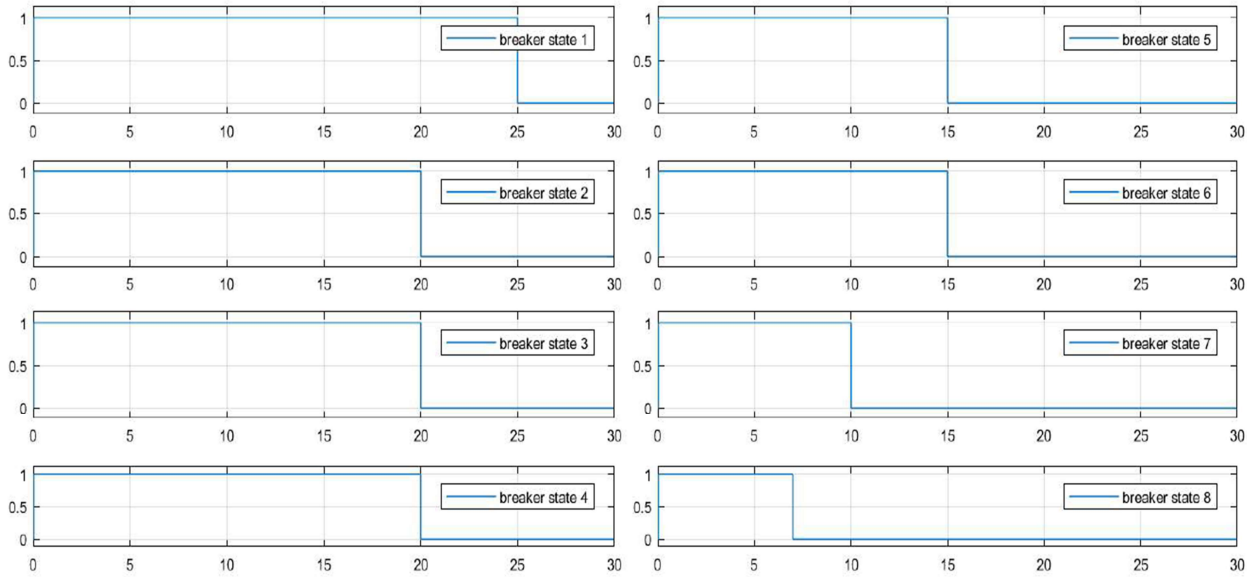

Figure 5.9: Dump load state

The state of each three-phase breaker, which switches a dump load on or off, is illustrated in Figure 5.9 and Figure 5.10 presents the frequency measurements. Note that the frequency is constant, which is due to the fact that the generator is driven by the speed. This means that the torque is infinite. Thus, switching loads on/off will have no effect on the RPM or frequency.

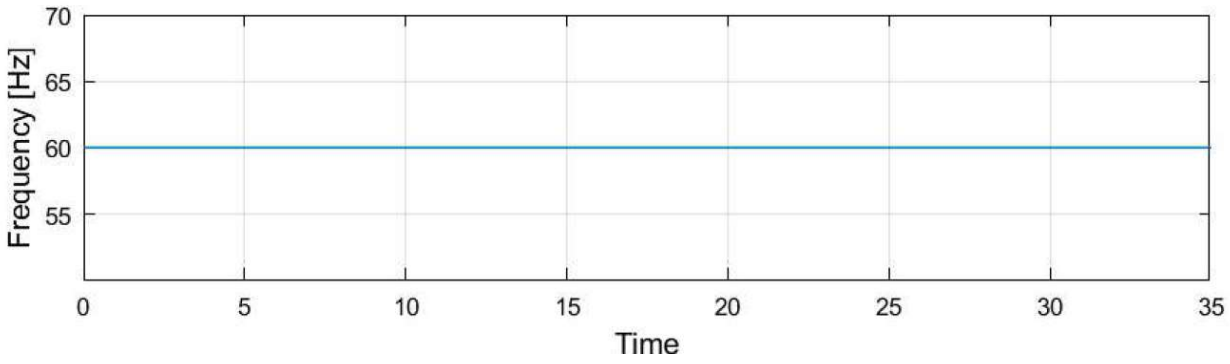

Figure 5.10: Frequency measurements first simulation

The simulation results of the second simulation whereby the turbine characteristics are taken into consideration is presented in the following sub section.

5.3.1 Simulations with theoretical data

This subsection discusses the simulations with the theoretical data obtained by using the affinity laws (see Equation 3 and 4) discussed in chapter 3. The difference between these simulations and the above are that the turbine characteristics are taken into consideration using a look-up table. The simulation results of the second simulation (simulation with 7m theoretical data) is presented in Figure 5.11 - Figure 5.13. If Figure 5.7**Error! Reference source not found.** and Figure 5.11 are compared, there is an average voltage drop in the two figures from 127 V to 125.75V. This drop in voltage is caused by the speed controller that imitates theoretical data of the Indalma turbine. In Figure 5.11 the max voltage is 127V and the min voltage is 124.5V, the average value of the voltage during the simulation is 125.75 V.

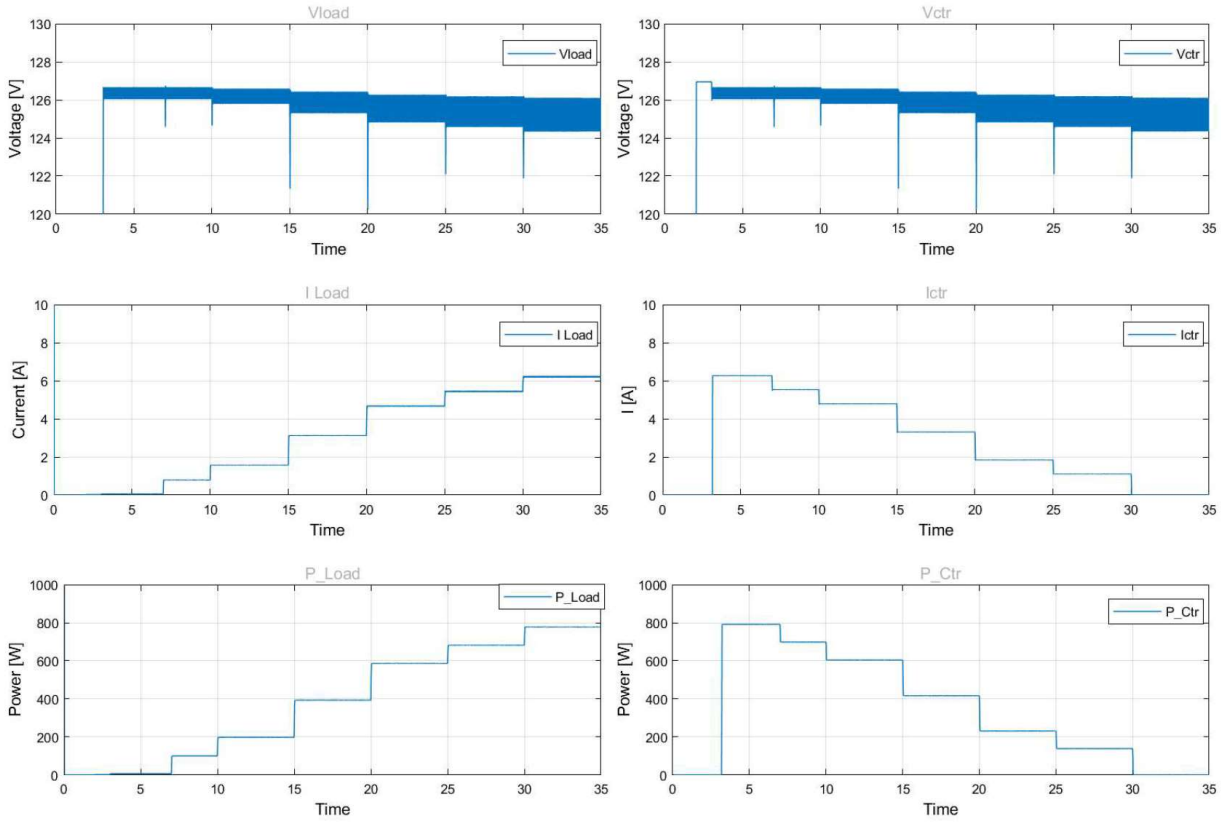

Figure 5.11: Simulation results with theoretical data

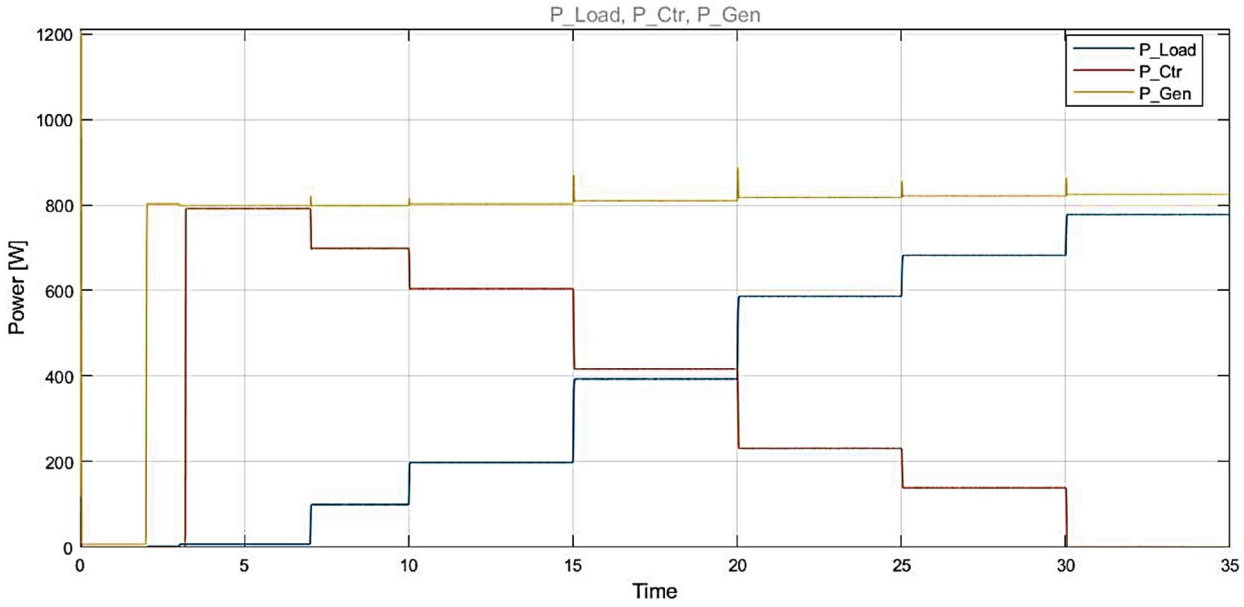

Figure 5.12: $P_{\_Load}$ vs $P_{\_Control}$ vs $P_{\_Generator}$ third simulation

Figure 5.12 and Figure 5.8**Error! Reference source not found.** are almost identical, their difference lies between t=20 - 35s. Between this interval Figure 5.8 has a higher power generation (around 20W give or take) due to neglecting of the turbine characteristics.

Figure 5.13 presents the dump load states for the third simulation. When comparing this to Figure 5.9 there are two differences. Breaker state 1 is switched off at t=30s instead of t=25s and breaker state 2 is switched off at t=25s instead of t=20s. The rest of the breaker states are switching off or on at the same time.

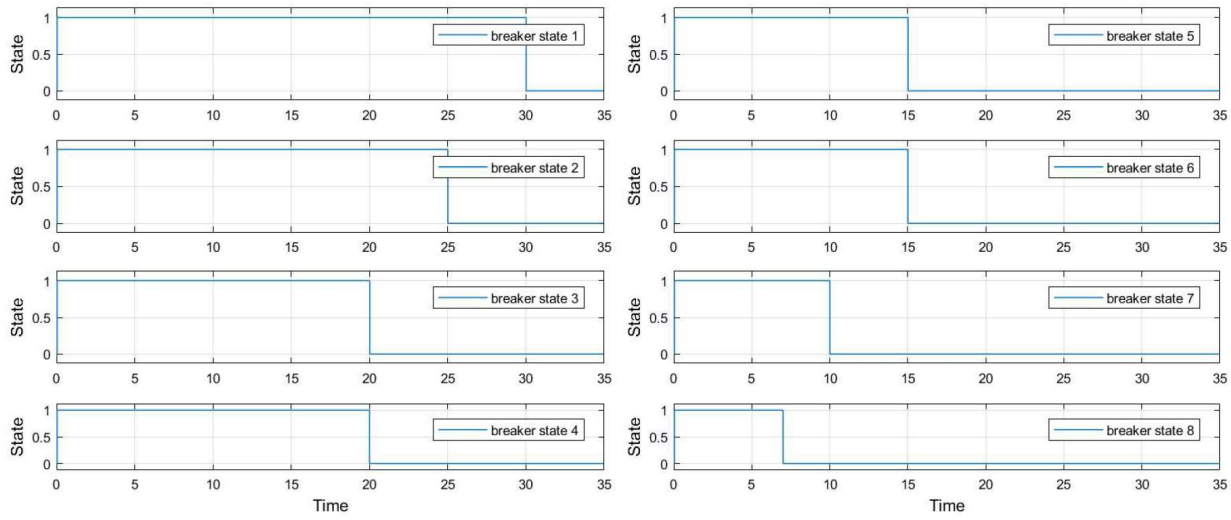

Figure 5.13: Dump load state third simulation

Comparing Figure 5.10 and Figure 5.14 a frequency drop is noticeable. In Figure 5.14 the frequency varies between 58 and 59.5 Hz.

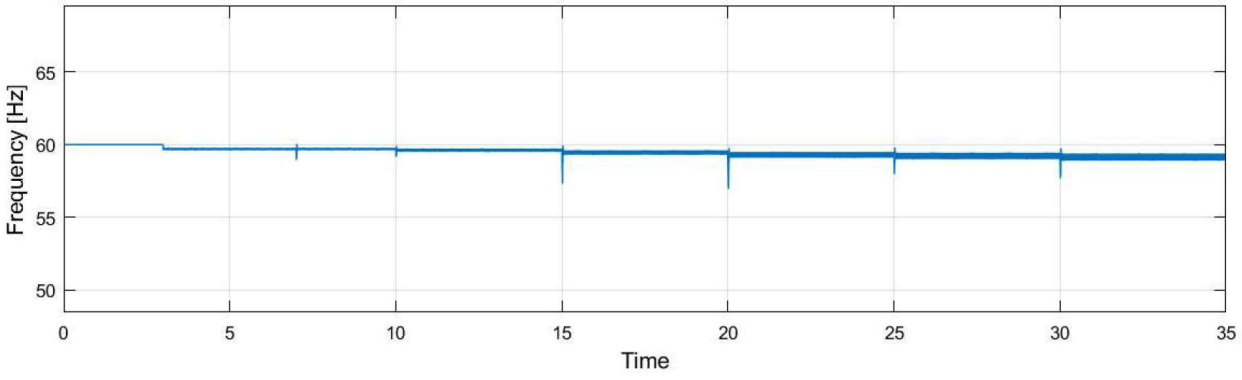

Figure 5.14: Frequency measurements second simulation

5.4 Modeling of a PI dump load controller

Unlike the simplified dump load controller, this subsection shows the modeling with a PI controller. This type of controller is chosen due to its low cost, it is easy to design and it does not have to predict near future errors. Furthermore it is widely used in industrial applications [55]. This controller is another design and is only simulated. These simulations are done to show that there is another possibility to design a control system, which meet the requirements of low cost, robust, easy to install and low maintenance. Note that this control system does not use relays and the dump load is capable of dissipating all the energy produced by the system. Previous study showed that a resistive dump load can be modeled as a first order function (Equation 14) [56].

$$Dump\ load\ first\ order\ function = \frac{1}{0.2s+1} \quad [14]$$

The designed model with PI controller is illustrated in Figure 5.15. Where the dump load is modeled as a first order function. Note that this block imitates a continuous dump load [56]. For this controller Equation 12 must always be valid, which was also the case with the previous designed controller. Since the controller focus is after the generation of electricity and the generator can generate a maximum around 800W, the reference value for voltage is 127V and for the current it is rounded to 6.3A. Due to the fact that the actual main load used during the research tests are incandescent lightbulbs, the cos φ is set to one (1). Tuning of this PI controller is done using the tuning function of Matlab and the values for P and I is given in Figure 5.16.

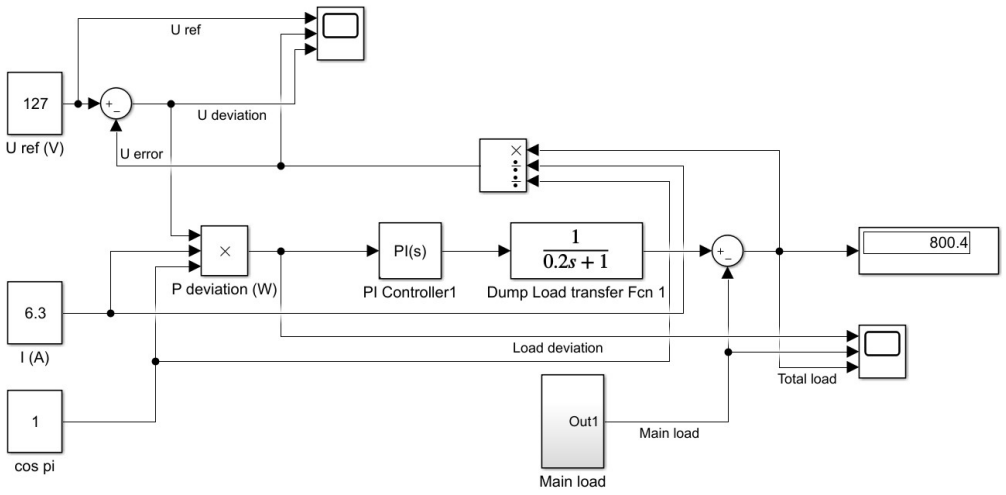

Figure 5.15: Simulation model (PI controller)

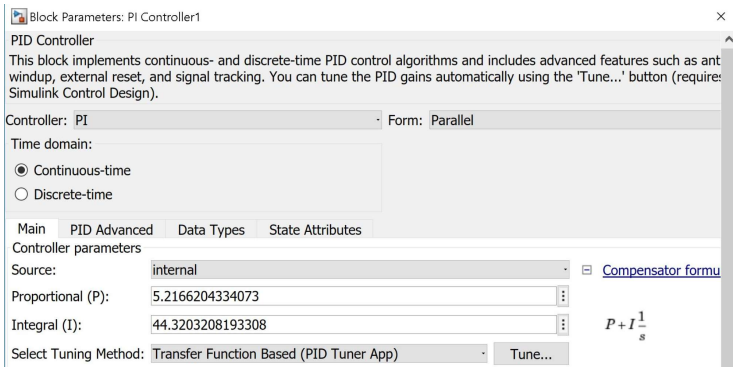

Figure 5.16: PI controller parameters

In Figure 5.17 the load deviation, main load and total load measurements are illustrated. The peaks in the load deviation and total load are due to the instantaneous on/off switching of the main load. Note that the peak of the load deviation or total load equals the main load switched on/off at that time. At the orange circles in Figure 5.17A the graph is zoomed in and this is illustrated in Figure 5.17B. From this graph the reaction time (time to respond to the change in load deviation) of the PI control system can be obtained, which is ± 0.4 seconds. This reaction time is constant no matter the main load on the system.

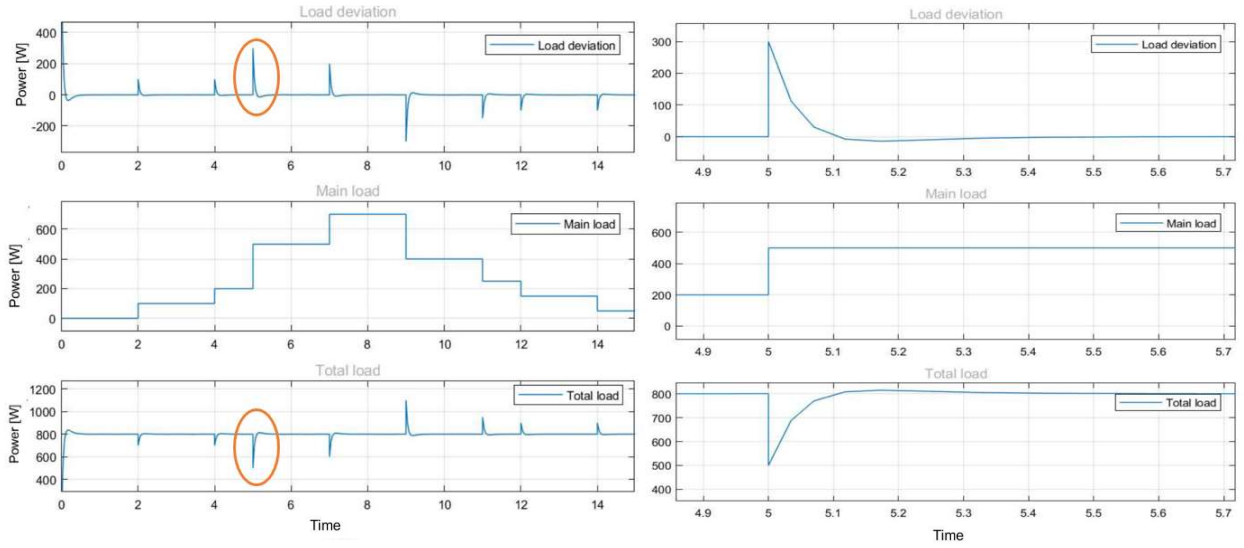

A *B*

Figure 5.17: Load measurements (A), zoomed in at t= 4.9-5.7 sec. (B)

In Figure 5.18 the reference voltage, the error and voltage deviation is illustrated. The peaks in the error and deviation are due to the instantaneous on/off switching of the main load. At the orange circles in Figure 5.18A the graph is zoomed in and this is illustrated in Figure 5.18B. From this graph the voltage drop at t=5 s equals 47 V (127V-80V), this occurs when a load of 300W is instantaneous switched on. This drop in voltage is acceptable since the voltage drop is only for a short while. It takes around 0.4 seconds to be precise for this voltage drop to be regulated to the reference value during the simulations. But if the voltage must stay at all times between the ± 10% margin than the max. main load switching should be around 100W. The voltage drop for a 100W main load switching equals 16V (127V - 111V), which is within the ±10% range of 127V.

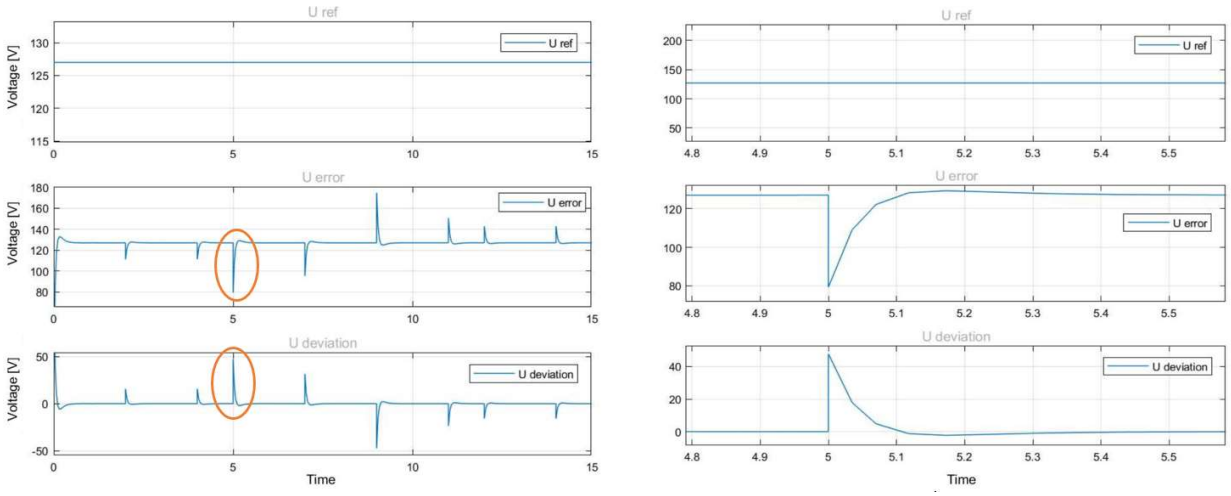

A *B*

Figure 5.18: Voltage measurements (A), zoomed in at t=4.8-5.5 sec.(B)

6 Results & discussions

This section of the thesis presents the experimental results and the discussions around the presented results. The designed control system and its performance is discussed, as well as the future work proposals that can be implemented in order to improve the designed controller. And also some recommendations for future studies are presented.

Figure 6.1 shows the controller operation performance, whereby the turbine effects are left out. Note that when the main load power increases, the dump load power decreases. Thus, keeping the power at the generator terminals almost constant. The spikes (these are illustrated in Figure 6.1 with the red circles) in the generator power curve are caused by the controller delay. This takes place when an extra load is connected and the controller needs some time to respond to the extra load. The time to respond is the controller delay time. Because of this delay (2.614 seconds, which is the time between two measurements or one can say it is the time needed to run the full Arduino script), the measured power spikes. The total power generated varies between 675-850 W, if the spikes are left out of the picture than the power fluctuates between 673 and 733 W. Due to minor losses in cables and the fact that the incandescent light bulbs power is related to the voltage applied, the total power is not at the designed value of 800 W, but rather somewhat lower. The ratings for the incandescent light bulbs used are 130V 100W. Thus, if the voltage which is applied, is lower than 130V the power drawn by the bulb will be lower than 100W. So, a 10 V decrease at the generator terminals corresponds to a power decrease of 7.69%.

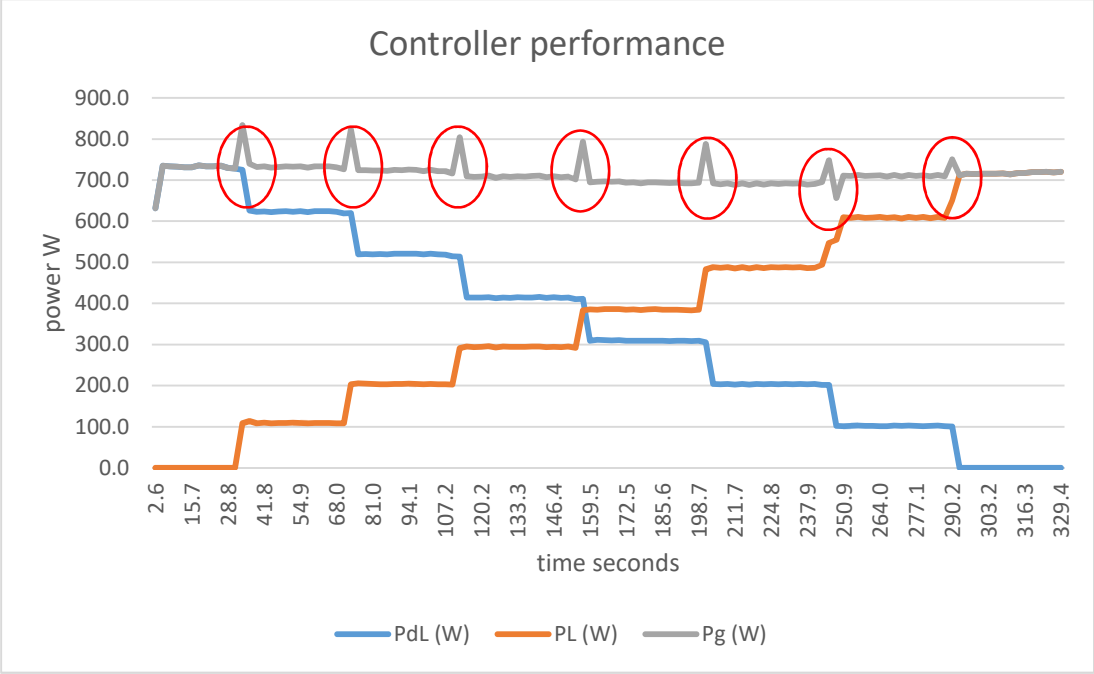

Figure 6.1: Controller performance without turbine characteristics

The second set of experiments are done with the turbine characteristics implemented in the drive (VFD), the method how this is done is discussed in section 5.3. Figure 6.2 shows controller operation, whereby the turbine characteristics are considered. In this graph the AC line to neutral voltage, dump load power (PdL), load power (PL), total power generation/demand (Pg) and the RPM are set out against the time of measurement.

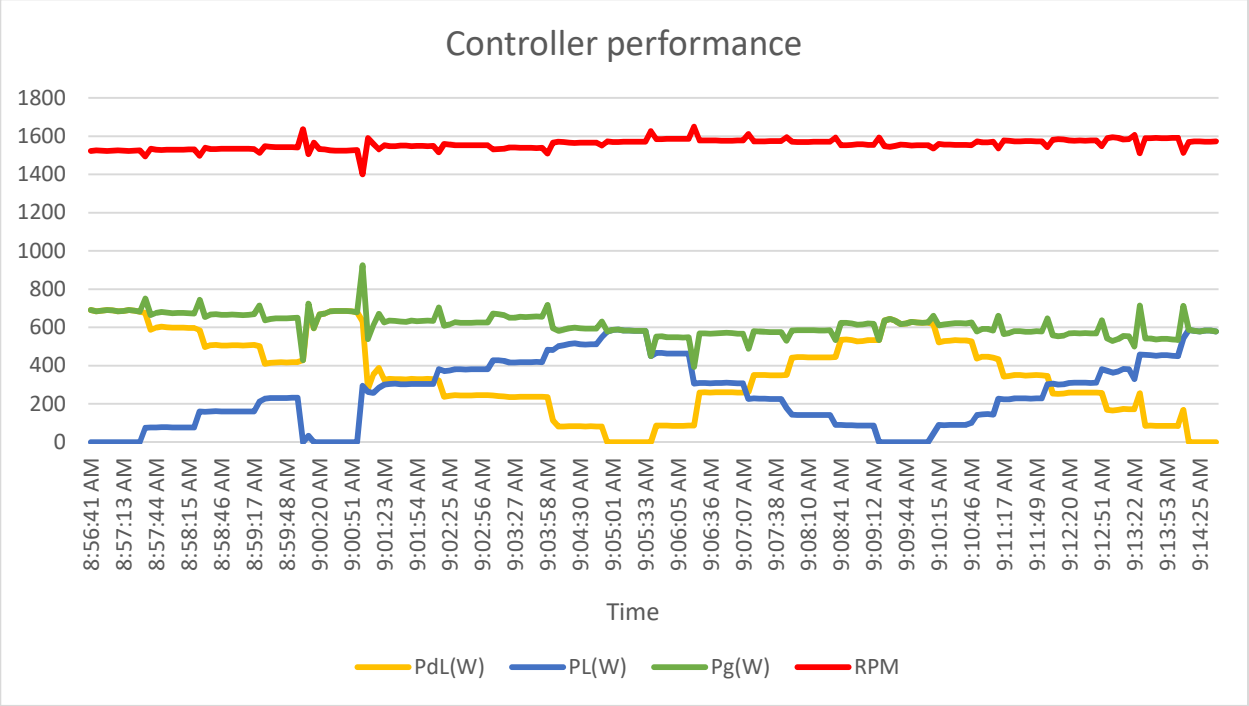

Figure 6.2: Controller performance with turbine characteristics

Figure 6.3 shows the voltage during the experiment with the turbine characteristics implemented. The voltage fluctuates between 97 V and 115 V, whereby its average value is around 108V. If this is taken as the base line than the voltage range should be between 118V (+10%) and 97V (-10%). Thus, the voltage fluctuation is within the voltage range. When the voltage is 97V the power demand equals 611W, which is 27.8% of the motor power (2.2KW). If the voltage is 115V the power demand equals 643W, which is 29.3% of the motor power.

This figure also illustrates that the frequency fluctuates between 46.7Hz and 55.0Hz, with an average of 51.5Hz. If this average is taken as a base line than the frequency fluctuations lies between -9.32% and +6.80%. If the base line frequency is 50Hz (motor is rated 50Hz, 2.2kW & 1700RPM) then the fluctuation in percentage equals -6.60 % and +10%.

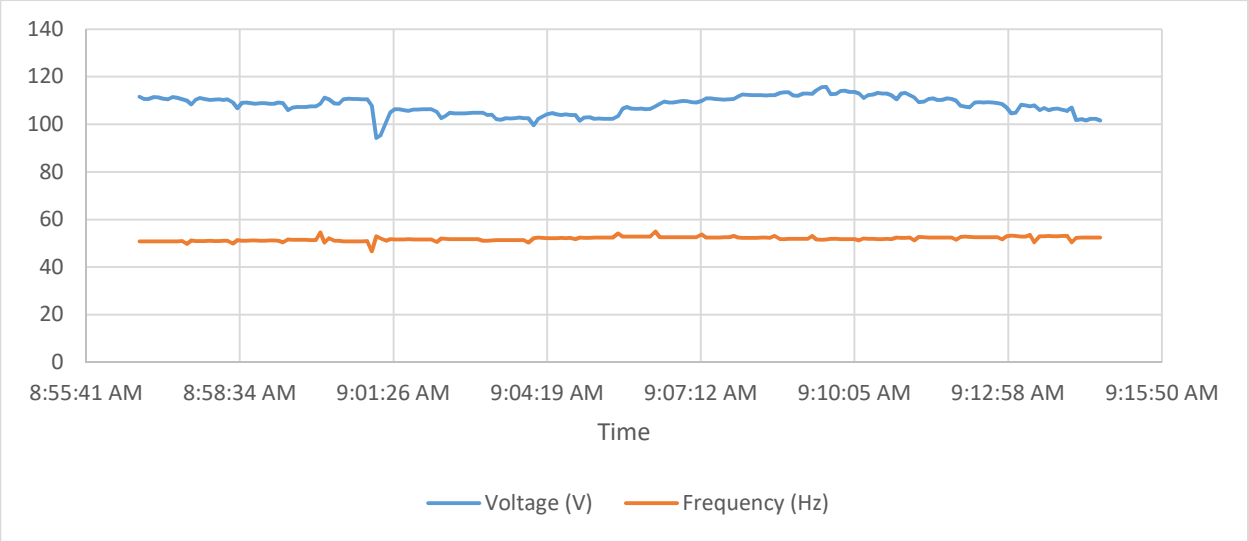

Figure 6.3: Voltage and frequency measurements with turbine characteristics

In Figure 6.4 the total power generated by the motor-generator set are presented against the time. Note that the average power equals 613 W. This graph is not a nice smooth line but it has dips and spikes in it. Which are created by the on off switching of the loads and dump loads. The first spike is between 08:57:07 and 08:57:50, which is the result of switching on a load while the controller did not react yet, thus all the dump loads were still active. This goes for all the spikes in the graph. The dips are the opposite of spikes and are caused when a load is switched off and the controller did not react yet to the new situation.

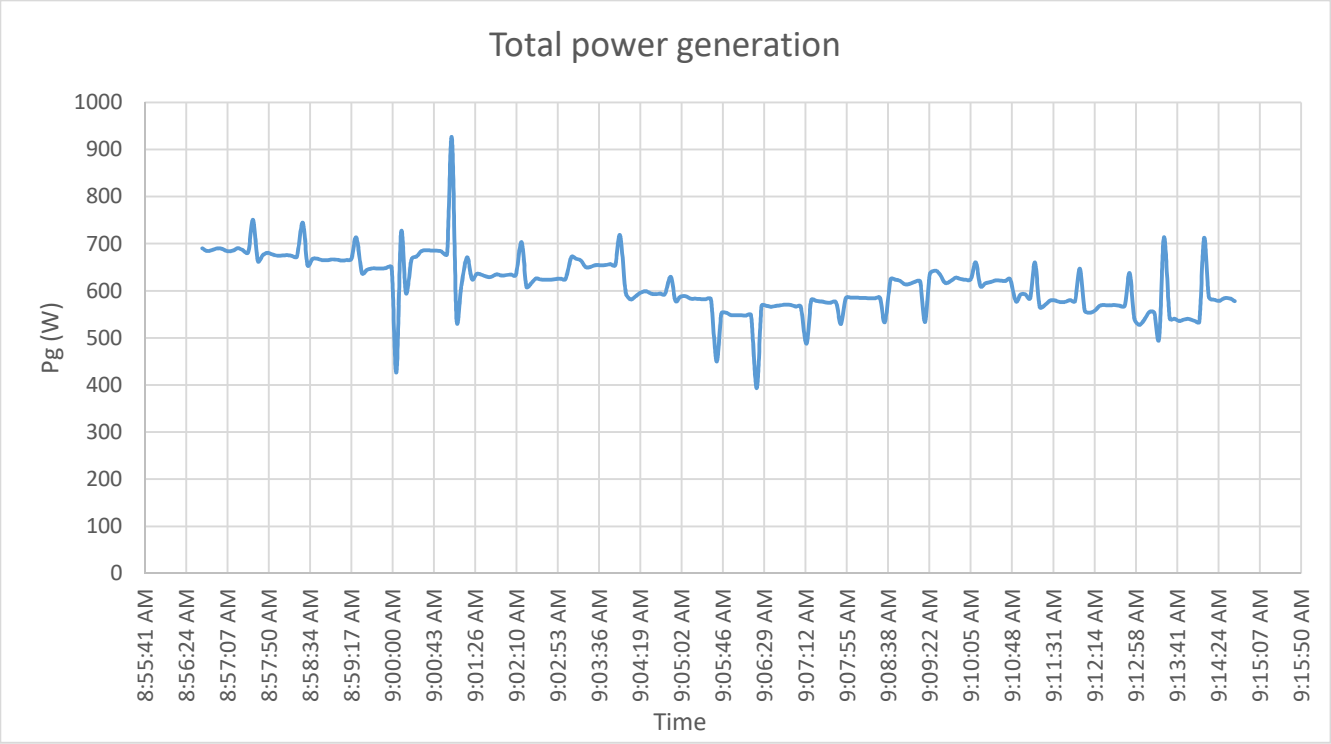

Figure 6.4: Total power generated with the turbine characteristics

If the simulated results of the designed dump load controller are compared to the simulated PI controller its obvious that the PI controller responds better to load changes. As the results indicated the voltage variation is smoother with the PI controller. This is due to the fact that the dump load controller works in a step range of 100W and the PI controller works with a variable dump load. This makes the PI controller more accurate. In practice such a PI controller can be build using power electronic for example a DC to DC converter.

Conclusions & Recommendations

Conclusions:

1. The first objective was to design the dump load control system, which will keep the frequency and voltage at the load terminals within respectively a -5% to +10% and ± 10% margin. This control was designed and presented in chapter 3 and 4, whereby the results of the experiments are presented and discussed in chapter 6. Experimental results indicate that the voltage fluctuates between 102 V and 115 V, whereby its average value is around 108V. If this is taken as the base line than the voltage range should be between 118V (+10%) and 97V (-10%). Thus, the voltage fluctuation is within the voltage range. The results also indicate that the frequency fluctuates between 46.7Hz and 55.0Hz, with an average of 51.5Hz. If this average is taken as a base line than the frequency range should be between 56.7 Hz (+10%) and 48.9 Hz (-5%). Thus, the frequency fluctuations exceeded the lower limit of this range resulting in a frequency fluctuation between -9.32% and +6.80%. The cause of this issue is the fact that the motor used in this research test setup was underrated (discussed in chapter 3). The controller can be improved by adding a frequency protection. If the frequency drops below -5%, which can happen if the load is larger than generated capacity or if the sudden load increase causes the frequency to instantly drop below the -5%. When either of these happens the frequency protection will act on the power from the generator to the load and dump load, thus keeping the frequency above -5%. This will solve the frequency issue and improve voltage fluctuation, since the voltage is correlated to the frequency.

2. The second objective was to simulate a control system for Pico hydropower systems, using a simplified model for the 6" Indalma turbine. This was done in Matlab R2017b software. From the simulation results presented in chapter 5 one can conclude that the designed micro hydropower model worked as it should be, which was to keep the voltage at the generator terminals within a ±10% margin and the frequency within a -5% to +10% margin. There is a fluctuation of max 2.5V (124.5 – 127V), which corresponds to 2 %. There is a fluctuation of max 1.5Hz (58 – 59.5Hz), which is within a -5% to +10% margin for the frequency. During these simulations the main load varied with constant values, either 100W or 200W. In practice this would be unrealistic, since the load connected to the grid is can be any

variable. So, in practice the dump load controller will only react to changes in the order of 100W, which will mean that demand will not always be equal to production of energy. This can lead to sudden voltage changes, due to sudden changes in main load.

Simulations results with the designed PI controller indicates that the on/off switching of main loads should be around 100W or less, to keep the voltage fluctuation between the ±10% margins of 127V. Since the dump load is not step controlled, but instead continuously controlled the voltage fluctuation is almost negligible. These fluctuations only occur during on/off switching. Furthermore this method is more accurate.

3. The third objective was to build the dump load control system as similar as possible to that of Gran Holo. From chapter 4 it can be concluded that this control system is built with the intension to be as similar as Gran Holo hydropower plant and to be used in the interior, thus using technology that is cheap and easy to replace. The only aspect is that the current prototype is not yet ready to be placed in the field. Due to budget constraint the PCB was not fabricated as it should and it is also not placed in a waterproof casing. Furthermore the dump load control system was tested using resistive loads. If a scaled up model is used at Gran Holo one must take into account that there will also be inductive, capacitive and motor loads connected on this entire system, which will have an impact on the active- and reactive power (also related to phase shift). So, there may be capacitors or inductors needed for cos φ improvement.

4. From all of the above it can be concluded that the design of the controller was successful, even though some parts are not fully executed or should be improved.

Recommendations for future studies:

1. The Pico hydropower laboratory should be implemented so that the experiments under real time conditions can be done using an actual turbine and water.

2. This control system should be tested using an actual Indalma turbine. The results presented in this chapter can then be evaluated / compared with the results of the experiments with an actual 6” Indalma turbine.

3. To improve results the delay time (presented in chapter 6) between measurement and execution should be decreased. This can be done by optimizing the code or using faster circuits.

4. A possibility to improve this control system is to use an R2R ladder system for the dump load control. This may give a more accurate dump load power depending on the main load variation.

5. For faster on and off switching of the dump loads, it is worth looking into a control system using solid state relays or power transistors. Note that this will be more expensive than using regular relays.

6. To get the fastest on and off switching of the dump loads, the control system can be built using power transistors. Note that this will be more expensive than using solid state relays.

7. If this research test setup is to be used for further research, the generator and motor should have better matching properties for the power, frequency and RPM. In this study the motor was underrated for the generator.

8. The dump load control system can be implemented using a PLC (programmable logic controller). This can make programming easier, but will be more expensive due to the cost of the PLC.

9. Further study is needed: (A) for the under frequency load shedding, (B) on the power flow when this control system is implemented in an actual electrical network and (C) on voltage and current measurements at the motor terminals, so that the torque can be calculated. This can be used to evaluate the virtual Indalma.

The design of a variable dump load controller for Pico hydropower plants was successfully done using relays, incandescent light bulbs and an Arduino. The contribution of this thesis is the implementation of the virtual Indalma turbine, which has never been done before for this hydraulic turbine. The second contributions of this work is the designed dump load controller, which can be

implemented for the Pico hydropower plants in the Amazon that are now in operation without any control system whatsoever.

Reference list

[1] J. Menke, *Mozaïek van het Surinaamse volk*. 2016.

[2] S. Murni, J. Whale, T. Urmee, J. Davis, and D. Harries, "The role of micro hydro power systems in remote rural electrification: A case study in the Bawan Valley, Borneo," *Procedia Eng.*, vol. 49, pp. 189–196, 2012.

[3] A. W. Dametew, "Design and Analysis of Small Hydro Power for Rural Electrification Chapter - One," *Glob. J. Res. Eng.*, no. January, 2016.

[4] A. Aboikoni, S. Alimoestar, and R. H. Van Els, "Potentials for renewable energy technology in the rural electrification of Suriname: technological and institutional challenges," Paramaribo, 2017.

[5] C. Lo kioeng shioe, "Suralco maintance intern report 2017," 2017.

[6] S. Naipal, "Verslag orietatie aan de bovenloop van de Suriname rivier en sipaliwinie rivier," 2003.

[7] S. Naipal, "Mini-Micro Hydropower – a Solution to Sustainable Development in the Interior of Suriname," 2012.

[8] A. Aboikoni and S. Alimoestar, "FINAL REPORT INTERNSHIP MSC RET," no. January, pp. 1–25, 2019.

[9] C. King, "Het belang van micro-centrales bij de ontwikkeling van het binnenland van Suriname," 1981.

[10] Del Prado, "Suriname's eerste mini watrkrachtcentrale," *ELDORADO*, vol. 2, pp. 30–40, 1982.

[11] R. H. Van Els, "De Puketi micro-waterkrachtcentrale in het binnenland van Suriname : implementatie , rehabilitatie en ervaringen," *Acad. J. Suriname*, vol. 2012, no. 3, pp. 276–

291, 2012.

[12] G. Orban, “Miniwaterkrachtcentrale mogelijk augustus in werking,” *De Ware Tijd*, Paramaribo, 04-Jul-2014.

[13] Obsession Magazine, “Zoveelste vertraging oplevering miniwaterkrachtcentrale Gran Olo Sula – Eén transformator ongeschikt voor stroomleverantie,” *Obsession magazine*, Paramaribo, Oct-2014.

[14] EBS, “Final Commissioning Report Phase 1 Gran Olo Mini Hydropower Plant.,” 2017.

[15] R. H. Van Els, “Report Gran Holo 2018_07_15,” 2018.

[16] S. Mbabazi and J. Leary, “Mini-project report 1 Analysis and Design of Electronic Load Controllers for Micro-hydro Systems in the Developing World,” no. March, 2010.

[17] A. Harvey, A. Brown, P. Hettiarachi, and A. Inversin, *Micro-Hydro-Design-Manual-Adam-Harvey.pdf*. 2013.

[18] G. Castillo, L. Ortega, M. Pozo, and X. Dominguez, “Control of an island Micro-hydropower Plant with Self-excited AVR and combined ballast load frequency regulator,” *2016 IEEE Ecuador Tech. Chapters Meet. ETCM 2016*, 2016.

[19] A. Poetoe, “spanningsproblemen als gevolg van de groei van de belasting in het EPAR systeem van de n.v. E.B.S. en mogelijke remedies,” 2004.

[20] IRENA, “Hydropower,” *Renew. Energy Technol. Cost Anal. Ser.*, vol. 1: Power s, no. 3/5, p. 44, 2012.

[21] World Energy Counsel, “World Energy Resources | 2016,” 2016.

[22] International Renewable Energy Agency (IRENA), *Renewable Power Generation Costs in 2018*. 2018.

[23] IRENA, “Renewable Energy and Jobs Annual Review 2019,” *Int. Renew. Energy Agency*, no. May, p. 12, 2019.

[24] R. A. J. K. Bairwa, “Types of plants,” *Environ. Prot.*, pp. 2002–2002, 2002.

[25] United Nations Industrial Development Organization (UNIDO) and International Center on Small Hydro Power (ICSHP), “World Small Hydropower Development Report 2016 Executive Summary,” 2016.

[26] A. S. Sánchez, E. A. Torres, and R. A. Kalid, “Renewable energy generation for the rural electrification of isolated communities in the Amazon Region,” *Renew. Sustain. Energy Rev.*, vol. 49, pp. 278–290, Sep. 2015.

[27] Practical Action, “MICRO-HYDRO POWER,” vol. 44, no. 871954, 2015.

[28] United States Department of Energy, “Types of Hydropower Plants | Department of Energy,” 2016. [Online]. Available: http://energy.gov/eere/water/types-hydropower-plants.

[29] R. Mac Donald and N. Sloot, “Experimental and Numerical Study of the Performance Characteristics of a Pico Hydro Turbine Manufactured by Indalma Industries Inc .,” 2014.

[30] S. Dixon and A. Hall, “Fluid Mechanics and Thermodynamics ofTurbomachinery. 6th ed.,” 2010.

[31] M. Sinagra, V. Sammartano, C. Arico, A. Collura, and T. Tucciarelli, “Cross-flow turbine design for variable operating conditions,” 2014.

[32] Ossberger, “Ossberger cross flow turbine,” 2017. [Online]. Available: https://ossberger.de/en/hydropower-technology/ossbergerr-crossflow-turbine/.

[33] Dongfang Power, “Dongfang power,” 2019. [Online]. Available: http://www.dfpower.biz/hpp-products/tubular-turbine-bulb-turbine.html.

[34] D. dos S. Oliveira, S. S. F. Rosa, and L. G. Noleto, “Modeling and Experimental Evaluation in the New Hydraulic Turbine Used in the Amazon Region,” *Glob. J. Eng. Sci. Res. Manag.*, vol. 2, no. 8, pp. 57–66, 2015.

[35] K. D. Alves, “Desenvolvimento de regulador de velocidade para Turbina Indalma com sintonia PID baseado em Otimização por Enxame de Partículas (PSO),” 2018.

[36] R. Thapar, “Modern_Hydroelectric_Engineering_Practice,” vol. II, pp. 147–173.

[37] S. N. Eduard Doujak, “The Gran-olo sula Project:MHP implementation in the Hinterland of Suriname,” 2008.

[38] B. Shakuntla, S. K. Aggarwal, and K. S. Sandhu, “Electronics Based Dump Load Controller (DLC) for an Grid Isolated,” 2015.

[39] N. P. Gyawali, “Universal electronic load controller for microhydro power plant,” *IEEE Int. Conf. Control Autom. ICCA*, vol. 2016-July, pp. 288–292, 2016.

[40] IEA DSM, “The Role of Advanced Metering and Load Control in Supporting Electricity Networks,” *Res. Rep. No 5 Task XV Int. Energy Agency Demand Side Manag. Program.*, 2008.

[41] IEA DSM, “Implementing Agreement on Demand-Side Management Technologies and Programmes,” *2009 Annu. report‖, task XIX Micro Demand Response Energy, January 2010, Stock.*, 2009.

[42] B. P. Vande Meerssche, G. Van Ham, D. Van Hertem, and G. Deconinck, “Balancing renewables by demand side management : local and global potential of loads,” 2013.

[43] P. Abaravicius, J.;Pyrko, “Load management from an environmental perspective, Energy & Environment,” 2006.

[44] A. B. Cuesta, F. J. Gomez-Gil, J. V. M. Fraile, J. A. Rodríguez, J. R. Calvo, and J. P. Vara,

"Feasibility of a simple small wind turbine with variable-speed regulation made of commercial components," *Energies*, vol. 6, no. 7, pp. 3373–3391, 2013.

[45] S. Mohod and M. Aware, "Laboratory development of wind turbine simulator using variable speed induction motor," *Int. J. Eng. Sci. Technol.*, vol. 3, no. 5, pp. 73–82, 2011.

[46] C. I. Martínez-Márquez, J. D. Twizere-Bakunda, D. Lundback-Mompó, S. Orts-Grau, F. J. Gimeno-Sales, and S. Seguí-Chilet, "Small wind turbine emulator based on lambda-Cp curves obtained under real operating conditions," *Energies*, vol. 12, no. 13, 2019.

[47] R. Mac Donald and N. Sloot, "Experimental Assessment and Numerical Analysis of an Indalma Hydraulic Turbine," pp. 2–5, 2014.

[48] P. . Randall W. Whitesides, "Basic Pump Parameters and the Affinity Laws," *PDH Online*, vol. 125, pp. 8–12, 2012.

[49] Songle Relay, "Power Relay SRD-5VDC-SL-C datasheet." pp. 1–2, 2000.

[50] B. Shakuntla, S. K. Aggarwal, and K. S. Sandhu, "Electronics Based Dump Load Controller (DLC) for an Grid Isolated," *Int. J. Emerg. Technol. 6(2) 09-14(2015)*, vol. 6, no. 2, pp. 9–14, 2015.

[51] P. R. Bevington, "First Year Physics Laboratory Manual," in *First Year Physics Laboratory Manual*, 2002, pp. xvii–xxviii.

[52] Anton de Kom Universiteit van Suriname, *Foutenleer diktaat 2013*. 2013.

[53] A. Aboikoni, "Design hydropower plant with Indalma turbine at the Tapawatra fall within the perspective of sustainable development," pp. 1–77, 2019.

[54] WEG, "Frequency Inverter WEG CFW700," *Energy*. 2014.

[55] K. S. Rao and R. Mishra, "Comparative study of P, PI and PID controller for speed control

of VSI-fed induction motor," *Int. J. Eng. Dev. Res.*, vol. 2, no. 2, pp. 2321–9939, 2014.

[56] J. Zhang, "MODELING, DESIGN AND SIMULATION OF A LOW COST SUPERVISORY CONTROLLER FOR RAMEA HYBRID POWER SYSTEM," *Pontif. Univ. Catol. del Peru*, vol. 8, no. 33, p. 44, 2014.

[57] WEG, "Variable speed drives," *Energy*. 1999.

Appendix A- VSD

The Variable speed drive (VSD) is a type of motor controller, which varies the frequency and voltage supplied to the electric motor in order to control the speed of such an electric motor. In Figure 41 the main components of this VSD is displayed. The VSD used for this system is a refurbished CFW700 manufactured and serviced by WEG in Brazil, which has a power range between 1.5HP and 150HP. The supply voltage to the VSD is 380 – 480 V and the motor voltage can vary between 220 – 480 V. The model number is CFW700C38P0T4DB20. From the WEG CFW700 inverter model number, CFW700C38P0T4DB20, most of its features can be decoded form the appendix tables, which is given by the manufacturer. This VSD inverter will be used to control the electric motor, which will drive the pump of the hydropower laboratory. The specifications for this VSD are displayed in Table A.1 [57].

Table A.1: VSD inverter model number decoded [57]

CFW700C38P0T4DB20	
CFW700	Series number of the inverter.
C	Frame size in mm: 378 x 220 x 293 (H x W x D)
38P0	Max. output current is 38A
T	Three-phase voltage
4	Rated voltage 380V – 480V
DB	Braking IGBT available
20	Degree of protection: IP20
Blank	No RFI filter
Blank	No STI function
Blank	No external power supply board

In some applications high inertia and short deceleration times are of great essential. With these kind of application a large amount of energy is returned from the motor to the VSD. Traditional VSDs handles this energy by dissipating it as heat in power resistors, which are usually large and very expensive. Another negative point is that the heat dissipation has to be taken into consideration during installation. This model inverter features a special braking method called

Optimal Braking, as an alternative to the use of braking resistors, where IGBT's are used. This innovation requires no resistor and still delivers rated torque with high performance [57].

The WEG CFW700 can be used for three-phase electrical motors for different applications, ex:

- Centrifugal pumps
- Fans / exhausters
- Compressors
- Conveyor belts
- Roller tables
- Granulators / palletizers
- Rotary filters
- Paper and Cellulose/ Wood Machines
- Chemical and Petrochemical process
- Ironworks and Metallurgy industries

Table A.2: CFW700 dimension, weight and temperature

Model	Frame size	NEMA1 Dimension mm (in) H	NEMA1 W	NEMA1 D	IP20 / IP21 H	IP20 / IP21 W	IP20 / IP21 D	IP20 Maximum surrounding air temperature with no derating °C (°F) _ ND/HD	NEMA1 / IP21 Maximum surrounding air temperature with no derating °C (°F) _ ND/HD	Weight kg (lb)	Braking IGBT
CFW700A06P0S2	A	305 (12.02)	145 (5.71)	227 (8.94)	247 (9.73)	145 (5.71)	227 (8.94)	50 (122)_ND/HD	50 (122)_ND/HD	6.3 (13.9)	Standard
CFW700A07P0S2								50 (122)_ND/HD	45 (113)_ND/HD		
CFW700A10P0S2								50 (122)_ND/HD	50 (122)_ND/HD		
CFW700A06P0B2								50 (122)_ND/HD	50 (122)_ND/HD		
CFW700A07P0B2								50 (122)_ND/HD	45 (113)_ND/HD		
CFW700A07P0T2								50 (122)_ND/HD	45 (113)_ND/HD		
CFW700A10P0T2								50 (122)_ND/HD	50 (122)_ND/HD		
CFW700A13P0T2								45 (113)_ND 50 (122)_HD	45 (113)_ND 50 (122)_HD		
CFW700A16P0T2								50 (122)_ND/HD	50 (122)_ND/HD		
CFW700B24P0T2	B	351 (13.82)	190 (7.46)	227 (8.94)	293 (11.53)	190 (7.46)	227 (8.94)	45 (113)_ND/HD	40 (104)_ND/HD	10.4 (22.9)	
CFW700B28P0T2								50 (122)_ND/HD	50 (122)_ND/HD		
CFW700B33P0T2								50 (122)_ND/HD	45 (113)_ND 50 (122)_HD		
CFW700C45P0T2	C	448.1 (17.64)	220 (8.67)	293 (11.52)	378 (14.88)	220 (8.67)	293 (11.52)	50 (122)_ND/HD	50 (122)_ND/HD	20.5 (45.2)	
CFW700C54P0T2								50 (122)_ND/HD	50 (122)_ND/HD		
CFW700C70P0T2								50 (122)_ND/HD	50 (122)_ND/HD		
CFW700D86P0T2	D	550 (21.63)	300 (11.81)	305 (12.00)	504 (19.84)	300 (11.81)	305 (12.00)	50 (122)_ND/HD	50 (122)_ND/HD	32.6 (71.8)	
CFW700D105T2								50 (122)_ND/HD	50 (122)_ND/HD		
CFW700E0142T2	E	735 (28.94)	335 (13.2)	358 (14.1)	620 (24.4)	335 (13.2)	358 (14.1)	45 (113)_ND/HD	45 (113)_ND/HD	650 (143.3)	Optional
CFW700E0180T2		828.9 (32.63)						45 (113)_ND/HD	45 (113)_ND/HD		
CFW700E0211T2								45 (113)_ND/HD	45 (113)_ND/HD		
CFW700A03P6T4	A	305 (12.02)	145 (5.71)	227 (8.94)	247 (9.73)	145 (5.71)	227 (8.94)	50 (122)_ND/HD	50 (122)_ND/HD	6.3 (13.9)	Standard
CFW700A05P0T4								50 (122)_ND/HD	50 (122)_ND/HD		
CFW700A07P0T4								45 (113)_ND 50 (122)_HD	40 (104)_ND 50 (122)_HD		
CFW700A10P0T4								45 (113)_ND/HD	45 (113)_ND/HD		
CFW700A13P5T4								50 (122)_ND/HD	50 (122)_ND/HD		
CFW700B17P0T4	B	351 (13.82)	190 (7.46)	227 (8.94)	293 (11.53)	190 (7.46)	227 (8.94)	50 (122)_ND/HD	50 (122)_ND/HD	10.4 (22.9)	
CFW700B24P0T4								50 (122)_ND/HD	40 (104)_ND 45 (122)_HD		
CFW700B31P0T4								50 (122)_ND/HD	50 (122)_ND/HD		
CFW700C38P0T4	C	448.1 (17.64)	220 (8.67)	293 (11.52)	378 (14.88)	220 (8.67)	293 (11.52)	50 (122)_ND/HD	50 (122)_ND/HD	20.5 (45.2)	
CFW700C45P0T4								50 (122)_ND/HD	50 (122)_ND/HD		
CFW700C58P5T4								50 (122)_ND/HD	50 (122)_ND/HD		
CFW700D70P5T4	D	550 (21.63)	300 (11.81)	305 (12.00)	504 (19.84)	300 (11.81)	305 (12.00)	50 (122)_ND/HD	50 (122)_ND/HD	32.6 (71.8)	
CFW700D88P0T4								50 (122)_ND/HD	50 (122)_ND/HD		
CFW700E0105T4	E	735 (28.94)	335 (13.2)	358 (14.1)	620 (24.4)	335 (13.2)	358 (14.1)	45 (113)_ND/HD	45 (113)_ND/HD	65.0 (143.3)	Optional
CFW700E0142T4								45 (113)_ND/HD	45 (113)_ND/HD		
CFW700E0180T4		828.9 (32.63)						45 (113)_ND/HD	45 (113)_ND/HD		
CFW700E0211T4								45 (113)_ND/HD	45 (113)_ND/HD		
CFW700B02P9T5	B	351 (13.82)	190 (7.46)	227 (8.94)	293 (11.53)	190 (7.46)	227 (8.94)	50 (122)_ND/HD	50 (122)_ND/HD	10.4 (22.9)	Standard
CFW700B04P2T5								50 (122)_ND/HD	50 (122)_ND/HD		
CFW700B07P0T5								50 (122)_ND/HD	50 (122)_ND/HD		
CFW700B10P0T5								50 (122)_ND/HD	50 (122)_ND/HD		
CFW700B12P0T5								50 (122)_ND/HD	50 (122)_ND/HD		
CFW700B17P0T5								50 (122)_ND/HD	50 (122)_ND/HD		
CFW700D22P0T5	D	550 (21.63)	300 (11.81)	305 (12.00)	504 (19.84)	300 (11.81)	305 (12.00)	50 (122)_ND/HD	50 (122)_ND/HD	32.6 (71.8)	
CFW700D27P0T5								50 (122)_ND/HD	50 (122)_ND/HD		
CFW700D32P0T5								50 (122)_ND/HD	50 (122)_ND/HD		
CFW700D44P0T5								50 (122)_ND/HD	50 (122)_ND/HD		
CFW700E53P0T5	E	735 (28.94)	335 (13.2)	358 (14.1)	675 (26.57)	335 (13.2)	358 (14.1)	45 (113)_ND/HD	45 (113)_ND/HD	65.0 (143.3)	Optional
CFW700E63P0T5								45 (113)_ND/HD	45 (113)_ND/HD		
CFW700E80P0T5								45 (113)_ND/HD	45 (113)_ND/HD		
CFW700E0107T5								45 (113)_ND/HD	45 (113)_ND/HD		
CFW700E0125T5								45 (113)_ND/HD	45 (113)_ND/HD		
CFW700E0150T5								45 (113)_ND/HD	45 (113)_ND/HD		

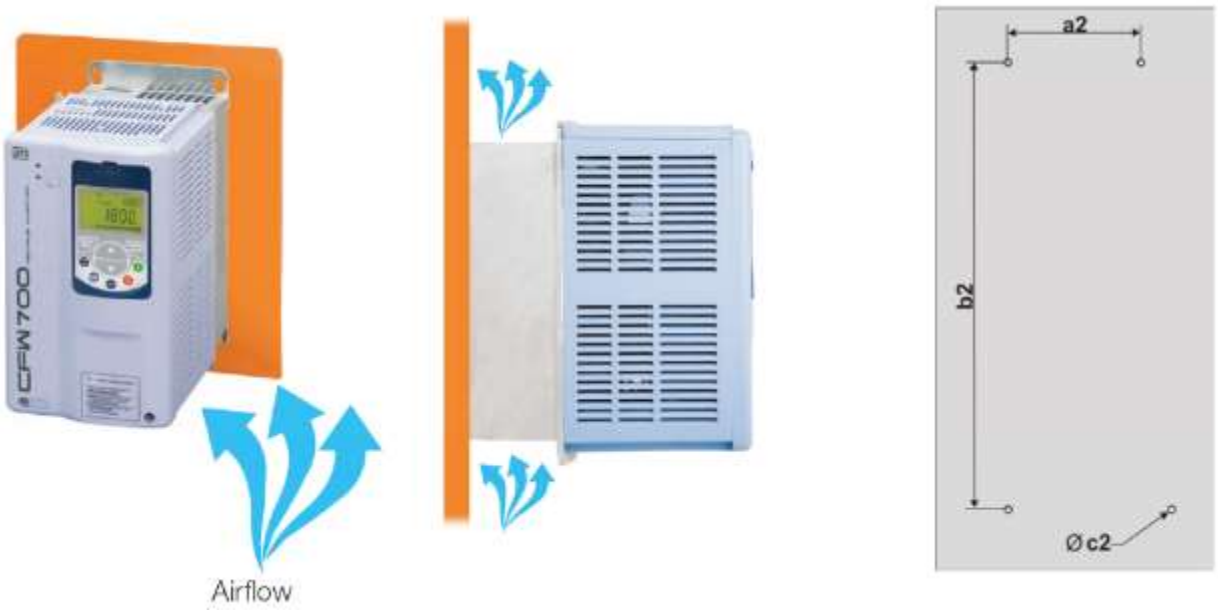

Figure A.0.1: VSD surface installation

Figure A.0.2: CFW700 Flange mounting

Table A.0.3: CFW700 frame size

Frame size	a2 mm (in)	b2 mm (in)	c2 (M)	a3 mm (in)	b3 mm (in)	c3 (M)	d3 mm (in)	e3 mm (in)
A	115 (4.53)	250 (9.85)	M5	130 (5.12)	240 (9.45)	M5	135 (5.32)	225 (8.86)
B	150 (5.91)	300 (11.82)	M5	175 (6.89)	285 (11.23)	M5	179 (7.05)	271 (10.65)
C	150 (5.91)	375 (14.77)	M6	195 (7.68)	365 (14.38)	M6	205 (8.08)	345 (13.59)
D	200 (7.88)	525 (20.67)	M8	275 (10.83)	517 (20.36)	M8	285 (11.23)	485 (19.10)
E	200 (7.8)	650 (25.6)	M8	275 (10.8)	635 (25)	M8	315 (12.40)	615 (24.21)

Table A.0.4: Distance between power and signal cables

Rated Output Inverter Current	Cable Length(s)	Minimum Separation Distance
≤ 24 A	≤ 100 m (330 ft) > 100 m (330 ft)	≥ 10 cm (3.94 in) ≥ 25 cm (9.84 in)
≥ 28 A	≤ 30 m (100 ft) > 30 m (100 ft)	≥ 10 cm (3.94 in) ≥ 25 cm (9.84 in)

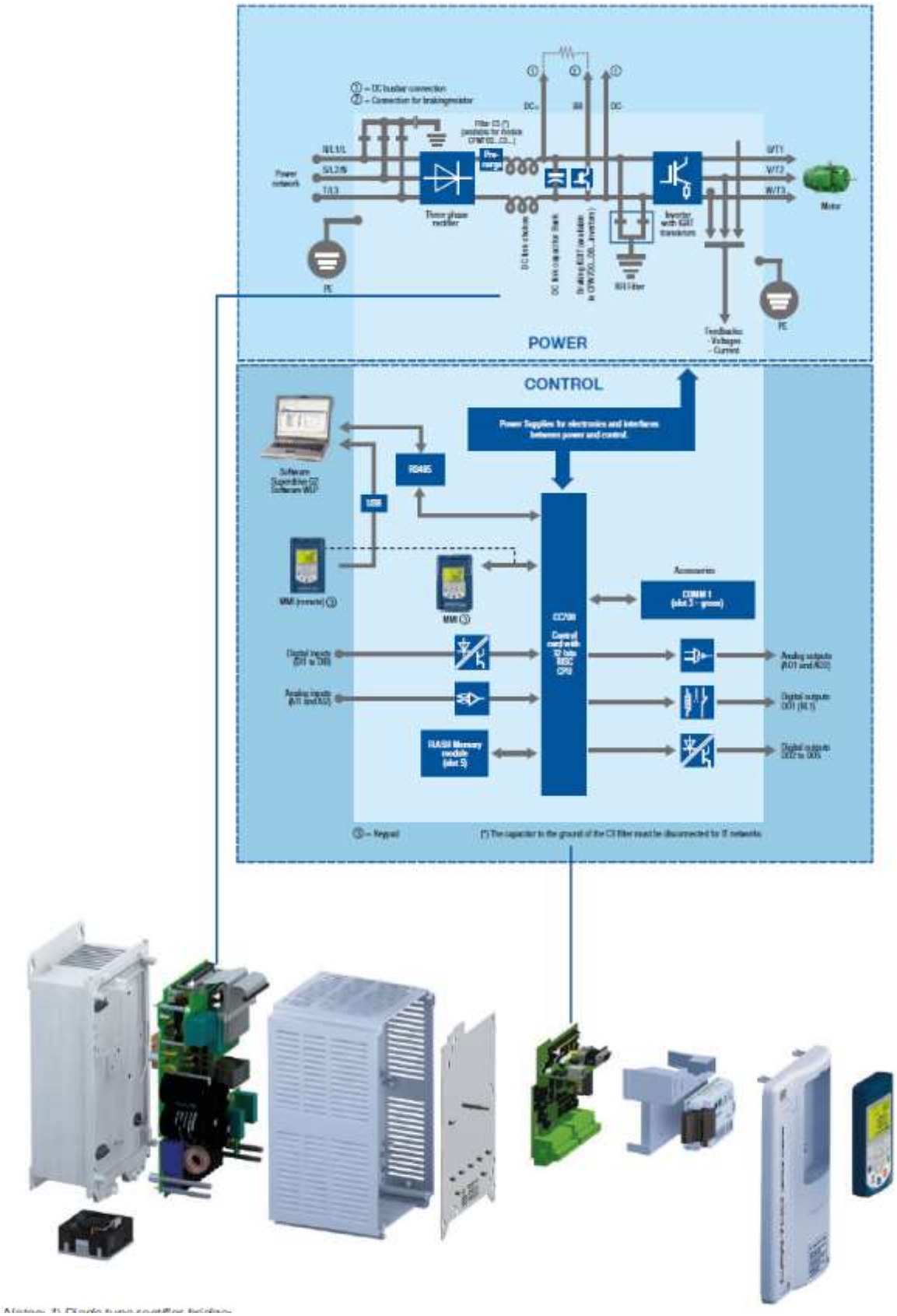

Figure A.0.3: WEG VSD

Appendix B1- Proposed test setup

In the figures below the proposed test setup is presented, which was designed during the internship. For further details of this setup open the following link:

https://drive.google.com/open?id=15sY4qz2iyLu0WkKohLCsj824regXI7Jf

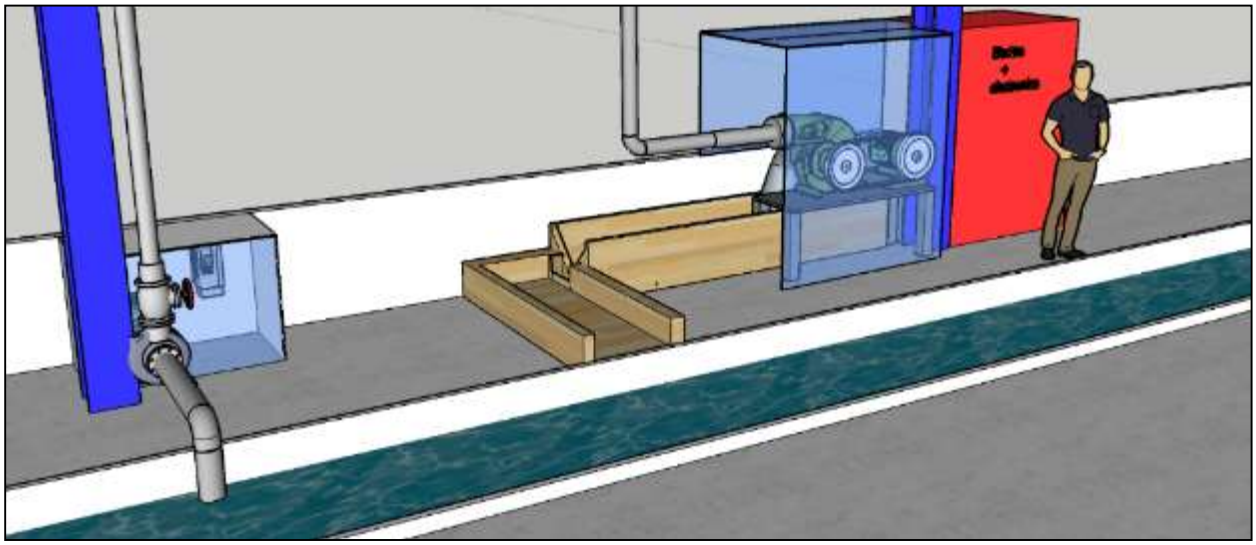

Figure B.1: Pico hydropower laboratory design 1

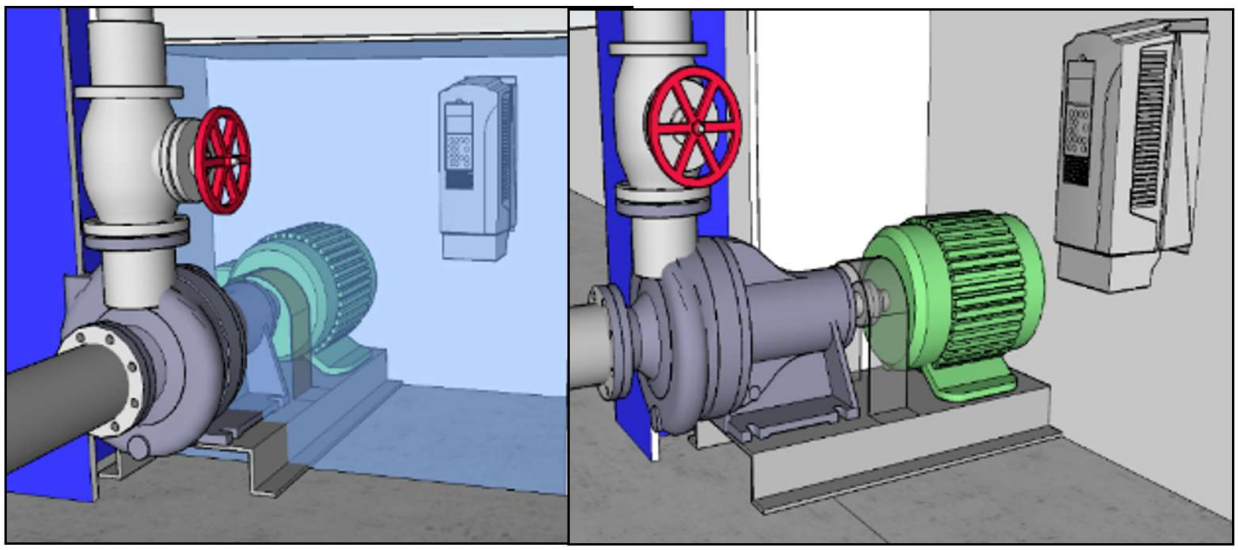

Figure B.2: Pico hydropower laboratory design 2

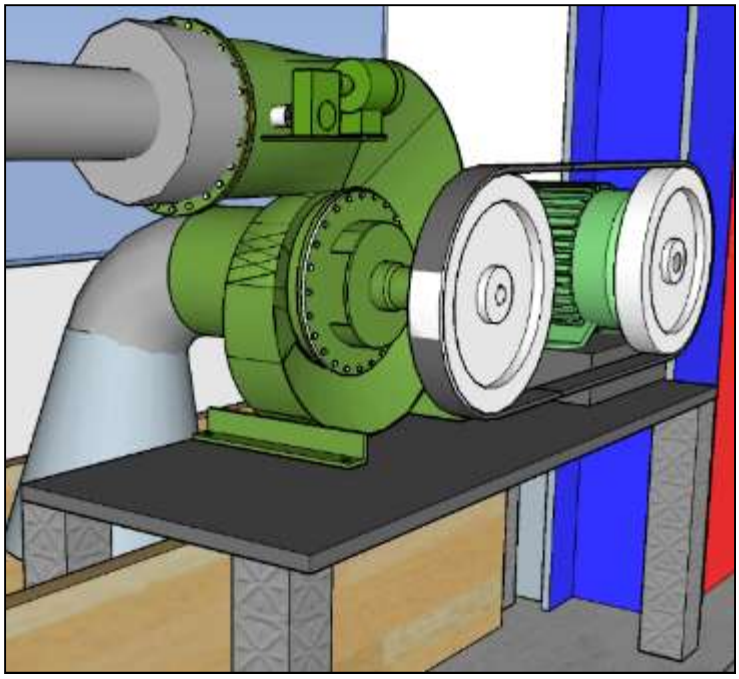

Figure B.3: Pico hydropower laboratory design 3

Appendix C- Arduino code

The full Arduino code (to control the dump loads and the virtual Indalma) is available for download:

https://drive.google.com/open?id=15sY4qz2iyLu0WkKohLCsj824regXI7Jf

Appendix D – Measurement tables

Table C.1: Measurement results

AC control with turbine characteristics								
Time	**AC (V)**	**IL (A)**	**IdL (A)**	**PdL(W)**	**PL(W)**	**Pgen(W)**	**RPM**	**F(Hz)**
08:56:41	111.58	0	6.19	690.24	0	690.24	1522.42	50.7
08:56:46	110.7	0	6.18	684.45	0	684.45	1525.13	50.8
08:56:51	110.7	0	6.2	686.49	0	686.49	1524.18	50.8
08:56:57	111.38	0	6.2	690.18	0	690.18	1522.45	50.7
08:57:02	111.31	0	6.19	688.56	0	688.56	1523.21	50.8
08:57:07	110.74	0	6.18	684.21	0	684.21	1525.24	50.8
08:57:13	110.45	0	6.2	685.14	0	685.14	1524.8	50.8
08:57:18	111.38	0	6.2	690.49	0	690.49	1522.31	50.7
08:57:23	111.11	0	6.18	686.86	0	686.86	1524	50.8
08:57:29	110.45	0	6.17	681.63	0	681.63	1526.44	50.9
08:57:34	110.02	0.68	6.15	676.26	74.53	750.79	1493.39	49.8
08:57:39	108.34	0.71	5.41	586.51	76.94	663.45	1534.85	51.2
08:57:44	110.25	0.69	5.43	598.57	76.47	675.04	1529.5	51.0
08:57:49	110.99	0.69	5.44	603.52	77.12	680.65	1526.9	50.9
08:57:54	110.7	0.7	5.42	600.17	77.13	677.3	1528.45	50.9
08:58:00	110.27	0.69	5.42	597.93	76.47	674.4	1529.8	51.0
08:58:05	110.32	0.69	5.42	598.29	76.65	674.94	1529.55	51.0
08:58:10	110.5	0.7	5.42	598.56	77.07	675.64	1529.23	51.0
08:58:15	110.25	0.69	5.42	597.51	76.45	673.96	1530	51.0
08:58:20	110.45	0.69	5.4	596.08	76.67	672.75	1530.56	51.0
08:58:26	109.15	1.46	5.36	585.23	159.46	744.69	1496.38	49.9
08:58:31	106.78	1.48	4.65	496.35	158.05	654.4	1538.99	51.3
08:58:36	108.99	1.47	4.65	506.79	160.48	667.27	1533.09	51.1
08:58:41	109.19	1.48	4.65	507.25	161.14	668.39	1532.58	51.1
08:58:46	108.9	1.47	4.64	504.96	160.23	665.19	1534.05	51.1
08:58:51	108.65	1.47	4.65	505.15	159.66	664.81	1534.22	51.1
08:58:57	108.9	1.47	4.65	506.48	160.17	666.65	1533.38	51.1
08:59:02	108.88	1.47	4.64	505.6	160.38	665.98	1533.69	51.1
08:59:07	108.65	1.47	4.64	504.03	160.01	664.03	1534.58	51.2
08:59:12	108.65	1.47	4.65	505.57	159.76	665.32	1533.99	51.1
08:59:17	109.1	1.47	4.65	507.42	160.64	668.07	1532.72	51.1
08:59:22	108.92	1.94	4.61	501.78	211.46	713.24	1511.55	50.4
08:59:28	105.99	2.15	3.87	410.07	227.41	637.48	1546.67	51.6
08:59:33	107.07	2.14	3.87	414.45	229.64	644.09	1543.68	51.5
08:59:38	107.34	2.15	3.88	416.58	230.76	647.33	1542.21	51.4

08:59:43	107.32	2.15	3.88	416.89	230.69	647.58	1542.1	51.4
08:59:48	107.3	2.15	3.88	416.63	230.38	647.01	1542.36	51.4
08:59:53	107.57	2.15	3.88	417.08	231.11	648.19	1541.82	51.4
08:59:59	107.5	2.15	3.89	418.26	231.28	649.53	1541.21	51.4
09:00:04	108.65	0	3.93	426.93	0	426.93	1635.57	54.5
09:00:09	111.22	0.29	6.22	692.22	31.99	724.21	1506.3	50.2
09:00:14	110.56	0	5.38	594.91	0	594.91	1565.59	52.2
09:00:20	108.74	0	6.14	667.29	0	667.29	1533.08	51.1
09:00:25	108.65	0	6.19	672.55	0	672.55	1530.66	51.0
09:00:30	110.47	0	6.19	683.99	0	683.99	1525.34	50.8
09:00:36	110.81	0	6.19	686.09	0	686.09	1524.36	50.8
09:00:41	110.68	0	6.19	685.17	0	685.17	1524.79	50.8
09:00:46	110.68	0	6.19	685.21	0	685.21	1524.77	50.8
09:00:51	110.47	0	6.19	683.75	0	683.75	1525.46	50.8
09:00:57	110.45	0	6.14	677.96	0	677.96	1528.15	50.9
09:01:02	107.75	2.72	5.86	631.82	293.28	925.1	1400.58	46.7
09:01:07	94.22	2.78	2.93	276.07	262.13	538.2	1590.01	53.0
09:01:12	95.43	2.69	3.71	354.43	256.72	611.15	1558.44	51.9
09:01:18	100.61	2.82	3.85	387.28	283.62	670.9	1531.42	51.0
09:01:23	104.96	2.86	3.1	325	299.98	624.99	1552.28	51.7
09:01:28	106.35	2.86	3.12	331.33	304.48	635.81	1547.42	51.6
09:01:33	106.4	2.87	3.1	329.34	304.85	634.19	1548.15	51.6
09:01:38	105.95	2.85	3.1	328.19	302.04	630.23	1549.93	51.7
09:01:43	105.7	2.86	3.1	327.6	301.78	629.38	1550.31	51.7
09:01:49	106.26	2.86	3.11	330.63	304.27	634.9	1547.83	51.6
09:01:54	106.17	2.86	3.09	328.54	303.78	632.32	1548.99	51.6
09:01:59	106.38	2.86	3.1	329.55	303.8	633.35	1548.53	51.6
09:02:04	106.4	2.86	3.1	330.09	304.47	634.57	1547.98	51.6
09:02:09	106.4	2.86	3.1	329.5	304.12	633.61	1548.41	51.6
09:02:15	105.32	3.61	3.07	322.94	380.3	703.24	1516.3	50.5
09:02:20	102.5	3.62	2.32	237.75	370.92	608.67	1559.53	52.0
09:02:25	103.47	3.62	2.33	241.33	374.52	615.85	1556.35	51.9
09:02:30	104.82	3.64	2.33	244.48	381.67	626.15	1551.76	51.7
09:02:35	104.64	3.63	2.33	243.75	380.21	623.96	1552.74	51.8
09:02:41	104.6	3.63	2.33	243.71	379.99	623.7	1552.86	51.8
09:02:46	104.6	3.63	2.33	243.58	380.2	623.78	1552.82	51.8
09:02:51	104.75	3.63	2.33	244.49	380.65	625.14	1552.21	51.7
09:02:56	104.82	3.63	2.34	244.8	380.96	625.75	1551.94	51.7
09:03:01	104.82	3.63	2.33	244.5	380.65	625.15	1552.2	51.7
09:03:07	104.82	4.08	2.32	243.66	427.78	671.44	1531.17	51.0
09:03:12	103.97	4.11	2.32	240.77	427.15	667.92	1532.79	51.1
09:03:17	104.01	4.08	2.3	239.28	424.87	664.15	1534.53	51.2
09:03:22	102.1	4.07	2.3	235.09	415.27	650.36	1540.83	51.4
09:03:27	101.89	4.08	2.31	235.46	415.31	650.77	1540.65	51.4
09:03:33	102.57	4.08	2.31	236.49	418.35	654.84	1538.79	51.3
09:03:38	102.41	4.08	2.31	236.42	417.61	654.04	1539.16	51.3
09:03:43	102.57	4.08	2.31	236.59	418.08	654.67	1538.87	51.3
09:03:48	102.8	4.08	2.31	237.3	419.25	656.56	1538.01	51.3
09:03:53	102.57	4.08	2.31	236.63	418.1	654.73	1538.84	51.3
09:03:58	102.57	4.71	2.29	234.57	483.02	717.58	1509.48	50.3
09:04:04	99.62	4.84	1.14	113.19	482.02	595.21	1565.46	52.2
09:04:09	102.34	4.9	0.79	80.59	501.13	581.72	1571.35	52.4
09:04:14	103.25	4.9	0.79	81.46	506.24	587.7	1568.75	52.3

09:04:19	104.15	4.93	0.79	82.47	512.96	595.43	1565.37	52.2
09:04:25	104.78	4.93	0.79	82.9	516.24	599.15	1563.73	52.1
09:04:30	104.19	4.91	0.79	82.32	512.01	594.33	1565.85	52.2
09:04:35	103.92	4.91	0.79	82.09	510.56	592.65	1566.59	52.2
09:04:40	104.15	4.91	0.79	82.25	511.79	594.04	1565.98	52.2
09:04:45	103.97	4.92	0.79	82.1	511.1	593.2	1566.34	52.2
09:04:51	103.92	5.28	0.78	81.48	548.19	629.67	1550.18	51.7
09:04:56	101.49	5.7	0	0	578.57	578.57	1572.72	52.4
09:05:01	102.82	5.71	0	0	587.34	587.34	1568.91	52.3
09:05:07	103	5.71	0	0	588.12	588.12	1568.56	52.3
09:05:12	102.34	5.7	0	0	583.1	583.1	1570.75	52.4
09:05:17	102.46	5.69	0	0	583.25	583.25	1570.69	52.4
09:05:23	102.28	5.69	0	0	582.21	582.21	1571.14	52.4
09:05:28	102.34	5.69	0	0	582.27	582.27	1571.11	52.4
09:05:33	102.34	5.69	0	0	582.11	582.11	1571.18	52.4
09:05:39	103.47	4.35	0	0	450.14	450.14	1626.3	54.2
09:05:44	106.58	4.37	0.81	86.03	465.8	551.82	1584.22	52.8
09:05:49	107.28	4.35	0.8	86.32	466.99	553.31	1583.59	52.8
09:05:54	106.62	4.34	0.8	85.49	462.9	548.39	1585.68	52.9
09:06:00	106.49	4.35	0.8	85.25	462.89	548.14	1585.79	52.9
09:06:05	106.6	4.34	0.8	85.36	462.67	548.03	1585.84	52.9
09:06:10	106.4	4.34	0.8	85.12	462.25	547.37	1586.12	52.9
09:06:15	106.53	4.34	0.8	85.58	462.64	548.22	1585.76	52.9
09:06:21	107.52	2.85	0.81	86.94	306.33	393.28	1648.81	55.0
09:06:26	108.63	2.85	2.38	258.55	309.42	567.96	1577.3	52.6
09:06:31	109.57	2.82	2.37	259.55	308.48	568.03	1577.28	52.6
09:06:36	109.1	2.82	2.37	258.89	307.15	566.05	1578.13	52.6
09:06:41	109.21	2.82	2.38	259.71	308.19	567.9	1577.33	52.6
09:06:47	109.55	2.82	2.38	260.31	309.17	569.47	1576.65	52.6
09:06:52	109.78	2.82	2.38	260.94	309.9	570.85	1576.06	52.5
09:06:57	109.64	2.82	2.37	260.25	309.43	569.68	1576.57	52.6
09:07:02	109.33	2.81	2.37	259.13	307.32	566.45	1577.96	52.6
09:07:07	109.1	2.81	2.38	259.49	306.93	566.42	1577.97	52.6
09:07:13	109.78	2.06	2.38	261.68	225.97	487.64	1611.07	53.7
09:07:18	110.92	2.06	3.17	351.31	228.97	580.27	1571.98	52.4
09:07:23	110.9	2.05	3.17	351.06	227.53	578.6	1572.71	52.4
09:07:28	110.65	2.05	3.16	350.06	227.37	577.43	1573.21	52.4
09:07:33	110.47	2.04	3.16	349.54	225.9	575.44	1574.07	52.5
09:07:38	110.41	2.04	3.16	348.98	225.52	574.49	1574.48	52.5
09:07:44	110.45	2.05	3.16	349.29	225.95	575.23	1574.16	52.5
09:07:49	110.61	1.61	3.17	350.99	178.22	529.21	1593.8	53.1
09:07:54	111.74	1.27	3.95	441.38	142.44	583.82	1570.44	52.3
09:07:59	112.48	1.26	3.95	444.36	141.3	585.66	1569.64	52.3
09:08:04	112.39	1.26	3.95	444.04	141.53	585.56	1569.68	52.3
09:08:10	112.3	1.26	3.95	443.38	141.47	584.86	1569.99	52.3
09:08:15	112.3	1.26	3.95	443.56	141.23	584.78	1570.02	52.3
09:08:20	112.25	1.26	3.95	443.06	140.88	583.94	1570.38	52.3
09:08:25	112.07	1.26	3.95	442.6	141.45	584.05	1570.34	52.3
09:08:30	112.25	1.26	3.95	443.42	141.23	584.65	1570.08	52.3
09:08:35	112.25	0.8	3.96	444.17	89.43	533.6	1591.95	53.1
09:08:41	113.15	0.79	4.73	535.25	89.01	624.26	1552.61	51.8
09:08:46	113.51	0.77	4.72	535.92	87.58	623.5	1552.94	51.8
09:08:51	113.49	0.77	4.7	533.48	87.41	620.89	1554.11	51.8

09:08:56	112.12	0.77	4.7	527.2	86.42	613.62	1557.34	51.9
09:09:01	112.03	0.77	4.71	528.07	86.44	614.51	1556.95	51.9
09:09:07	112.97	0.77	4.71	532.5	87	619.5	1554.73	51.8
09:09:12	112.93	0.77	4.71	532.37	86.95	619.32	1554.81	51.8
09:09:17	112.75	0	4.73	533.56	0	533.56	1591.97	53.1
09:09:22	114.28	0	5.56	635.13	0	635.13	1547.73	51.6
09:09:28	115.63	0	5.56	642.84	0	642.84	1544.25	51.5
09:09:33	115.79	0	5.47	633.64	0	633.64	1548.4	51.6
09:09:38	112.7	0	5.47	616.81	0	616.81	1555.93	51.9
09:09:44	112.73	0	5.51	620.83	0	620.83	1554.14	51.8
09:09:49	114.06	0	5.51	627.88	0	627.88	1550.98	51.7
09:09:54	114.17	0	5.48	625.17	0	625.17	1552.2	51.7
09:09:59	113.6	0	5.49	623.63	0	623.63	1552.88	51.8
09:10:05	113.6	0	5.5	625.04	0	625.04	1552.26	51.7
09:10:10	112.95	0.39	5.45	616.12	44.31	660.43	1536.23	51.2
09:10:15	111.04	0.8	4.69	520.89	88.93	609.82	1559.03	52.0
09:10:20	112.25	0.79	4.7	527.47	88.27	615.74	1556.4	51.9
09:10:26	112.48	0.79	4.71	529.72	88.83	618.55	1555.15	51.8
09:10:31	113.2	0.79	4.71	532.81	89.51	622.32	1553.47	51.8
09:10:36	112.93	0.8	4.71	531.74	89.84	621.58	1553.8	51.8
09:10:41	112.93	0.79	4.7	531.1	89.5	620.6	1554.24	51.8
09:10:46	112.28	0.88	4.68	525.66	98.88	624.54	1552.48	51.7
09:10:52	110.54	1.28	3.94	436.08	141.72	577.81	1573.05	52.4
09:10:57	112.93	1.29	3.96	446.67	145.26	591.93	1566.9	52.2
09:11:02	113.15	1.29	3.95	446.48	145.9	592.37	1566.7	52.2
09:11:07	112.25	1.28	3.93	440.82	143.27	584.09	1570.32	52.3
09:11:12	111.35	2.04	3.89	432.82	227.27	660.09	1536.39	51.2
09:11:17	109.24	2.05	3.13	342.01	223.74	565.75	1578.26	52.6
09:11:23	109.57	2.05	3.16	346.45	224.23	570.67	1576.14	52.5
09:11:28	110.7	2.07	3.17	350.65	228.77	579.42	1572.35	52.4
09:11:33	110.9	2.07	3.16	350.14	229.25	579.38	1572.36	52.4
09:11:38	110.29	2.07	3.16	348.06	228.16	576.22	1573.73	52.5
09:11:43	110.25	2.06	3.17	349.17	227	576.17	1573.76	52.5
09:11:49	110.9	2.07	3.16	350.93	229.36	580.29	1571.97	52.4
09:11:54	110.7	2.07	3.16	349.41	228.72	578.13	1572.91	52.4
09:11:59	109.93	2.74	3.14	345.34	301.55	646.89	1542.41	51.4
09:12:04	107.79	2.83	2.35	253.64	304.79	558.43	1581.4	52.7
09:12:09	107.39	2.81	2.35	252.42	301.27	553.68	1583.43	52.8
09:12:14	107.1	2.83	2.37	254.18	302.72	556.9	1582.05	52.7
09:12:20	109.1	2.83	2.37	259.11	309.22	568.33	1577.14	52.6
09:12:25	109.33	2.84	2.37	259.43	310.08	569.51	1576.64	52.6
09:12:30	109.12	2.84	2.38	259.19	309.74	568.94	1576.88	52.6
09:12:35	109.28	2.84	2.37	259.49	310.11	569.6	1576.6	52.6
09:12:40	109.1	2.84	2.38	259.19	309.48	568.67	1577	52.6
09:12:46	108.88	2.85	2.37	258.5	310.09	568.59	1577.03	52.6
09:12:51	108.45	3.51	2.37	256.72	380.87	637.58	1546.62	51.6
09:12:56	106.96	3.49	1.57	168.1	372.85	540.94	1588.84	53.0
09:13:01	104.55	3.47	1.57	164.55	363.07	527.62	1594.47	53.1
09:13:06	104.82	3.53	1.6	167.77	369.71	537.48	1590.31	53.0
09:13:12	108.18	3.53	1.6	173.15	382.33	555.48	1582.66	52.8
09:13:17	107.91	3.53	1.6	172.19	380.45	552.64	1583.87	52.8
09:13:22	107.52	3.05	1.59	171.33	328.47	499.79	1606.06	53.5
09:13:27	107.88	4.24	2.37	255.77	457.92	713.69	1511.34	50.4

09:13:33	105.93	4.3	0.81	85.32	455.85	541.17	1588.75	53.0
09:13:38	106.92	4.26	0.8	85.78	454.93	540.71	1588.94	53.0
09:13:43	105.95	4.25	0.8	85.04	450.72	535.76	1591.04	53.0
09:13:48	106.42	4.26	0.8	85.36	453.77	539.13	1589.61	53.0
09:13:53	106.62	4.27	0.8	85.33	454.82	540.16	1589.18	53.0
09:13:59	106.13	4.25	0.8	85.07	450.99	536.06	1590.91	53.0
09:14:04	105.72	4.25	0.8	84.69	449.59	534.28	1591.66	53.1
09:14:09	107.03	5.08	1.57	168.36	543.98	712.34	1511.98	50.4
09:14:14	101.76	5.77	0	0	586.69	586.69	1569.19	52.3
09:14:20	102.12	5.69	0	0	580.9	580.9	1571.71	52.4
09:14:25	101.67	5.69	0	0	578.5	578.5	1572.75	52.4
09:14:30	102.34	5.71	0	0	584.01	584.01	1570.36	52.3
09:14:36	102.34	5.7	0	0	583.83	583.83	1570.43	52.3
09:14:41	101.67	5.68	0	0	577.99	577.99	1572.97	52.4